NASA Contractor Report 179600

Study of the Generator/Motor Operation of Induction Machines in a High Frequency Link Space Power System

Thomas A. Lipo and Pradeep K. Sood
University of Wisconsin
Madison, Wisconsin

March 1987

Prepared for the
Lewis Research Center
Under Grant NAG3-631

National Aeronautics and
Space Administration

Contents

Chapter 1

Introduction

Static power conversion systems have traditionally employed dc links for distribution of power and to accomplish temporary energy storage required for decoupling. A key factor behind the wide spread use of dc as the link quantity has been the ease and effectiveness by which the energy storage function can be implemented. In particular, electrolytic capacitors provide low-cost, high density energy storage in popular *dc voltage* link systems. DC inductors perform a similar function, although somewhat less effectively, in the *dc current* link systems frequently employed in high power ac drives. Another important consideration is that relatively simple converter topologies have been available for power conversion to and from dc enabling competition in a cost sensitive market.

With continued progress in the development of power devices and components, improvements in the performance capabilities of dc link systems are to be expected. However, dramatic gains in such areas as improved system response, higher converter bandwidths, increased output frequencies, greater power densities, reduction in audible and electrical noise associated with power conversion process, increased safety, and others will require advances in power conversion circuit configurations in addition to continued progress in the area of power components. These advances become necessary because the dc link approach to power conversion subjects the system to a number of basic constraints which ultimately limit its overall performance.

The "hard" switching of the power devices is largely responsible for the simplicity of dc link power converters but is also responsible for high levels of losses and device stresses during the switching intervals. As a result, switching frequencies in traditional dc link converters have failed to rise substantially even with the arrival of new large power BJTs and GTOs. In turn, the output frequency, converter bandwidth, power density, and other such capabilities related to switching frequency are severly limited. Also, high device stresses

have had an adverse effect on the reliability of such power converters. An indirect consequence of this limitation has been that device manufaturers have spent considerable amount of development effort to make devices capable of withstanding high switching stresses resulting in undesirable compromises in other areas of device performance.

Recently, resonant switching techniques have been applied to reduce or eliminate some of the undesirable effects of "hard" switching [1- 5]. By permiting increased switching rates with less than corresponding increases in losses or device stresses, resonant converters have generally been able to improve converter performance. However, continued use of traditional dc link approach (or variations thereof) for the energy storage function has generally prevented its application to a broader range of power conversion systems.

A fundamentally different approach to static power conversion is the use of an ac link in place of the conventional dc link. Power conversion systems that utilize an ac link for power distribution can employ transformers within the link to meet possibly conflicting voltage level requirements in the system. With adjustable link voltage, each converter in the system can then be operated from a link voltage that is optimal for its needs. An ac link provides increased flexibility in power distribution since entire sections of the link can be operated at voltage levels higher or lower than that of the rest of the system. Electrical isolation is readily achieved to allow safer grounding practices and a more effective noise suppression in the system. Alternating link voltage also makes it easier to detect and quickly isolate faulty converters in the system and thus, further increases the safety and reliability of the entire system. The penalty of size, weight and efficiency that would normally be associated with the use of transformers in the power conversion system can be minimized by choosing a high value (20 kHz or above) for the link frequency. High frequency ac (mostly nonsinusoidal) link systems have been used successfully in dc-to-dc power conversion for quite some time. However, because of real or perceived difficulties in transforming the ac link voltage to anything but dc, application of ac link approach has generally been confined to the area of dc-to-dc power conversion.

1.1 Objective of the Research

The objective of this research is to demonstrate the feasibility of a high frequency sinusoidal voltage link power conversion system which is not conversion-function specific. The proposed system is envisioned as a utility type distribution system serving dc or ac, single or three-phase, voltage or current type loads and sources. In particular, an ac voltage (rather than an ac current) link is proposed to help realize a distributed power structure. The choice of a sinusoidal voltage for the link is employed to facilitate passive energy storage in the link and to minimize adverse effects due to the parasitic elements in the system. Reduced order systems requiring only specific type of conversion function can be treated as special

cases of this generalized configuration. However, conversion at megawatt power levels or power distribution over very large distances (more than a few hundred meters) is outside the scope of this research.

A link frequency of 20 kHz or more is used to permit high power densities and substantial reductions in audible noise associated with link-side transformers and other magnetic components operating at link frequencies. Interface converters are envisioned which would perform one-step power conversion to interface a wide variety of loads and sources to the link. A special switching strategy called pulse density modulation or *PDM* is used to allow high speed switching in interface converters without incurring high switching losses, to provide effective control over the generated voltage or currents, and to permit bi-directional flow of power. As a result of high switching rates, higher converter bandwidths, faster system response, and increased output frequencies are expected. Higher output frequencies, in turn, will allow the use of high speed ac machines resulting in additional reductions in size and weight of the overall system. Another promising characteristic of a high frequency link system is that while it would process power at low frequencies (including dc), the noise associated with power processing occurs at high frequency ranges where it is both easier to suppress and less troublesome to instrumentation and other sensitive apparatus.

1.2 Applications of High Frequency Link Converters

1.2.1 Orbiting Space Station

Power system requirements for the orbiting space station are being projected at 75 kW for the initial operation capability (IOC) with a steady growth over a period of a few years to the 300 kW level [6,7]. Because of the large power levels involved and the need to distribute this power over distances of more than 100 meters, the ac link appears to have a number of advantages. In particular, an ac link system offers a utility type system configuration with ease of voltage level changes and electrical isolation by means of transformers on the link side. With voltage shifting achieved at the link, most conversion needs are met with one additional stage of power conversion. Also, switching and protection are made easier due to the frequent reversal of the link voltage.

Figure 1.1 shows a possible configuration which may be used to implement a power management and distribution (PMAD) space power system [7]. Three-phase fixed frequency utility converters for actuator control and control of compressors for the environmental control all require low-distortion three-phase outputs of controllable frequency and amplitude. The PDM converter described in this report can generate such outputs and is capable of bi-directional power flow required for such loads. Resonant converters need be

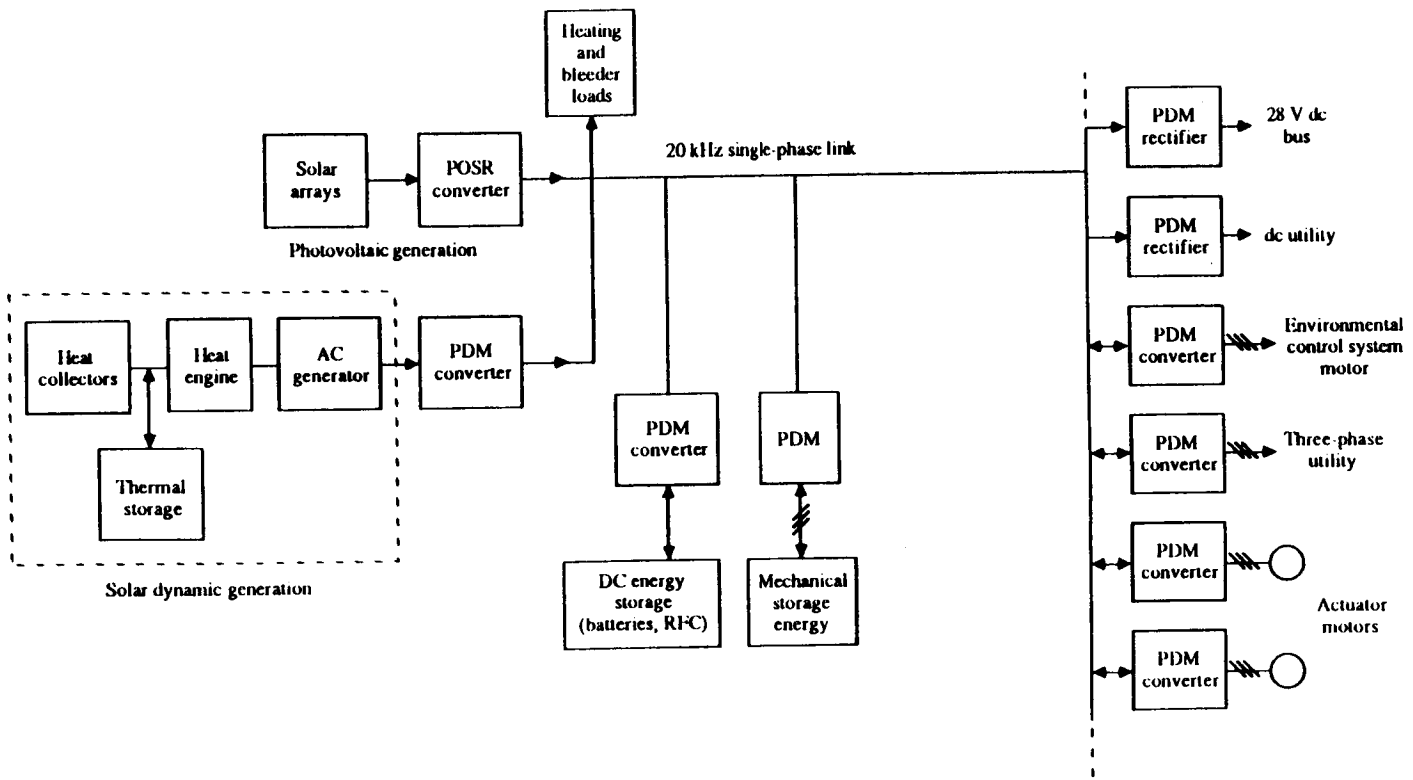

Figure 1.1: Application of High Frequency Link to Space Station Power System.

used only for interfacing dc sources to the link, a function to which they are well suited. For unidirectional dc power flow out of the link, transformer/rectifiers can be used. When tighter regulation is needed, the rectifier can be replaced by a unidirectional PDM converter with possible natural commutation of the devices.

In normal operation of such a system, link voltage build up and control would be performed through a parallel output, series resonant (POSR) converter [7,8]. PDM converters would interface the remaining loads/sources in the system and maintain average power balance at all times. The distinguishing features between traditional POSR converters and the PDM converter will be described in subsequent chapters of this report. Because a large number of converters in the system are of one basic type, the proposed implementation produces a higher degree of uniformity in the system. This can be expected to result in increased reliability of the system. Inherent bi-directional power flow capability of the PDM converter means that the management of power in the overall system becomes somewhat easier requiring no topological or control system changes. The proposed PMAD implementation is also well suited to the modular growth that is projected for the space station power system.

1.2.2 Aircraft Secondary Power System.

Another potential application of a high frequency link power conversion system is in the secondary power system of an aircraft. Secondary power in aircraft is needed for environment control, lighting, utility power, landing gear control, flight controls, de-icing, and a host of other aircraft operation and environment related functions. In conventional aircraft, these functions are handled by separate electric, hydraulic (primarily for flight control) and pneumatic (anti-icing, environmental air supply, etc.) power systems that can add up to equivalent power ratings of several hundred kilowatts.

Technical studies have shown that considerable advantages are to be obtained by using electric power systems based on a high frequency sinusoidal voltage link for all secondary power needs in the aircraft. For example, Hoffman and associates [9] have reported that if a 200 passenger modern transport aircraft such as Boeing 767 were to be redesigned with an all electric secondary power system based on a 20 kHz, 440 V rms single-phase sinusoidal voltage link, then aircraft weight savings of as much as 7700 Kg (17000 lb) would result. The associated saving in fuel consumtions have been estimated at approximately 9 per cent.

Figure 1.2 suggests how the secondary power system of an aircraft may be implemented using the 20 kHz link power system. The schematic shows one- half of the dual redudant system in which all primary sources have access to either of the two links. Again, PDM converters would be used as the primary interface converter in the system with a POSR

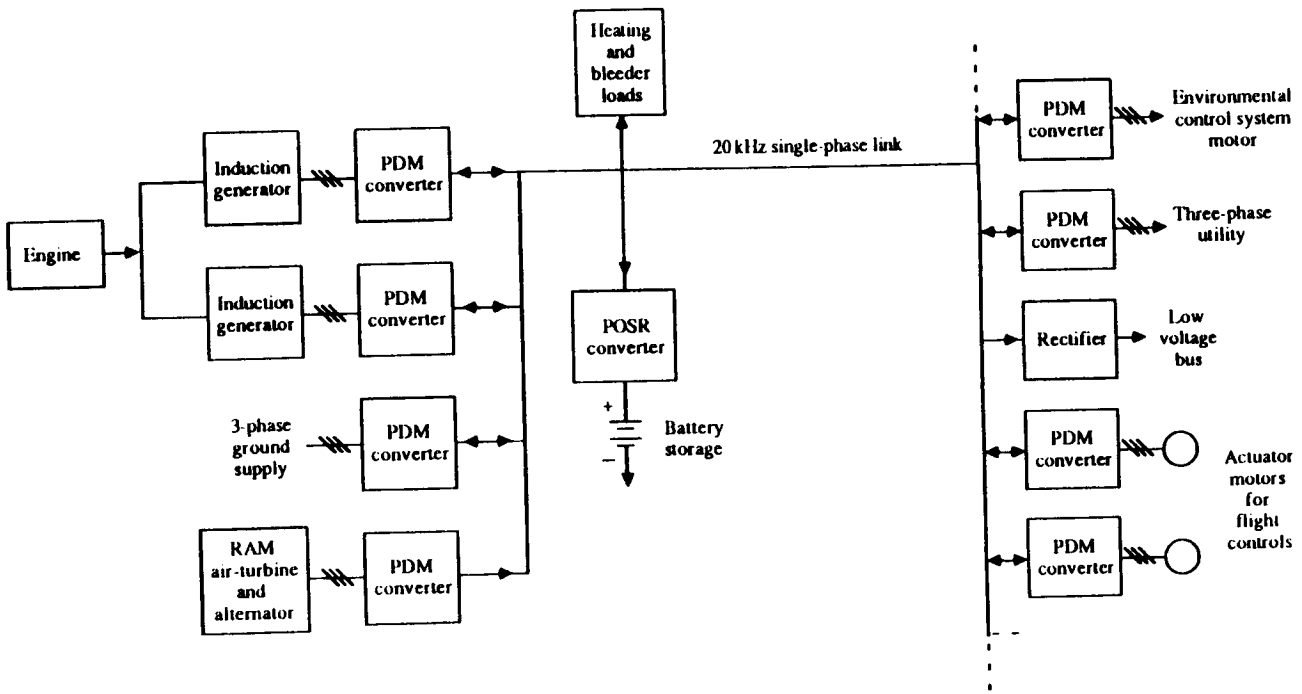

Figure 1.2: Application of High Frequency Link Configuration to the Secondary Power System of an Aircraft. Figure Shows One-Half of a Dual Redundant System.

converter used only to convert dc power into the link. Two 90 KVA induction generators would operate from each of the two engines. The sizing of these machines, discussed in detail in [9], is such that all essential loads can be supplied from just one machine so that the system can operate with one engine and one generator out of service. In normal operation, PDM converters would power the induction machines as motors to start the engines and then operate them as generators for feeding the power into the link. A POSR converter running from the battery supply can be used to build up and maintain the link voltage required by the PDM converters. Galley and de-icing loads could be supplied directly from the high frequency bus with minimal power processing. PDM converters would provide the individual variable frequency supplies needed for controlling the actuators in flight control systems. Fixed frequency utilities and environmental control system motors are supplied with PDM converters.

The uniformity obtained in the system due to the versatility of the PDM converters simplifies the implementation and increases reliablity of the overall system. Another major advantage of the proposed implementation is that it is better able to manage the power flow in the system due to the inherent capability (requiring no changes in circuit topology or overall control strategy) of the PDM converter to reverse direction of power flow.

1.3 Brief Summary of This Report

A brief review of induction machine/high frequency link interface characteristics are outlined in Chapter 2 and the important properties required of these interface converter with induction machine load/sources are summarized. Existing ac link topologies (most of which are conversion function specific) are also discussed in Chapter 2. A parallel output series resonant (POSR) type of high- frequency sinusoidal voltage link converter is examined in Chapter 3.

Chapter 4 introduces the concept of zero voltage switching which is critical to the efficient operation of interface converters and proposes a new pulse density modulated (PDM) converter utilizing a parallel resonant LC tank to support the ac voltage link. The remainder of Chapter 4 is devoted to a discussion of the technique of area-comparison pulse-density-modulation (AC-PDM) which enables the realization of low frequency waveforms of controllable frequency, amplitude and waveshape in spite of the zero voltage restriction on converter operation.

Chapter 5 examines the overall operation of the experimental system. In particular, interaction of the proposed POSR and PDM interface converters with the high frequency link has been studied both with computer simulation and in hardware. Subsequently, steady state and startup performance of the entire power conversion system has been examined. Oper-

ation with and without an excitation inverter has been investigated analytically. Chapter 6 examines system operation of the PDM converter with a variety of loads and sources. Alternative PDM configurations are discussed. Chapter 7 summarizes the important aspects and conclusions of this research and identifies areas suitable for further work. Finally, Chapter 8 lists some of the bibliography relevant to this research. Computer models have been used quite extensively in this study. Development and experimental verification of these models has been described in Appendices A to C at the end of this report.

To complete this introduction, a few remarks regarding the terminology appear relevant. Many of the converters discussed in this report are capable of generating voltage or currents waveforms at the low frequency end. In order to avoid repeated usage of *current or voltage*when either is possible, the word *signal* has been used as a generic electrical variable. The term does not necessarily imply low power levels as the usage of this term sometimes does. Of course, the terms *current* and *voltage* are used individually wherever they are specifically intended. When power converters with capability of bi-directional power flow are involved, usage of *input* and *output* to refer to the converter ports (terminals) can sometimes be confusing. Where misunderstandings appear possible, converter ports have been referred to as *high frequency end* or *low frequency end* because of the wide frequency separation that exists in the majority of converters discussed in this report.

1.4 References

1. J. G. Kassakian, *New current mode sine wave inverter*, IEEE Trans. Ind. Appl., vol. IA-18, pp. 273-278, May/June 1982.

2. R. L. Steigerwald, *High-frequency resonant transistor dc-dc converters*, IEEE Trans. Ind. Elect., vol. IE-31, pp. 181-191, May 1984.

3. D. M. Divan, *The resonant dc link converter - a new concept in static power conversion*, Conf. Rec. 1986 Annu. Meet. IEEE Ind. Appl. Soc., pp. 648-655.

4. K. H. Liu and F. C. Lee, *Zero voltage switching technique in DC/DC converters*, in Conf. Rec. 1986 Annual Meeting, IEEE Power Electronics Specialist's Conf., pp. 58-70.

5. J. Mildice, *Bi-directional power converter control*, NASA CR-175070, 1986.

6. R. R. Rice, *Space Station Power System Selection*, 21st Intersociety Energy Conversion Engineering Conference (IECEC), San Diego, CA, Aug., 1986.

7. I.G. Hansen and G.R. Sundberg, *Space station 20-kHz power management and distribution system*, 1986 Power Electronics Specialist's Conference, Vancouver, Canada, June 23-27, 1986.

8. N. Mapham, *An SCR inverter with good regulation and sine-wave output*, IEEE Trans. on Ind. and Gen. Appl., vol. IGA-3, pp. 176-187, March/April 1967.

9. A. C. Hoffman, I. G. Hansen, R. F. Beach, et. al., *Advanced secondary power system for trasport aircraft*, NASA Technical Paper 2463, 1985.

Chapter 2

Induction Machine - High Frequency Link Interface Considerations

A key to the successful application of an ac or dc link power distribution system is the ability of ac induction machines to operate from the distribution network. The squirrel cage induction machine is an enormously versatile and extensive class of electrical machine which can readily operate in both the motoring or the generating mode. The induction machine inherently requires a three phase power source in order to maximize its iron and copper utilization and to provide smooth electromagnetic torque. Since a high frequency link constitutes, in effect, a single phase supply and it is clear that a power circuit interface will be needed to supply three-phase voltages at the machine terminals from the single-phase fixed frequency regulated voltage link. However, before discussing specific interface circuit topologies for this purpose, it will be useful to first examine the basic terminal characteristics of an induction machine during both motoring and generating operation.

2.1 Terminal Characteristics of Induction Machines

2.1.1 Reactive Power Requirements

It can be said that an induction machine is unique from all other electrical machines in that it must obtain its excitation power from the same terminals through which the real power flow also occurs, that is, through its stator terminals. When the machine is connected to a source of reactive power such as the utility supply, the excitation component of power is inherently supplied to the machine from the utility supply. However, if the network

receiving the generated power is incapable of providing the required reactive power (for example, a passive load in a stand alone induction generator system) then a dedicated system (exciter) must typically be provided for this purpose.

2.1.2 Operation with Sinusoidal Supply Having Fixed Frequency and Amplitude.

Figure 2.1 shows the speed- torque characteristics of a three-phase squirrel cage induction machine supplied from a fixed frequency, balanced, sinusoidal voltage source. When operated from a fixed frequency supply, it can be noted that normal steady state operation is limited to a narrow speed range around synchronous speed. This speed, *synchronous speed* is equal to the supply frequency divided by the number of pole pairs. At synchronous speed no currents can be induced in the rotor bars and as a result the machine develops zero torque. For shaft speeds below synchronous speed, i.e. for positive values of slip, the electromagnetic torque is positive and the machine operates as a motor. Operation at speeds lower than the maximum positive torque (motoring breakdown torque) is normally not feasible due to static instability of the resulting operating point. When shaft speeds are higher than the synchronous speed, the power flow is reversed and the machine operates as a generator converting mechanical energy into electrical energy which is then returned to the supply. Operation at speeds above the maximum value of generating torque (generating breakdown torque) is again not feasible as a normal operating condition.' Figure 2.2 shows an equivalent circuit that is typically used to predict the steady state behavior of an induction machine. Using this equivalent circuit, phasor diagrams for machine operating as a motor (Fig. 2.3 (a)) and as a generator (Fig. 2.3 (b)) can be constructed. In this diagram the reference direction of current flow has been taken as positive when flowing into the machine so that when the machine is generating the stator current has a negative real component. The phasor diagrams demonstrate that the machine draws a lagging current from the supply during both motoring and generation. This is a direct consequence of fact that the excitation flux in a induction machine must be induced from the stator side regardless of the direction of the real power flow.

2.1.3 Sinusoidal Supply Having Variable Frequency and Amplitude.

While some speed control is possible with fixed frequency operation, useful shaft speeds are typically limited to speed variations less than ten percent on either side of the synchronous speed due to the breakdown torque limitation. An effective method of extending the useful speed range is to simply adjust the supply frequency such that the synchronous speed is in the vicinity of the desired shaft speed. However, if the stator frequency is changed without

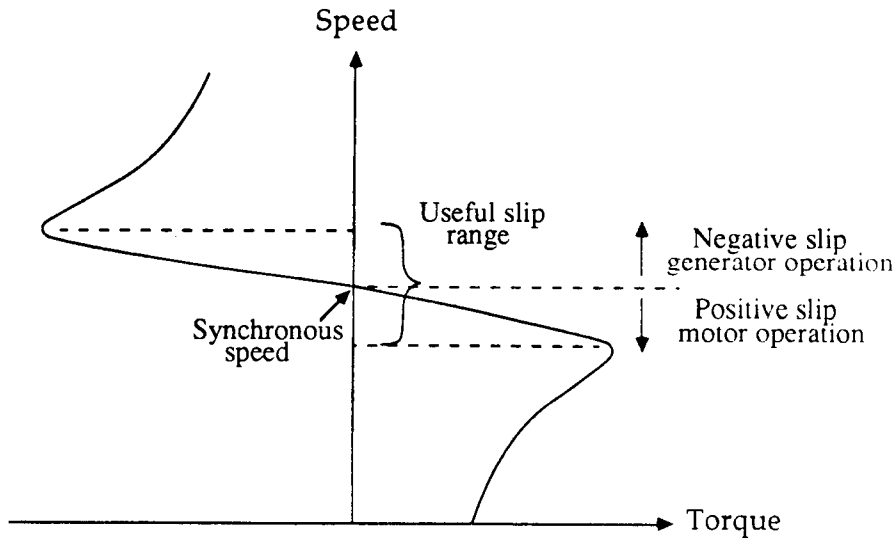

Figure 2.1: Torque-Speed Curves of a Three Phase Squirrel Cage Induction with a Balanced, Three Phase, Sinusoidal, Fixed Frequency Supply.

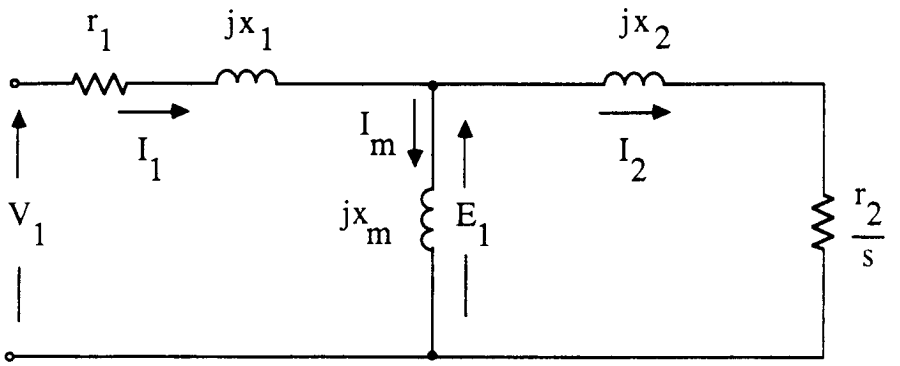

Figure 2.2: Per Phase Squirrel Cage Induction Machine Equivalent Circuit.

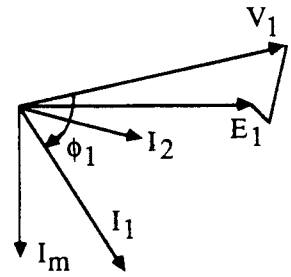

(a) Phasor Diagram for Motoring

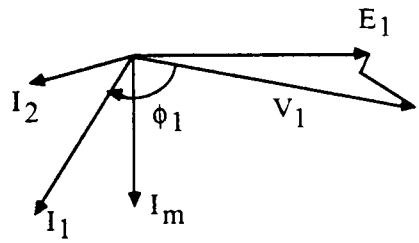

(b) Phasor Diagram for Generation

Figure 2.3: Phasor Diagrams for Motoring and Generation.

altering the magnitude of the stator voltage, the airgap flux increases (decreases) as the stator frequency is decreased (increased) due to the frequency dependent voltage drop across the stator impedance. This change in operating flux reduces the machine's torque capability at higher frequencies and causes machine saturation at lower frequencies. On the other hand, if the stator voltage is adjusted in proportion to the supply frequency, (i.e. constant Volts/Hertz) a machine with nearly constant air gap flux results. Such a constraint between voltage and frequency permits the speed-torque characteristics to be translated nearly unaltered along the speed axis (Fig. 2.4). As a practical matter, at very low frequencies, stator resistive drop becomes significant and a voltage boost beyond the constant Volts/Hertz relationship is required in order to prevent a decrease in the desired value of the air gap flux in the machine [1,2]. The proper algorithm for maintaining constant Volts/Hertz becomes very complicated as the speed of the machine approaches zero.

2.1.4 Operation from a Converter Supply.

Power converters are commonly used to provide the controllable amplitude variable, frequency supply that is needed to make the induction machine operate at variable shaft speeds. Successful operation of the combined converter-machine system requires not only that the converter be able to impress voltages (or currents) of controllable frequency and amplitude on the machine, but at the same time *be able to accomodate the resulting lagging currents (or leading voltages in the case of a current source) of variable amplitude and phase.* In addition, converter outputs are typically nonsinusoidal. Harmonics present in the impressed voltages must be minimized in order to reduce undesirable effects such as heating and large current peaks.

2.2 Desirable Characteristics of the Interface Converter

Induction motors can be considered as the workhorse of industry and would necessarily form an important part of the load in any power distribution system. In addition, induction machines are increasingly being considered for use as generators, with operation in the motoring mode occuring only occasionally for starting or for similar noncontinuous duty. Induction machines are also widely used as actuators in which case frequent transitions between motoring and (re)generation may be needed. The characteristics of the interface converter differs in the two cases in terms of the converter capability for inherent bi-directional power flow. When interfacing a power converter with an induction generator, this motoring capability is desirable but not essential provided that some adaptations are possible which allow for the occasional motoring operation. On the other hand, actuator type applications require frequent torque reversals and must use converters with bi-directional power flow

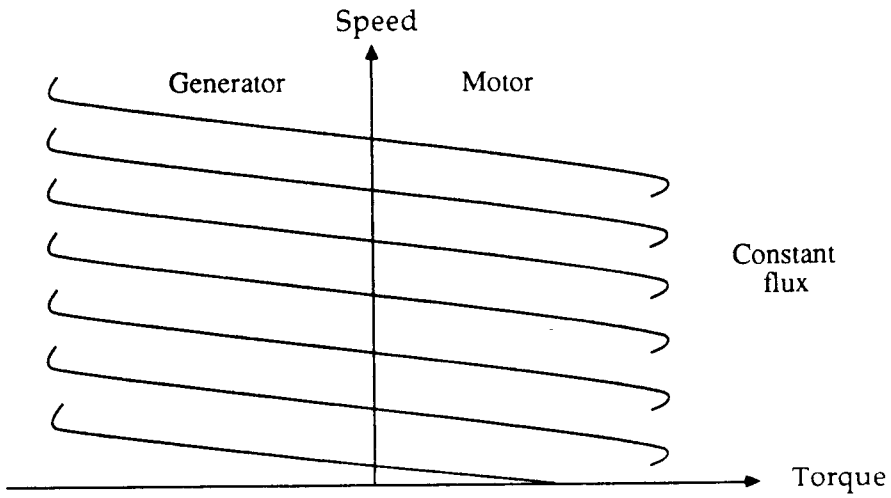

Figure 2.4: Torque-Speed Characteristics for Various Frequencies with Constant Volts/Hertz Operation.

capability. To avoid separate treatment of interface converters with otherwise similar requirements, the bi-directional power flow capability will be taken as a desirable feature, but converter topologies having only unidirectional power flow capability will not be automatically excluded from consideration as a candidate interface converter.

Considerations which influence the choice of the interface converter topology are:

High Efficiency of Power Conversion. Poor efficiency not only implies loss of valuable power but also results in increased system bulk and/or poorer reliability due to the need to dissipate the losses.

Bi-Directional Power Flow Capability. This feature permits smooth transitions between motoring and generation as discussed above.

Low Distortion Output to at Least 1000 Hz. Required in order to permit direct operation of high speed machines for additional gains in system mass, volume and efficiency.

Simple and Reliable Means of Output Control. Control strongly influences the converter topology and its performance capability.

Minimization of Voltage or Frequency Disturbances to the Link. Disturbances to the ac link increases the degree of coupling among the various sources/loads operating from the link.

2.3 Interface Converter Topologies.

Figure 2.5 shows converter topologies which might be considered for interfacing of a three-phase induction machine to a single-phase high frequency link. A brief description of each topology is given below. Table 2.1 summarizes the primary strengths and limitations of each configuration.

2.3.1 Intermediate DC Link Converter, Fig. 2.5(a)

The intermediate DC link converter of Fig. 2.5(a) utilizes two ac-to-dc converters to establish an intermediate dc voltage or current link. DC energy storage provides a good buffer between the load and the link resulting in a system that is well decoupled in terms of harmonics and local transients. Although dc-to-low frequency conversion portion can employ established technology, conversion to dc from an existing high-frequency voltage with inherent bi- directional power flow needs to be demonstrated. An uncontrolled rectifier may

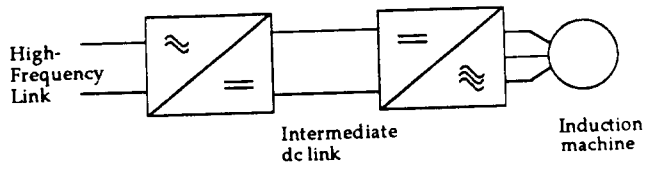

(a) Intermediate DC Link Converter

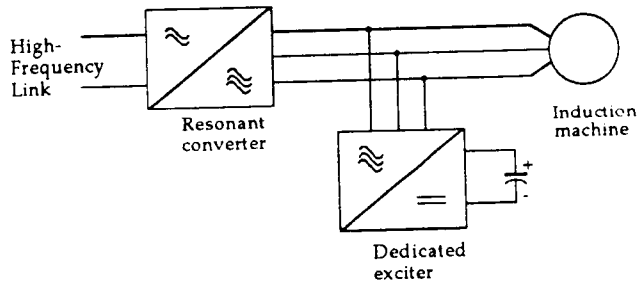

(b) Resonant Converter with an Auxiliary Exciter

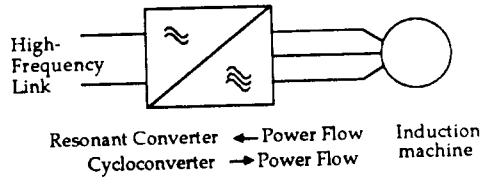

(c) Resonant Converter without Auxiliary Exciter

Figure 2.5: Converter Topologies for Single Phase to Three Phase Power Conversion

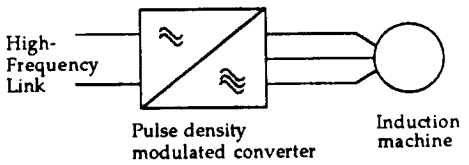

(d) Phase Controlled Cycloconverter

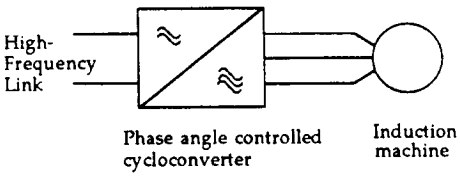

(e) Pulse Density Modulated Converter

Figure 2.5: Converter Topologies for Single Phase to Three Phase Power Conversion

Configuration	Block Schematic	Major Advantages	Major limitations
Intermediate-dc	Fig. 2.5 (a)	Known tecknology for uni-directional power flow. Good decoupling through dc energy storatge.	Two-step power handling. Show feasibility of operating from a high-freq. link with bi-directional power flow. Limited output freq.
Resonant conv-erter with exicter	Fig. 2.5 (b)	Straight forward machine excitation control.	Demonstrate feasibility of resonant converter interface. Combined power rating greater than machine rating.
Resonant conv-erter without exciter	Fig. 2.5 (c)	Efficient, one-stage power conversion.	Seeks dual role for resonant converter neither of which has been demonstated as individually feasible.
Phase-controlled cycloconverter	Fig. 2.5 (d)	One-stage power conversion. Inherent bi-directional power flow capability. Known Tech-nology.	Very high switching losses. Varying (and lagging) power factor reflected to the high-frequency link. Sharp voltage transients.
Pulse-density-modulated converter	Fig. 2.5 (e)	Efficient, one-stage power conversion with inherent bi-directional power flow. Usable with most type of sources/loads.	Needs an ac filter.

Table 2.1: Comparison of Converter Topologies

be used rather than the controlled bridge but the bi-directional power flow capability would clearly be sacrificed.

2.3.2 Resonant Converter with an Exciter, (Fig. 2.5(b).

The resonant converter topology is particularly suitable for interfacing an induction generator with the high frequency link. The configuration could use a dedicated exciter to meet the excitation needs of the generator and to maintain regulated ac voltages on the machine terminals. Resonant converters, possibly one single-phase unit for each phase, would then convert the low frequency three-phase generator output into the single-phase high frequency voltage of the link. The Parallel Output Series Resonant (POSR) converter is favored for the choice of resonant circuit topology because of its ability to generate high-frequency sinusoidal power with high efficiency. However, the total rating of the exciter and the resonant converter can be expected to be higher than the generator rating since they represent the algebraic (rather than the vector) sum of the excitation and the load components of the generator kVA.

2.3.3 Resonant Converter Without an Exciter, Fig. 2.5(c).

This topology is also suitable primarily for interfacing generators to a high frequency link. It would seek to perform the dual role of providing machine excitation as well as the conversion of low-frequency three-phase generator power into single-phase high-frequency link power. The converter would also be suitable for interfacing a conventional alternator or a permanent magnet generator to the link. Potential efficiencies are high due to resonant mode of power conversion. The power circuit of the individual converter may be adaptable for the occasional motoring operation that may be needed to start the generator by operating as a conventional cycloconverter.

2.3.4 Phase Controlled Cycloconverter, Fig. 2.5(d).

The conventional phase-controlled cycloconverter is able to generate three- phase low frequency voltages of controllable amplitude or frequency thereby allowing motor or generation operation without any circuit modifications. The approach, however, would require a link side filter to provide the necessary reactive power the commutate the bridge.

2.3.5 Pulse Density Modulated Converter, Fig. 2.5(e)

Another class of converters which can perform the task of providing an interface between the low and high frequencies are converters which operate on the principle of switching only at points of zero voltage on the high frequency side. A zero-voltage-switching power converter could synthesize three-phase low frequency voltages for the machine with power flow in either direction. The technique of pulse density modulation would permit control of amplitude and frequency of the synthesized signals in the presence of the zero-voltage switching constraint. The scheme requires a link side filter for harmonic decoupling.

2.4 Topologies Studied in This Report

While closest to conventional technology, the dc link topology of Fig. 2.5(a) is not desirable since it involves two-stage power conversion. In addition, voltage stresses and switching losses resulting from the "hard switching" used in such conventional dc link converters are likely to severely limit the capabilities and efficiency of this interface converter topology. In this investigation, such a dc link converter interface for induction machine has not been studied further.

The configurations of Figs. 2.5(b) and 2.5(c) were identified at the beginning of this investigation with a hope to extend the favorable characteristics of such POSR's operated from dc voltages sources to power conversion from low frequency ac sources. The power circuit rating of the configuration with a dedicated exciter is significantly higher than it is for a one-step power conversion (although still better than for the case of the intermediate dc link). This advantage exists because the excitation and the real power component of the machine current are handled separately resulting in a total power rating which depends on the algebraic rather than the vector sum of these components. The topology of Fig. 2.5(c) is an attempt to remedy this limitation and make the resonant circuit Figs. 2.5(d) and 2.5(e). Section 3 of this report examines the feasibilty of these resonant circuit based topologies and identifies some of the problems associated with the implementations.

The converter circuits of Figs. 2.5(d) and 2.5(e) are very similar in their power circuit configuration but utilize fundamentally different techniques of control. Chapter 4 of this report identifies some of the limitations of conventional phase angle control when it is used in a high frequency link system (Fig. 2.5(d)). The report then goes on to propose a particular pulse density modulated converter topology (Fig. 2.5(e)) and discusses how it may be used successfully for the interfacing with a three-phase induction machine for either generator or actuator type applications.

Chapter 3

Resonant Circuit Based Interface Converter

Resonant converters are, perhaps, the oldest family of power converters having been developed before the age of modern solid state power devices. The family of resonant converters is probably also the largest class of power converters since numerous circuit variations exist which produce series or parallel resonance. One of the most useful of all resonant converters is the series resonant configuration in which the load is connected in parallel with the capacitor of the resonant LC tank. This converter has been called the Mapham converter in honor of its inventor [1]. Recent work [2,3] has demonstrated that the Mapham converter, hereinafter termed the Parallel Output Series Resonant (POSR) converter, is a very effective topology for conversion of dc voltages into low distortion high frequency sinusoidal voltages. There is, therefore, considerable interest in adapting the POSR circuit for use with ac inputs and in particular, for developing a topology for interfacing of induction machines to the high frequency link. The first phase of the work in this project was directed towards this goal and is described in this chapter.

3.1 The Parallel Output Series Resonant (POSR) Circuit

Figure 3.1 shows the basic circuit of a Parallel Output Series Resonant circuit in which the inductor L and capacitor C form a series resonant circuit. It is important to note that the load, represented by resistor R, is in parallel with the capacitor and not in series with the resonant circuit as used commonly in induction heating type applications [4]. Unlike the series connection, where the load sees essentially a constant current source, the parallel load sees a nearly constant voltage source which is well suited to link type applications and is

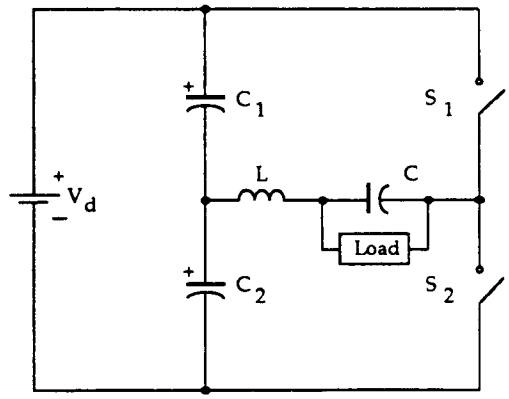

(a)

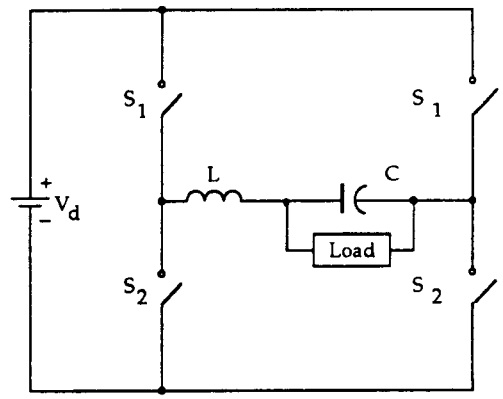

(b)

Figure 3.1: Parallel output series resonant (POSR) converter. (a) Half-bridge configuration. (b) Full-bridge.

much less prone to stability problems.

A high frequency sinusoidal voltage of the desired frequency, f_o can be generated across the capacitor by gating the switch pairs S_1, S_4 and S_2, S_3 alternately with frequency f_o. The frequency ratio f_o/f_r,where f_r is the resonant frequency given by

$$f_r = \frac{1}{2\pi\sqrt{LC}} \tag{3.1}$$

The per unit quantity f_0/f_r is an important parameter of the POSR converter. Converter operation is possible for the values of the switching frequencies both above and below the resonant frequency. Operation above the resonant frequency is characterized by the need for forced commutated devices, negligible turn-on losses in the main switches, and the use of purely capacitive snubbers [2]. Conversely during operation below the resonant frequency, $f_o/f_r < 1.0$, the tank circuit current leads the voltage applied across the circuit and makes natural commutation of the switches possible [1,2]. In addition, the switch turn on losses become nearly negligible since the converter switches now operate at the current zero point. Because of its desirable properties, the naturally commutated POSR circuit is the only class of resonant converter configuration that has been considered further in this investigation.

Figure 3.2 shows a modified form of the POSR circuit in which the resonant inductor has been split and placed symmetrically in series with each of the converter switches. In this manner the resonant inductor is made to perform the additional role of the di/dt inductors which would be otherwise needed. The smooth transfer of current resulting from this modification lowers the turn on losses in the converter switches, increases the circuit turn-off time somewhat and simplifies circuit protection due to the increased impedance of the shoot through path.

3.1.1 Circuit Operation of POSR Converter.

Circuit operation of the POSR converter is best described for the case of continuous capacitor current using naturally commutated devices. Over frequencies of interest, a fast thyristor reverse diode combination functions satisfactorily as the switch with the bi-directional current and unidirectional voltage blocking capability. The frequency ratio, f_o/f_r for these conditions of operation is likely to be in the range of 0.6 to 0.8. This range of frequency ratio occurs because the lower values tend to produce a discontinuous capacitor current resulting in markedly increased distortion and poor regulation of the generated high frequency voltage. For example, $f_o/f_r = 0.5$ guarantees discontinuous operation. Operation much closer to the resonant frequency, on the other hand, reduces the circuit turn off times and leads to larger than needed circulating currents.

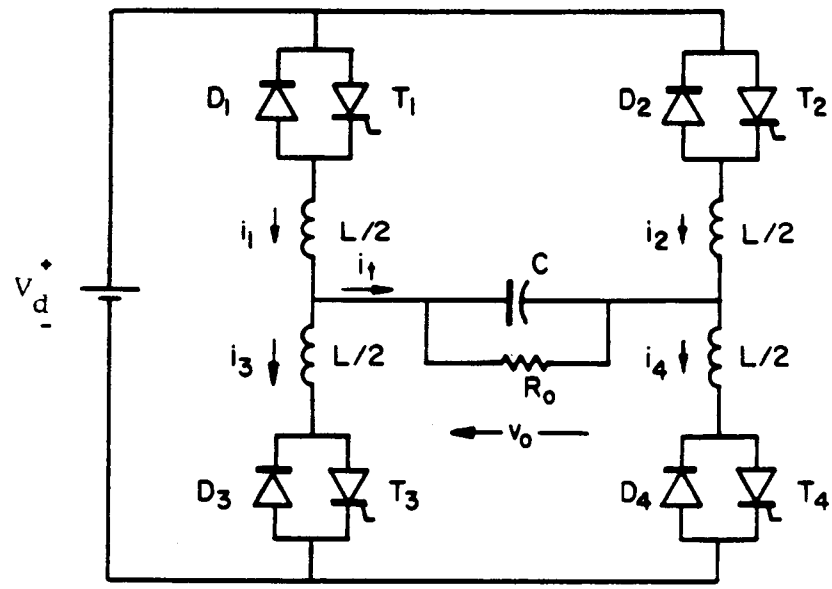

Figure 3.2: Modified POSR circuit with the resonant inductor split and placed symmetrically in series with converter switches.

Over the frequency range of interest, three modes of circuit operation can be identified for each half cycle of the generated high frequency voltage. Figure 3.3 shows the waveforms and circuit diagrams associated with each of the three modes. In mode I, Fig. 3.3 (b), a pair of thyristors conduct. As a result, the capacitor voltage charges with a resonant current pulse in the forward direction. When the charge on the capacitor reaches and then exceeds the supply voltage, the current pulse begins to decrease in amplitude. Mode I ends at the instant the current pulse returns to zero and the conducting thyristors begin to turn-off. Mode II, Fig. 3.3 (c), is then initiated by the capacitor which has now charged to its peak value and which forces the reverse connected diodes into conduction. Firing of the second pair of thyristors initiates mode III, Fig. 3.3 (d), in which the current transfers from the reverse connected diodes to the incoming thyristor pair. Note that mode III would be nonexistent if the inductances were lumped together into a single resonating inductance L and placed in series with capacitor C in the manner of Fig. 3.1 or if the capacitor current becomes discontinuous.

In order to improve understanding of the POSR converter a computer model of the converter of Fig. 3.2 has been developed and verified. The model is described in detail in Appendix B. Figure 3.4 shows an example set of circuit waveforms obtained using this simulation model. In this Figure the input dc voltage is 90 V. The frequency ratio is approximately 3/4.

3.1.2 Converter Losses.

Converter losses are a key limiting factor when weight, size and cost are of major concern. An important property of a POSR converter is that it can operate at tens of kilohertz without the switching losses becoming prohibitively large. At turn-off, the voltage across the device is limited by the reverse conducting diode. This turn off property ensures that the thyristor turn-off losses remain small. The turn-on losses are also small if split inductances (Fig 3.2) are used because the series inductances prevent the device current from rising to high levels during the period of turn-on when the voltage across the device is still falling.

Since the converter operates with a fixed amount of circulating current it, therefore, has fixed conduction losses. As a result, the total losses in a POSR converter do not vary substantially with the load. Thus, efficiencies are generally lower under light load conditions. However, at designed loads, efficiencies in the neighborhood of 95 percent can be expected when switching at 20 kHz. By comparison, conventional topologies are likely to perform much less efficiently at such a high frequency. The comparison becomes even more favorable if losses associated with filtering, EMI suppression etc., which are needed with conventional circuits, are taken into account.

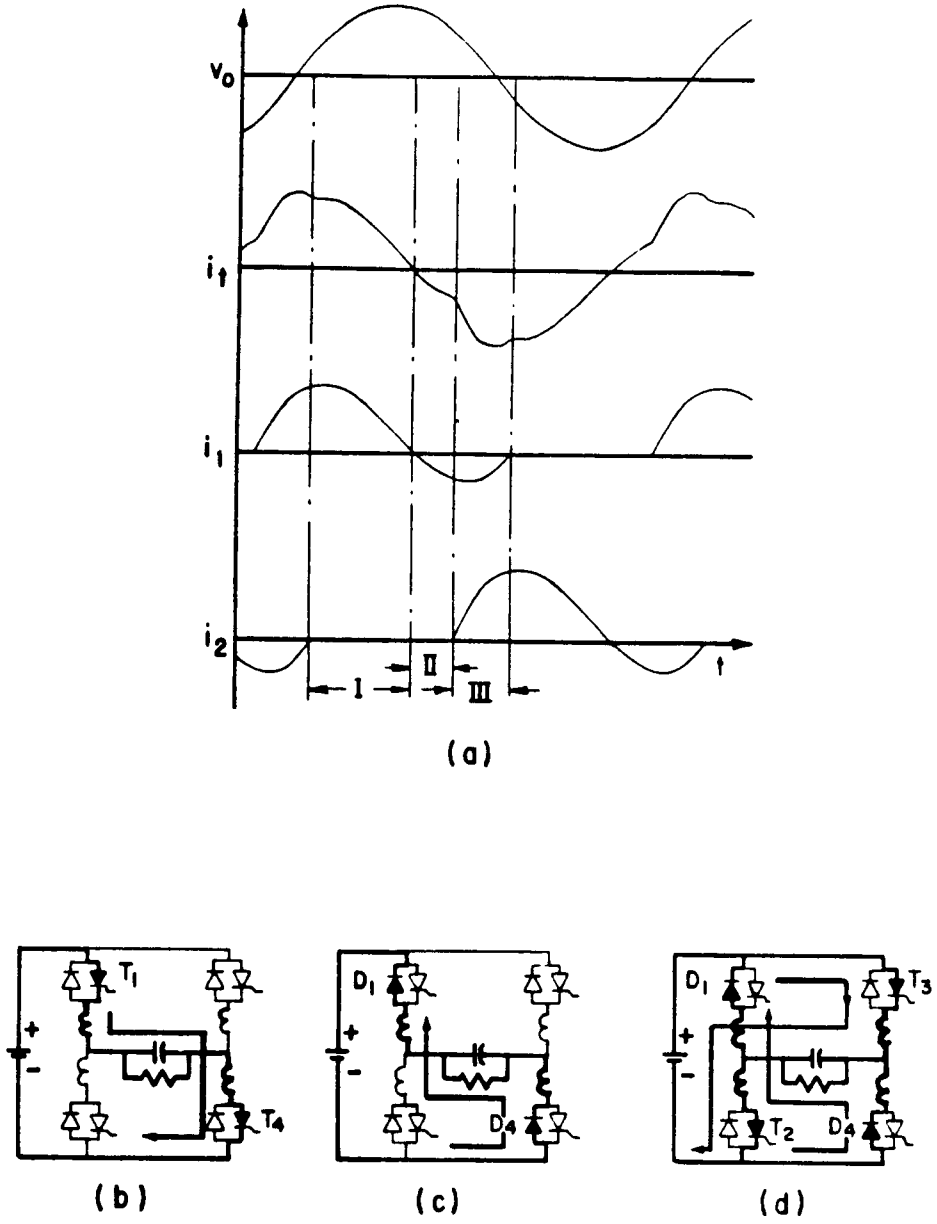

Figure 3.3: POSR circuit operation. (a) Typical circuit waveforms. (b) Mode I, pair of thyristors conduct. (c) Mode II, reverse diodes conduct. (d) Mode III, current transfers from diodes to the next pair of thyristors.

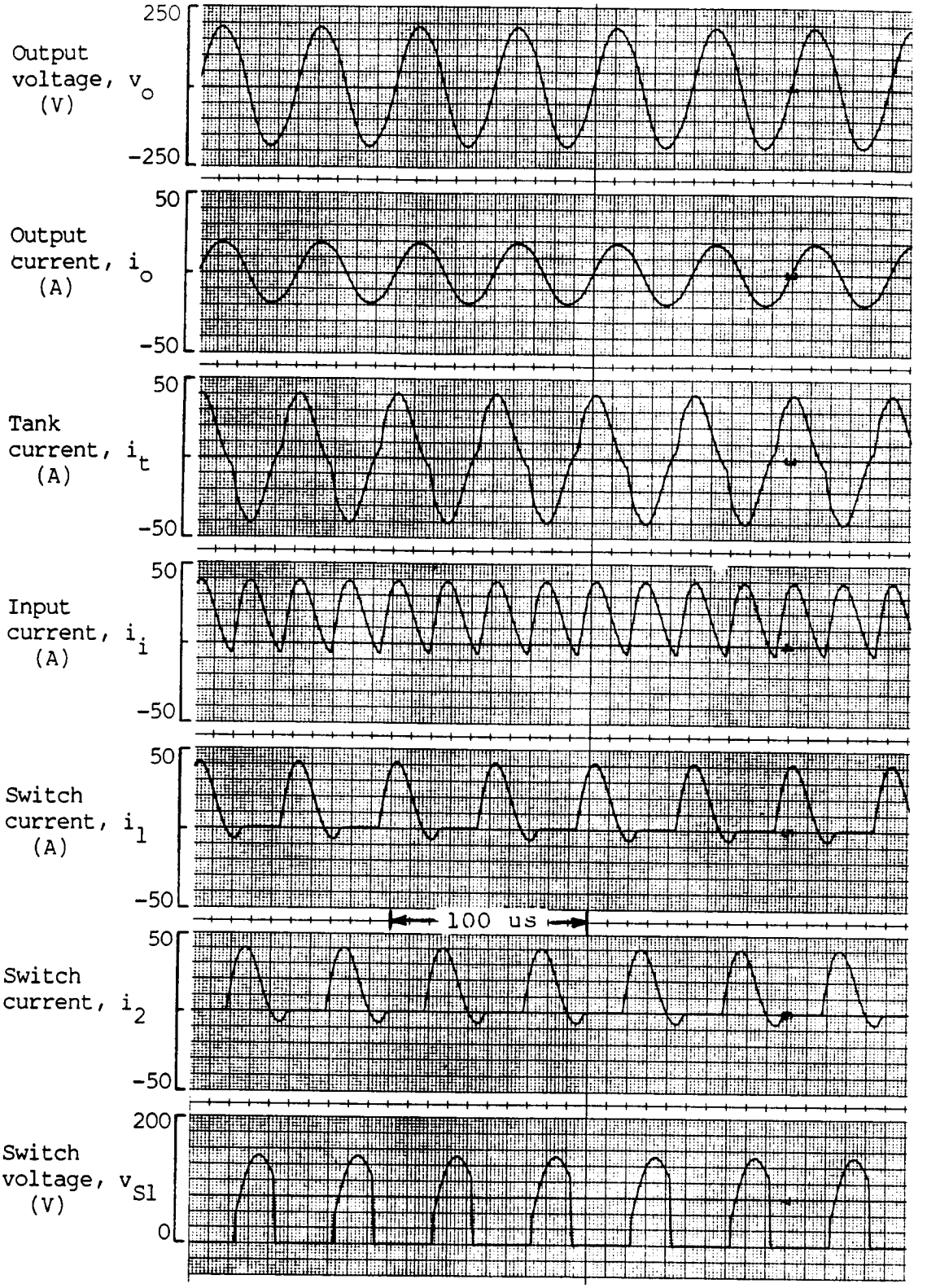

Figure 3.4: Typical set of waveforms predicted by the model. $f_o/f_r = 3/4$.

3.1.3 Effect of Loading.

Figure 3.5 shows simulated circuit waveforms of a POSR converter with a steadily increasing resistive load. The input voltage is kept constant but otherwise no attempt is made to regulate the high frequency voltage. These waveforms demonstrate the inherent voltage regulation capability of a POSR converter (better than 10 percent). Circuit turn-off time,seen from the conduction time of the reverse diode (see waveforms of i_1 and i_2) decrease as the load increases. If the load is increased beyond its design value, commutation failure may result if the devices are naturally commutated. Figure 3.6 shows the effect on converter waveforms as the frequency ratio is steadily increased. It can be noted that the frequency ratio, f_o/f_r , strongly affects the load and regulation capability of the POSR converter.

Although a POSR converter works best with a resistive load, the converter can supply non-unity power factor loads. A non-unity power factor (PF) load presents an equivalent inductance or capacitance in parallel with the resonant capacitor, thus altering its resonant frequency. Hence, a lagging PF load is analogous to operating at a lower value of frequency ratio, f_o/f_r , causing increased distortion and a poor load regulation in the generated HF voltage. The situation with a leading PF is just the opposite. Operation is closer to the resonant frequency, i.e. a higher f_o/f_r ratio. Although the regulation and distortion are improved, circuit turn-off time is reduced. It is easy to recognize that the original choice of frequency ratio determines the ability of the converter to handle nonunity PF loads. In addition to the effects noted, discontinuous capacitor current or even loss of commutation may also result if the load PF is worse than the minimum anticipated value.

3.1.4 Control of High Frequency Voltage.

In a POSR converter either the output frequency or the output voltage, but not both, may be controlled. For a high frequency (HF) link type application, the POSR converter is likely to be operated with a constant frequency. As noted earlier, the circulating current nature of POSR converter operation gives it a built-in voltage regulation capability. If the inherent voltage regulation is inadequate, then alternate means of regulating the capacitor voltage are required. One possibility is to regulate the input voltage by the same degree as the regulation required in the output voltage. When input voltage regulation is not possible or is undesirable, the output voltage can still be regulated by series connection of two phase shifted POSR converters if they are clocked at the identical frequency. The net voltage as well as the current for an assumed resistive load, is leading with respect to the capacitor voltage in one converter and lagging in the other. The converter that sees the leading current operates with an effective frequency ratio which is higher than its no load value and as a results develops higher voltage and carries the larger portion of the load. Similarly, the

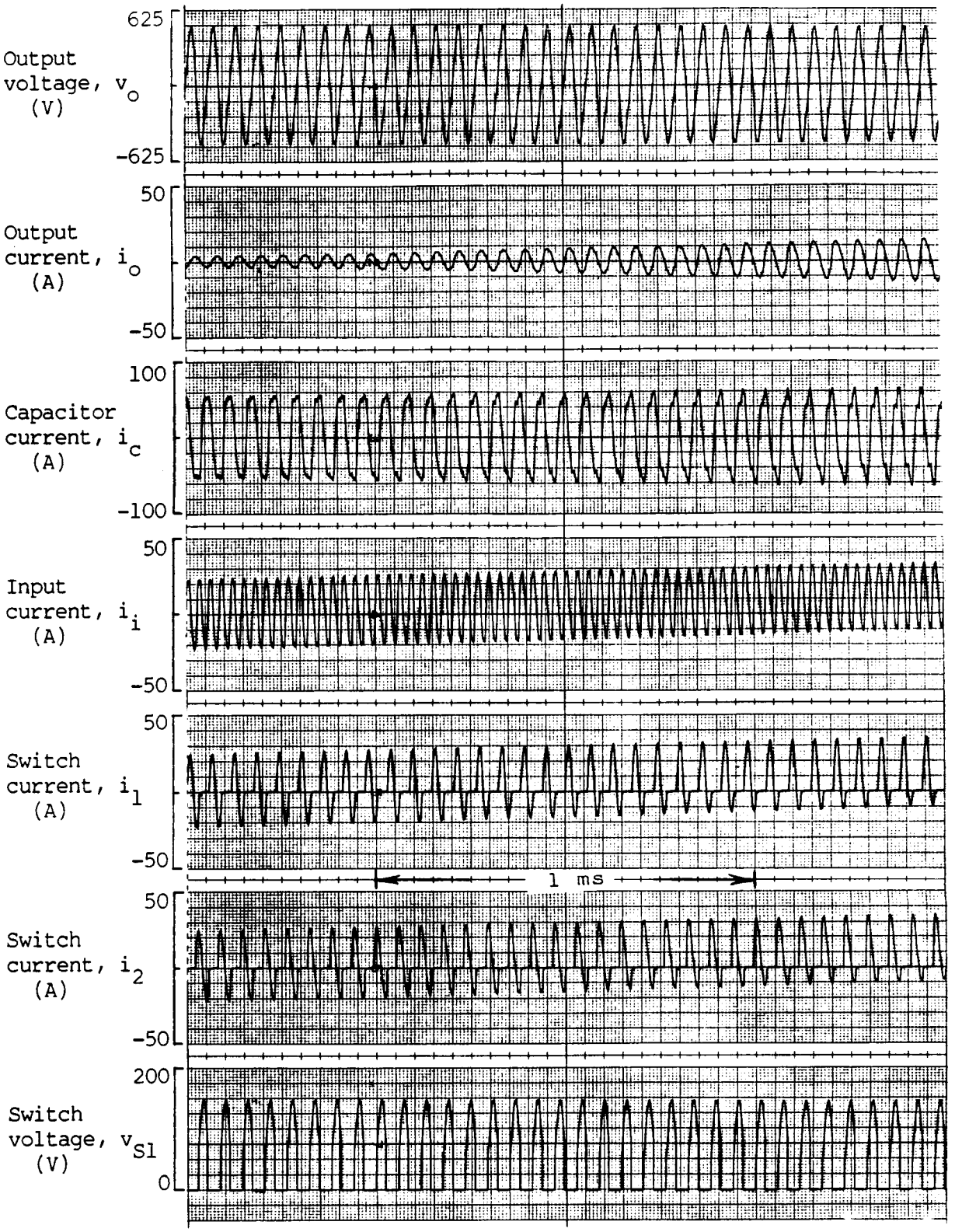

Figure 3.5: Operation with a steadily increasing resistive load.

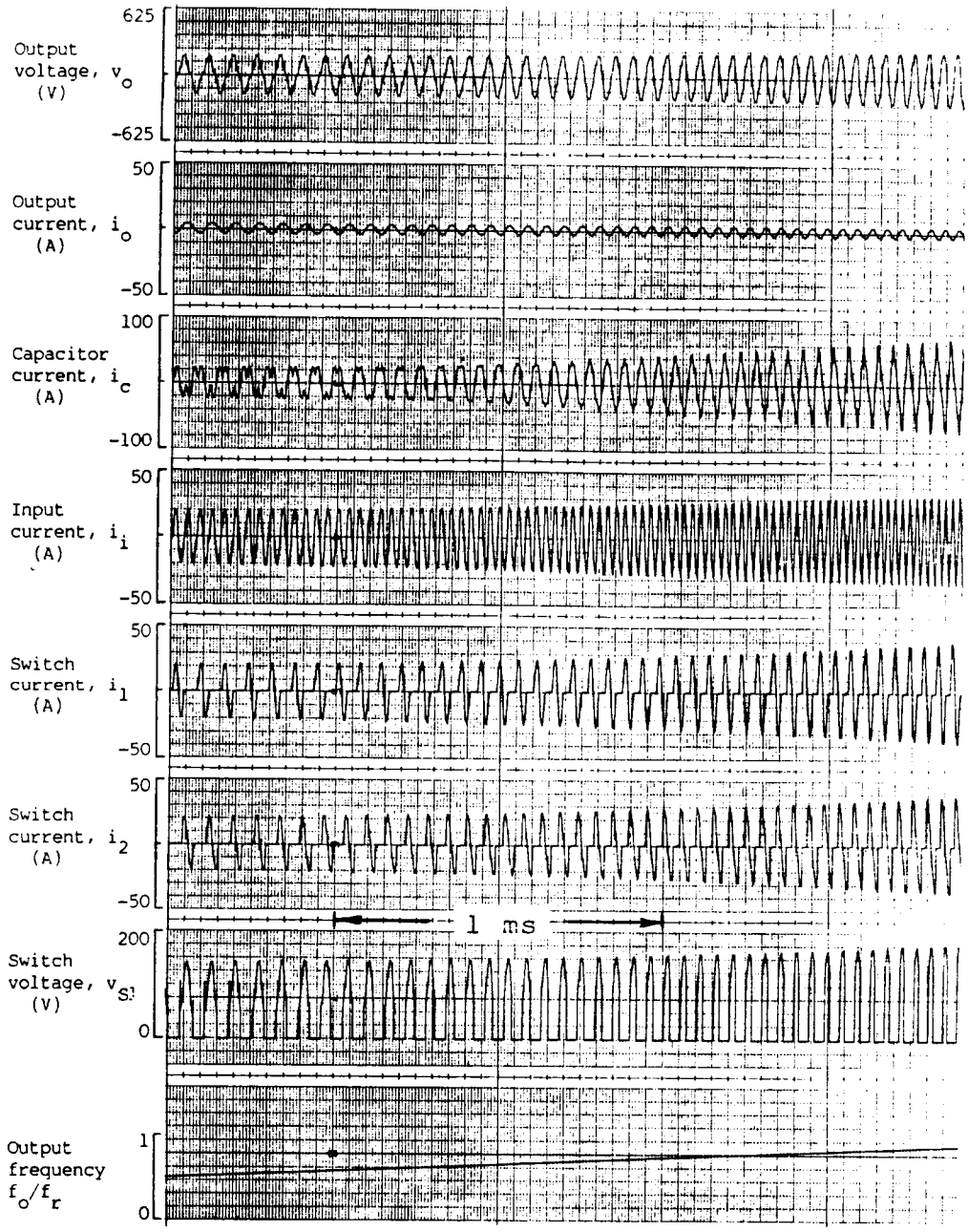

Figure 3.6: Operation with steadily increasing frequency ratio, f_o/f_r .

other converter sees a lagging power factor and develops a voltage that is less than its no load value. Thus, voltage control using series connection of phase shifted converters may require careful attention to load sharing when the phase angles become large.

3.2 Circuit Adaptation for AC Inputs

A single-phase ac signal cannot be expected to generate a constant amplitude HF signal since the output cannot be sustained when the input is going through its zero crossings. Nonetheless, circuit operation with a single-phase input is of interest since it provides information useful for the more practical case of conversion from a three-phase input.

Operation from ac input requires that the devices have full bi- directional capability. Besides the ability to conduct current of either direction, the switches are now required to block voltage of either polarity. A reverse connected inverter grade pair of thyristors has been assumed but clearly other device combinations are possible.

Figure 3.7 shows the circuit of a POSR converter modified for operation with an ac input. Assume first that the ac source impedance represented by R_i and L_i and the decoupling capacitor C_i is not present. During the positive half cycle of the input, operation is the same as for dc input except that the reverse connected thyristors perform the feedback diode duty. Clearly, the changing level of input voltage must modulate the high frequency (HF) output. When the input voltage changes to a negative polarity, it is possible to either retain the firing sequence $1-4,\ 2-3,\ 1-4$ used during the positive half cycle or to reverse it to $2-3,\ 1-4,\ 2-3$. The subtle difference arising from this change of sequence is of consequence only when adding two or more such signals, for example when working from a three-phase input. In either case, the HF output voltage is modulated by the LF (low frequency) input signal. Diode duty in the negative half-cycle is performed by the forward connected thyristors. Figure 3.8 shows the simulated circuit waveforms for an ac input of 100 V peak and a frequency of 1 kHz. No sequence change was done for this set of waveforms.

3.2.1 Adverse Affects of Source Impedance.

The impedance of the AC source appears in series with the resonant components L and C. Generally, the resistive component is small and its effect on the converter operation is secondary. However, the reactive component, which can be of the same order of magnitude as the resonant inductance L, adds with the resonant inductance reducing the effective value of the resonant frequency. If the operating frequency is unchanged, as would be the case

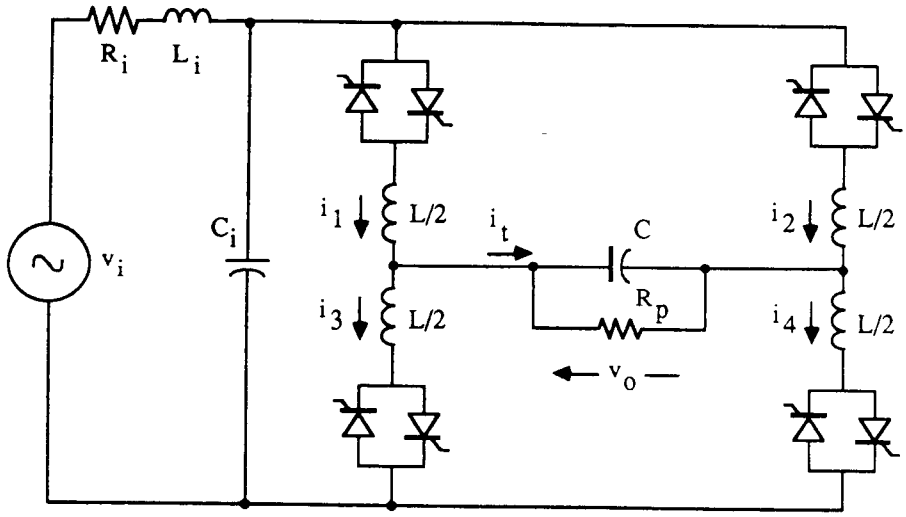

Figure 3.7: POSR converter modified for operation with an ac input. Note the use of bi-directional switches.

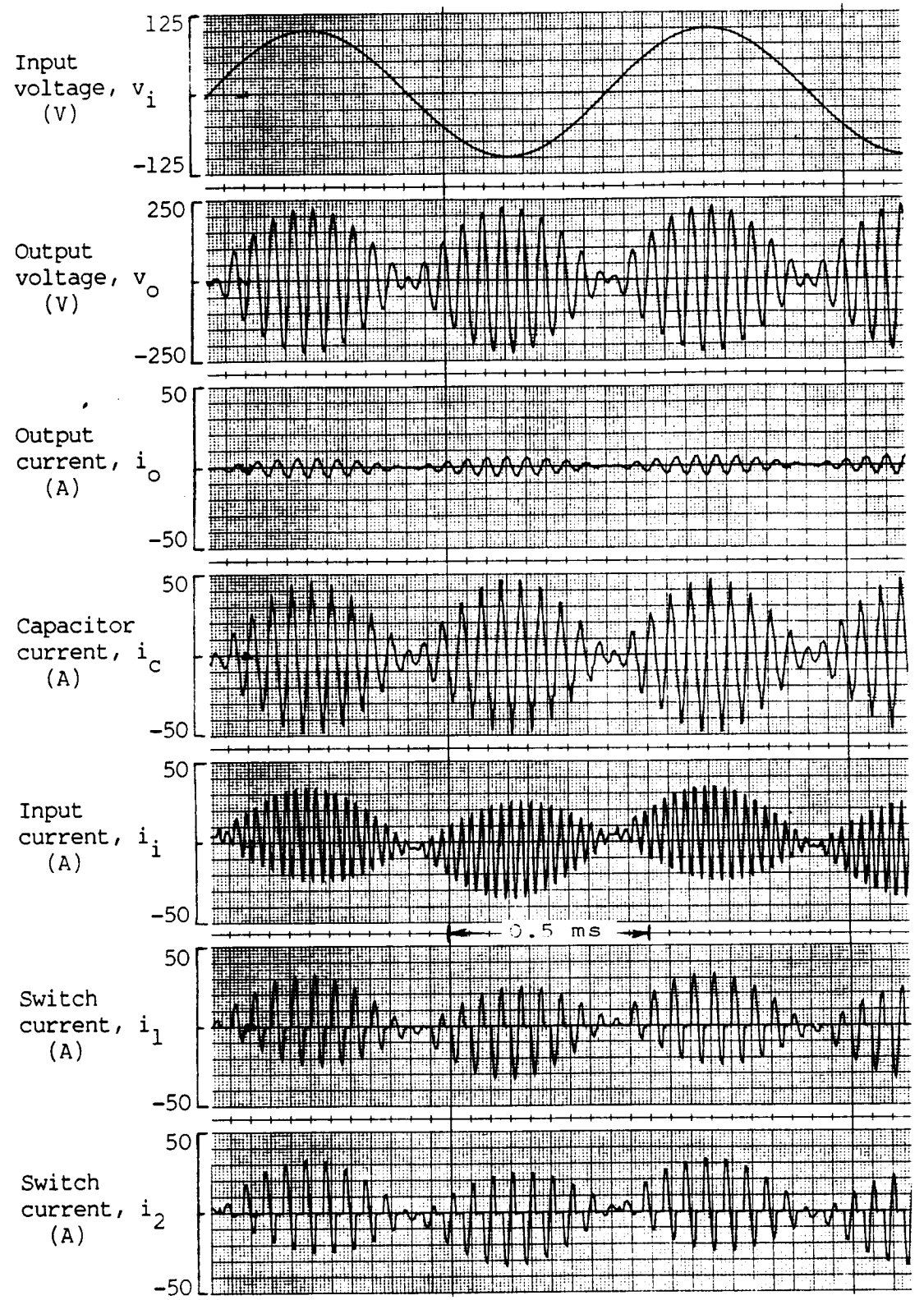

Figure 3.8: Circuit waveforms when operated from an ideal ac source of 100 V peak and a frequency of 1000 Hz.

normally, the frequency ratio, f_o/f_r is effectively increased. This results in reduced circuit turn-off times and the possible loss of the ability to naturally commutate the devices. If the source impedance is known and relatively constant, it might be possible to incorporate it in the design as part of the resonant inductor. This might be feasible in some special cases. However, a more general approach would be to avoid the interaction completely by tuning out the source reactance from the resonant circuit by means of a small shunt capacitor.

3.2.2 Decoupling Effect of an Input Capacitor.

Connecting a suitably sized capacitor in parallel with the input (C_i of Fig. 3.7) isolates the source reactance from the resonant circuit. Simulation studies conducted in during this investigation have shown that it is adequate to select C_i so that the product L_iC_i is at least three times the value of LC of the resonant circuit. Figure 3.9 shows the decoupling effect of different sized input capacitors when the source impedance is R_i/Z = 0.25 and L_i/L = 1.0. Fig. 3.9 (a) shows operation with a low value of L_iC_i/LC of only 1.3. Waveforms improve significantly when the value of L_iC_i/LC of 3.3 is used (Fig. 3.9 (b)). Figure 3.9 (c) shows that subsequent increase to 5 yields relatively smaller gains. Effectiveness of this decoupling under load conditions is demonstrated by the waveforms of Fig. 3.10.

3.3 Circuit Topology and Operation for Three-Phase Input

Figure 3.11 shows a circuit topology in a generalized form that appears to be promising for direct operation from a three-phase ac input. Although one POSR converter for each phase is shown, the following discussion should apply to the case where two converters are used in each phase and operated with phase difference for amplitude control (as discussed earlier in Sec. 3.1). Depending upon the turns ratios and the polarities assigned to each of the three transformers, several combinations of the three outputs can be realized. Operating frequencies and the phase shifts assigned to each converter are the other degrees of freedom in this generalized configuration.

Frequencies of the individual converters are likely to be same, since unequal frequencies create an unbalance for the low-frequency source supplying the converters. Choices for the phase shifts are more numerous. Two of these options have been investigated in detail.

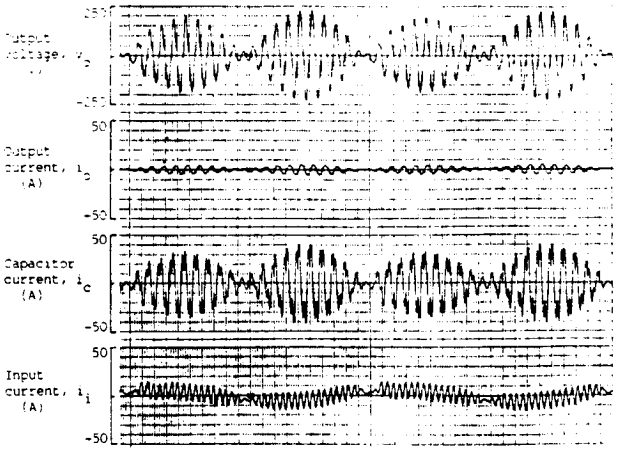

(a)

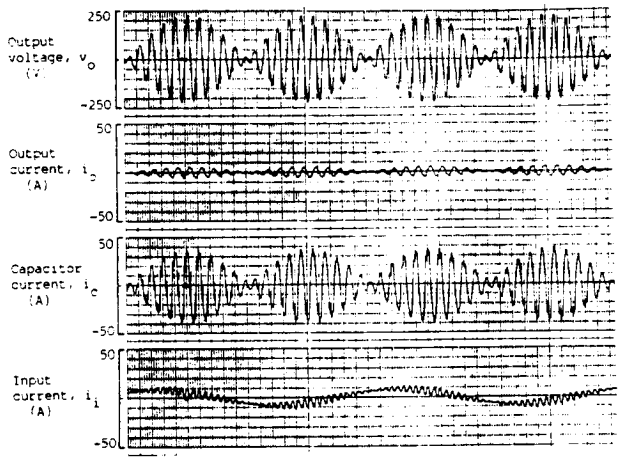

(b)

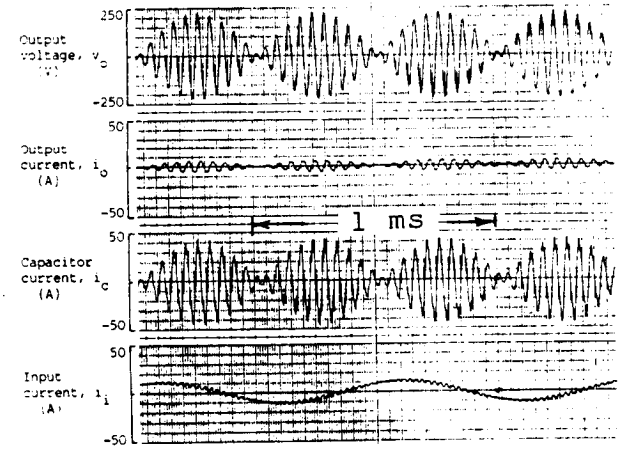

(c)

Figure 3.9: Decoupling of the source reactance by using an input capacitor.

Source impedance is: $R_i/\sqrt{L/C}$ = 0.25 and L_i/L = 1.0. (a) L_iC_i/LC = 1.3. (b) L_iC_i/LC = 3.3. (c) L_iC_i/LC = 5.0.

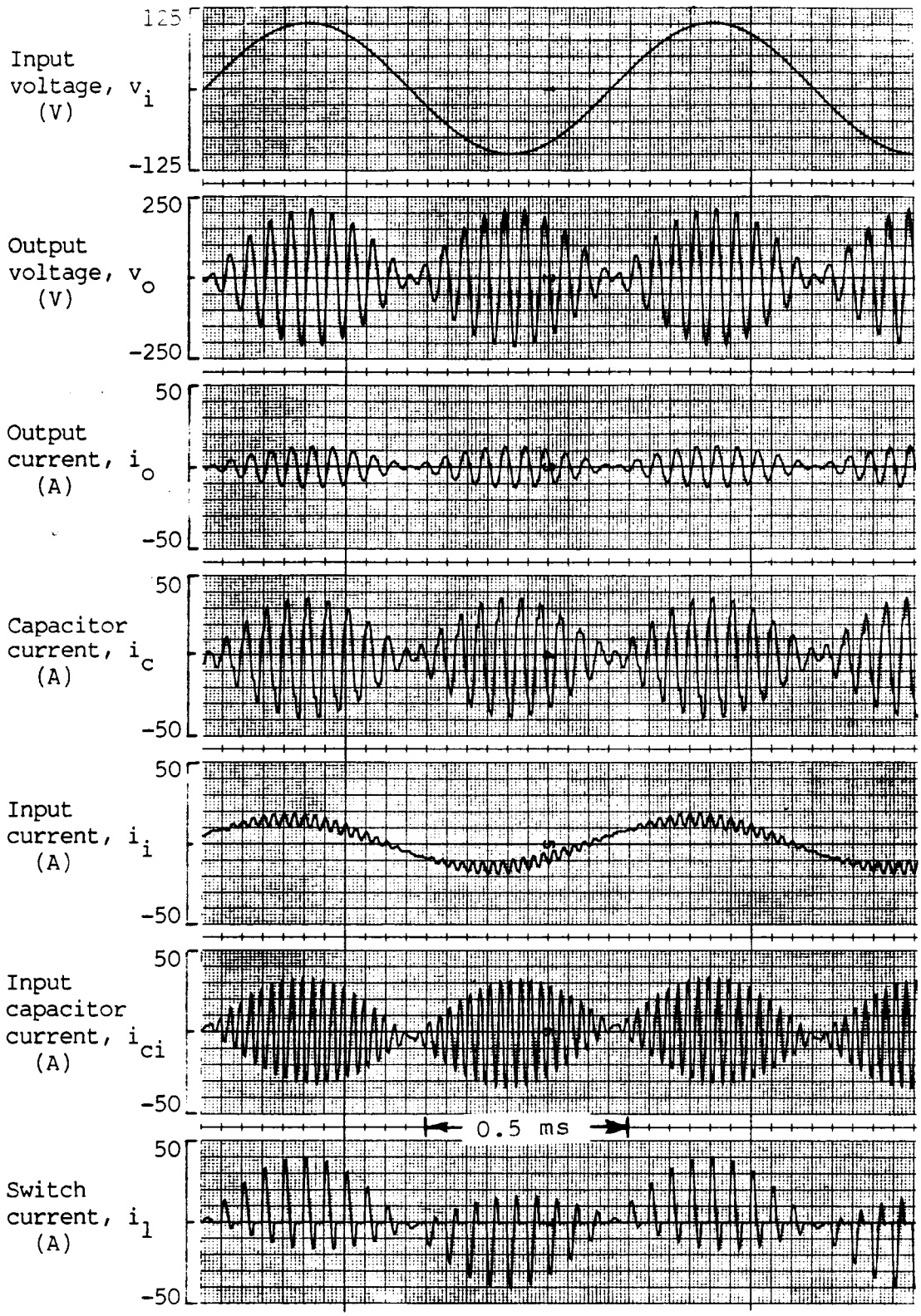

Figure 3.10: Decoupling under load conditions.

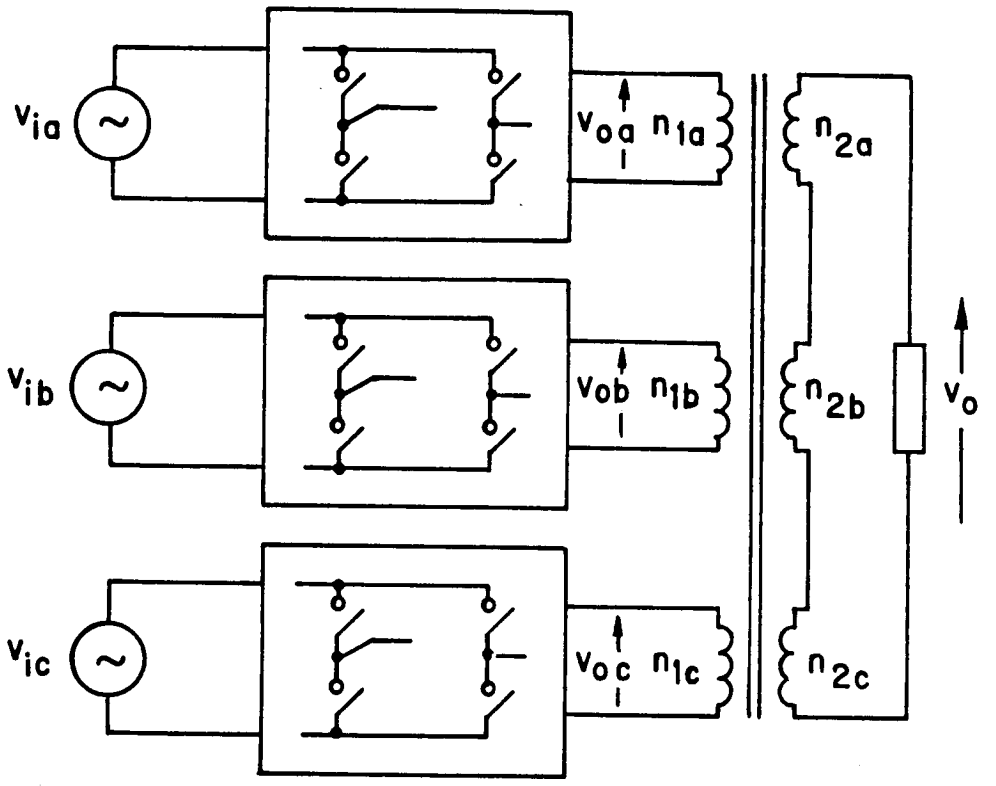

Figure 3.11: Three-converter configuration of POSR converter for operation from a three-phase low-frequency ac.

3.3.1 120° Phase Shifted Gating.

In this case converters are operated so that the gating of the converter in phase b is phase delayed with respect to the converter in phase a by 120° of the high frequency cycle, that of phase c with respect to phase b and so on. Individual outputs, each one a high frequency signal modulated by the low frequency input signal, are then combined in $a+b+c$ fashion. The combined signal is an unmodulated HF signal. However, its frequency is not the same as the gating frequency of converters. It is, instead, a beat frequency, being the difference of the gating and the input signal frequency. The simulated waveforms of Fig. 3.12 show the individual and the combined signals. These results can be confirmed by the following simple analysis.

Let the low frequency input voltage having an angular frequency ω_i be expressed as

$$v_{ia}(t) = V_m \sin(\omega_i t) \tag{3.2}$$

$$v_{ib}(t) = V_m \sin(\omega_i t - \frac{2\pi}{3}) \tag{3.3}$$

$$v_{ic}(t) = V_m \sin(\omega_i t + \frac{2\pi}{3}) \tag{3.4}$$

Then each of the modulated outputs are given by

$$v_{oa}(t) = V_m \sin(\omega_i t) \sin(\omega_o t) \tag{3.5}$$

$$v_{ob}(t) = V_m \sin(\omega_i t - \frac{2\pi}{3}) \sin(\omega_o t - \frac{2\pi}{3}) \tag{3.6}$$

$$v_{oc}(t) = V_m \sin(\omega_i t + \frac{2\pi}{3}) \sin(\omega_o t + \frac{2\pi}{3}) \tag{3.7}$$

The combined signal is,

$$v_o(t) = v_{oa}(t) + v_{ob}(t) + v_{oc}(t) \tag{3.8}$$

which, after substitution and simplification, is given by the expression

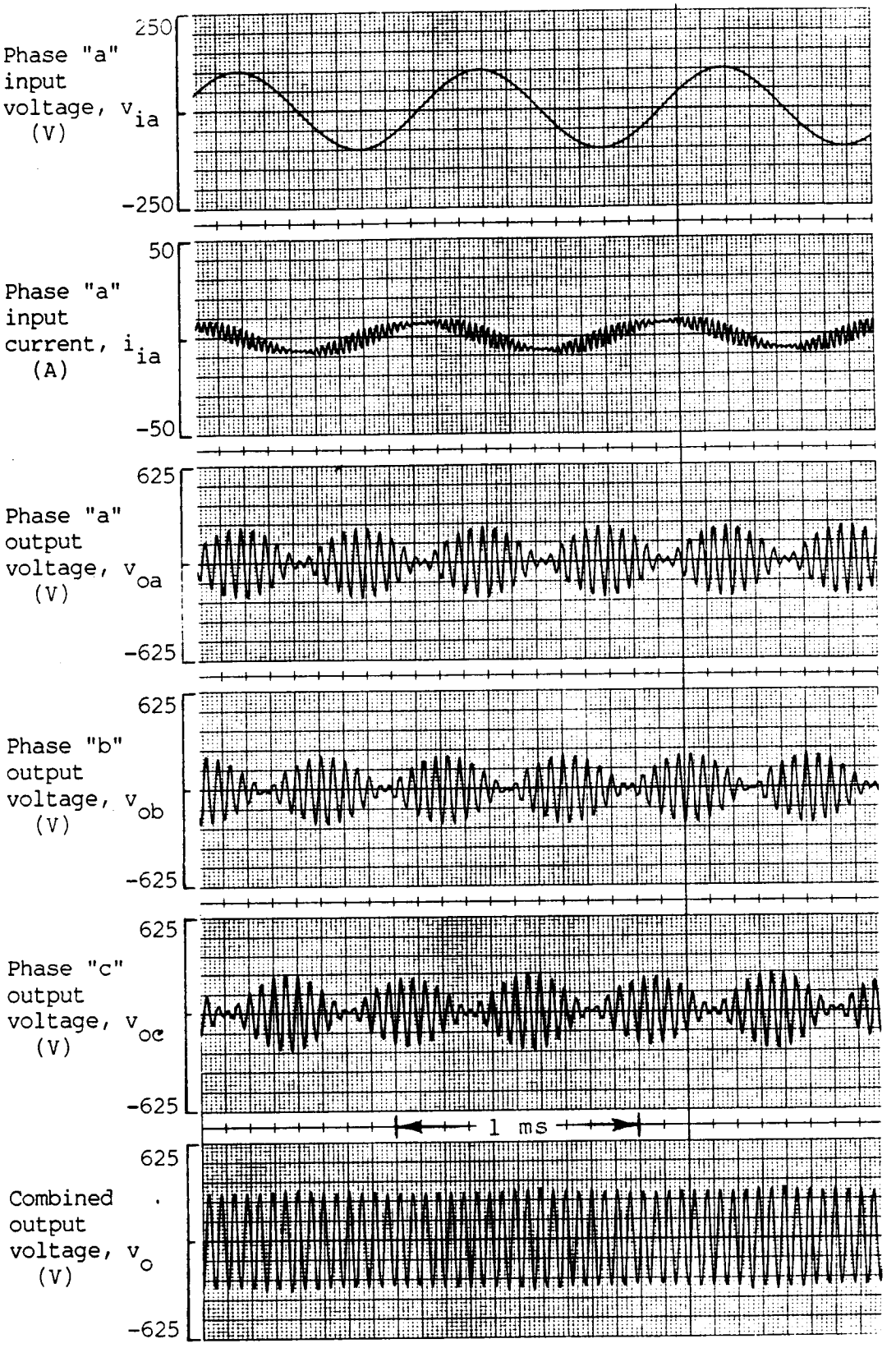

Figure 3.12: 120° phase shifted firing of three POSR converters. Individual outputs combined as $a + b + c$.

$$v_o(t) = \frac{3}{2} V_m \cos(\omega_o - \omega_i)t \tag{3.9}$$

This result confirms that the combined voltage is an unmodulated HF voltage which has an amplitude of (3/2) times the amplitude of the low-frequency input. Its frequency is the difference between the switching frequency and the low-frequency source frequency.

Other combinations of the individual outputs can be tried by combining (3.5) to (3.7) with different gains and polarities. For example, $a - b/2 - c/2$ combination commonly used in machine theory, gives

$$v_o(t) = -\frac{3}{4} V_m \cos(\omega_o + \omega_i)\, t \tag{3.10}$$

which is also an unmodulated HF signal of beat frequency but has the magnitude of one-half the value realized in (3.9). An $a + b - c$ combination generates

$$v_o(t) = \sqrt{\frac{3}{2}} V_m \sin(\omega_o + \omega_i)\, t - (V_m \sin \omega_o t) \cdot \sin \omega_i t \tag{3.11}$$

which is the combination of an unmodulated and a modulated term. The corresponding simulated waveforms are shown in Fig. 3.13.

The beat frequency seen in the combined signal of (3.11) poses a two fold problem. Dependence on the uncontrolled input frequency makes it difficult to keep the link frequency under strict control which is likely to be a system requirement. Worse still, even a resistive loading of the combined signal is reflected back to individual converters as a load of varying power factor because the frequency of the reflected current, being the same as the frequency of the combined signal, is different from the frequency of the individual output voltages.

3.3.2 Synchronized Gating.

When individual converters are operated in synchronism but with no other alteration in their operation, the combined voltage can be shown to be either zero or a modulated signal for all linear combinations of individual outputs. To appreciate this, (3.5) to (3.7) can be modifiedto produce zero phase shift in the HF term and an expression for the combined output can be derived in the manner of (3.9).

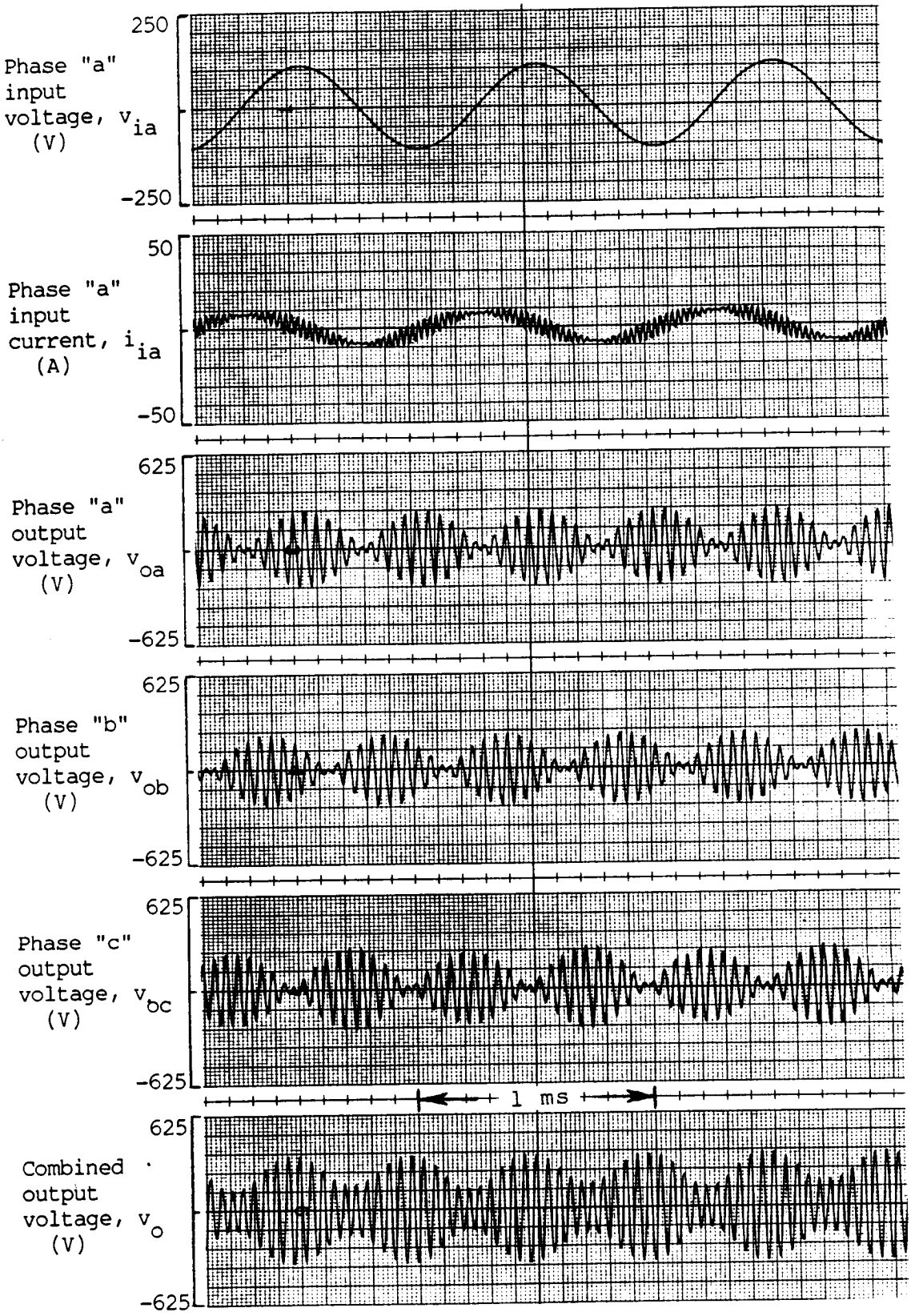

Figure 3.13: 120° phase shifted firing of three POSR converters. Individual outputs combined as $a + b - c$.

3.4 Feasibility of POSR Converter as an Interface Converter

As observed previously, a key performance characteristic is the performance of a converter as an interface between the single phase HF link and a three phase ac generator. In the study of the feasibility of such a configuration, it was decided that it was adequate to represent the machine output as a three-phase voltage source. However, if an induction generator is to supply power to the POSR converters then a mechanism of building up and regulating the generator output must be found. One method might be the use of a special power converter separate from the resonant converters just for this purpose. Such a dedicated exciter would allow separation of the voltage generation and power conversion functions but would add substantially to the overall power rating of the system. An alternative approach might be to combine the two functions and use the resonant converters for the dual role of generator voltage control and power conversion into the high frequency link. It can be recalled from the discussion of Sec. 2.1, however, that the excitation control of an induction machine requires that the machine be supplied with a lagging current of controllable magnitude and phase. Thus, a dual role for the resonant circuit topology operating from an induction generator would require the capability of controlling the magnitude and phase of the input current of the converter while they simulaneously perform the power conversion function with varying load conditions.

The work reported in the preceeding section has demonstrated that the three-phase low-frequency to single-phase high frequency conversion function, although appearing possible, has unresolved problems associated either with maintaining a constant link frequency or an unmodulated voltage amplitude. As for the control of the phase angle of the input current of the POSR converter, no mechanism is known at present. In addition, input capacitors proposed for decoupling of the machine reactance from the resonant circuit of the converter represent an additional component which cannot be eliminated. This feature is likely to also further complicate any control mechanism that may be found which may enable regulation of the phase angle of the input link current.

These unresolved problems concerning the resonant circuit topology for the interface converter (for now, at least) have lead to the search for alternative topologies which are capable of the high potential efficiencies of the resonant converter approach but which pose fewer difficulties in their realization. One such topologly is discussed in the next chapter.

3.5 References

1. N. Mapham, *An SCR inverter with good regulation and sine-wave output*, IEEE Trans. on Ind. and Gen. Appl., vol. IGAa-3, pp. 176-187, March/ April 1967.

2. R. L. Steigerwald, *High-frequency resonant transistor dc-dc converters* IEEE Trans. Ind. Elect., vol. IE-31, pp. 181-191, May 1984.

3. J. Mildice and L. Wappes, *Resonant ac power system proof-of-concept*, NASA CR-17069, 1986.

4. B. R. Pelly, *Latest developments in static high frequency power sources for induction heating*, IEEE Trans. Ind. Electronics & Contr. Instrum., vol. IECI-17, pp. 297-312, June 1970.

Chapter 4

Pulse Density Modulated Interface Converter

During the course of this investigation, a zero voltage switching ac- to-ac converter configuration was identified which appears well suited to the role of interfacing three-phase induction machines to the high frequency link. The converter has the advantage of a one-stage power conversion but unlike the resonant circuit topology discussed in the previous section, it is easier to implement and more versatile. This section describes the concept and advantages of zero voltage switching, a control technique that is especially designed for synthesizing signals with zero voltage switching and a power converter that uses this control technique to interface induction machines to a high frequency link.

4.1 Modulation Considerations

4.1.1 Limitations of Phase Angle Control Cycloconverters.

One-stage power conversion from a three phase ac source has been conventionally implemented using phase-angle controlled cycloconverters. Phase angle control permits continuous control over the frequency and amplitude of the synthesized signal and hence could be employed with a single phase ac link [1]. However, the technique becomes increasingly unsuitable as the frequency of the link increases. This result occurs because the phase angle control normally employed with these converters causes the current reflected back to the link to have a variable (and lagging if naturally commutated) phase angle and also causes the synthesized voltages to have high values of dv/dt. Even more serious is the fact that

the loss per switching cycle in phase angle control is inherently high due to both the voltage and current being nonzero during the switching interval. At high frequencies this feature would lead to excessive switching losses in the converter.

4.1.2 Advantages of Zero Voltage Switching

It appears that the limitations outlined above for the conventional cycloconverters can be eliminated by restricting the device switching to the zero crossings of the high frequency voltage. In this case, the switching losses are dramatically reduced since the voltage across the switch is at or near zero value and therefore, the product of the switch voltage and current during the switching interval is inherently low. Low voltages during switching interval reduce voltage stresses on the device and allow the use of purely capacitive, lossless snubbers. In addition, zero voltage switching causes the current reflected to the link to be always in phase (or 180 degrees out of phase) with the link voltage which makes it much easier to control the frequency and distortion of the link voltage. Also, the voltages synthesized with zero voltage switching become free of abrupt transients.

4.1.3 Technique of Pulse Density Modulation (PDM)

With the switchings restricted to the zero crossing point of the link voltage, a half cycle of the link voltage become the basic unit of synthesis of lower frequency signals. Figure 4.1 illustrates how a lower frequency voltage having a nearsinusoidalfundamental component may be "patched" from the half cycles of the high frequency voltage at the link.

Waveforms such as the synthesized voltage of Fig. 4.1 may either be directly programmed (analogous to programmed PWM for dc link systems) or, they may be generated by using a regulation scheme (analogous to the Sine-Triangle PWM). Figure 4.2(a) shows the block schematic of new proposed technique based on the concept of area comparison. In this scheme. the area under the reference signal is compared with the area of the synthesized signal. If the comparison indicates that the area of the synthesized signal is more (less) than desired, the controller causes the next half cycle pulse to be applied so that this area is decreased (increased). In this manner, voltages or currents having fundamental component of dc, sinusoidal ac or any other smooth waveformmay be synthesized using one integrator, comparator and a few logic gates. This simple implementation results in the density of the half cycle pulses in the synthesized voltage to be modulated in accordance with the amplitude of the reference signal. The term *Area Comparison - Pulse Density Modulation* (AC-PDM) is suggested to differentiate it from the possible programmed method of generating PDM waveforms.

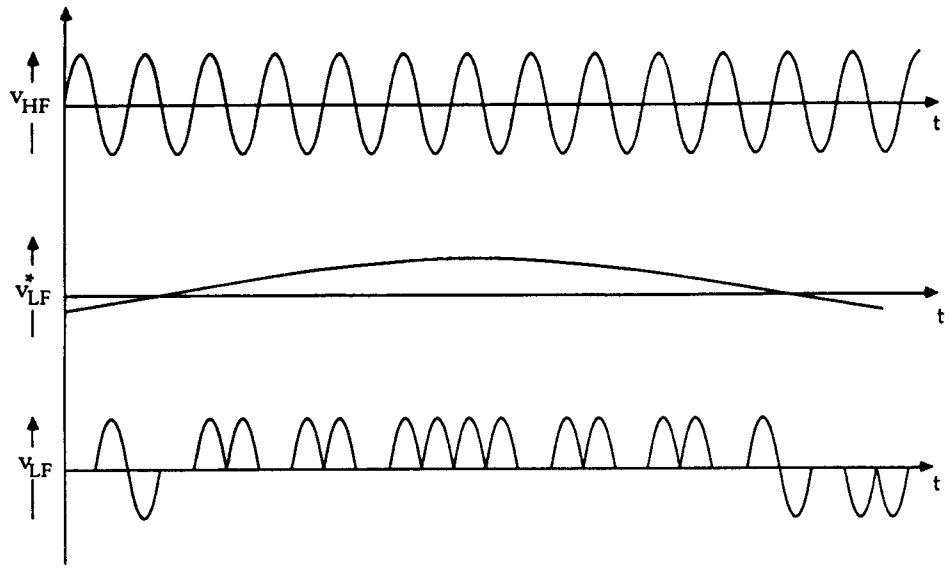

Figure 4.1: Pulse-density-modulated synthesis of a low frequency voltage.

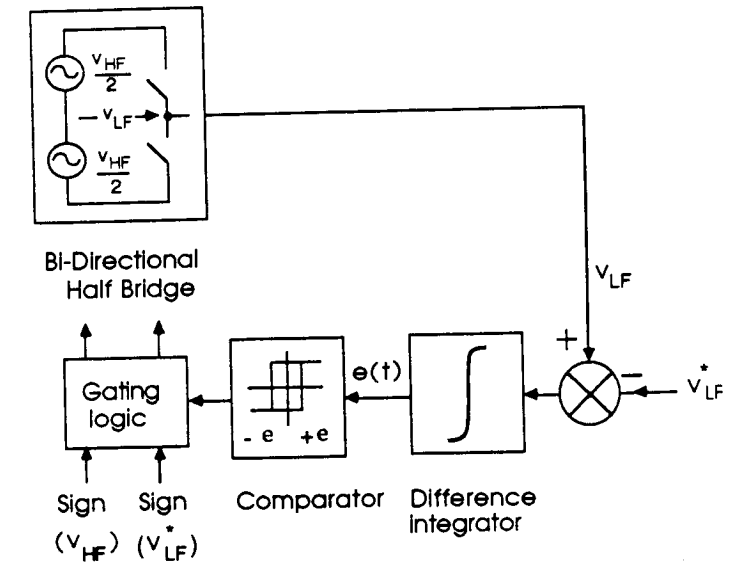

(a)

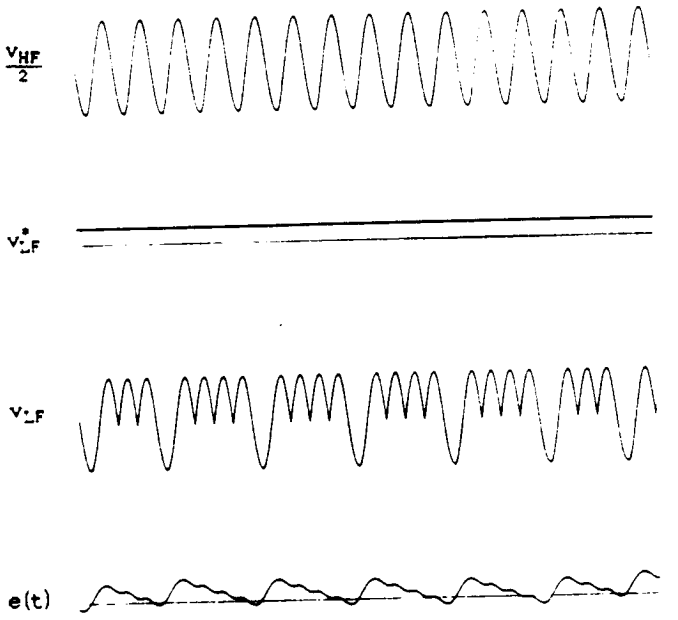

(b)

Figure 4.2: Area comparison - pulse density modulation (AC-PDM) scheme. (a) Block diagram schematic. (b) Associated waveforms when the reference signal is a dc voltage.

4.1.4 Fundamental Relationships in Pulse Density Modulation.

. Figure 4.2(b) shows the waveforms associated with the controller of Fig. 4.2(a) when the reference signal is a dc voltage. Although Fig. 4.2(a) shows voltage feedback directly from the synthesized signal, it is more practical to sense the fixed frequency ac link voltage and then realize from it a scaled value of v_{LF} by applying the same logic that drives the power circuit. When synthesizing currents, of course, a direct feedback of current can be used.

The fundamental relationship of pulse density modulation for voltage synthesis can be written as

$$\frac{e(t)}{K} = \int [\, v^*_{LF}(t) - v_{LF}(t) \,]\, dt \tag{4.1}$$

where K is the total gain associated with the difference integrator and $v^*_{LF}(t)$ and $v_{LF}(t)$ are the desired and the actual values respectively of the low frequency signal. The term on the right is the volt-time area difference between the synthesized and the reference signal. The feedback action of the controller has the effect of reducing this difference to the minimum attainable in a given system. Clearly, if the commanded value of the voltage remains beyond a maximum value then the controller will saturate. This maximum reference signal level is given by

$$V_{LFmax} = \frac{V_{HF}}{\pi} \tag{4.2}$$

where V_{LFmax} is the maximum level of the dc signal or the peak value of an ac signal that can be synthesized from a high frequency link voltage of peak value V_{HF}. If the reference signal is increased beyond this value, the controller enters into a saturated operating mode where the behavior depends on the nature of the reference signal. For a dc reference signal, onset of saturation is well defined and results in the synthesized signal having the waveform of the rectified high frequency signal. In the case of a sinusoidal voltage reference, the saturation begins at the peak region and gradually extends to full saturation as the reference signal is steadily increased in magnitude. When fully saturated, the synthesized voltage becomes a square wave composed of rectified half-cycles of the link voltage. Thus, if the increased harmonic distortion is not a problem, the fundamental component of the sinewave synthesized voltage voltage may be increased beyond the value given in Eq. 4.2 by a factor of $4/\pi$. It should be noted that the transition into saturation is automatic and gradual unlike pulse width modulated inverters (PWM) in which sudden jumps in output voltage fundamental occur when the inverter approaches maximum output.

In establishing the voltage relationships above, it has been assumed that the volt-time area error is negligible. It can be shown [2] that the upper bound for this error is given by

$$e_{A\,max} \leq \frac{(1 + m)\,V_{HF}}{2\pi f_{HF}} \tag{4.3}$$

where $m = V_{LF}/V_{LFmax}$ is defined as the modulation index and V_{HF} is the peak of the link voltage. This inequality shows that for a given value of the link voltage,determined by requirements of the signal amplitudes to be synthesized, the maximum error decreases with an increase in the link frequency. This result states that the higher the link frequency the better is the fidelity of the synthesis (i.e. reduced lower frequency harmonics and inreased frequency at which the distortion occurs). Note that Eq.4.3 establishes a bound on the error, the actual error is much smaller than this maximum value for the majority of half cycles. When synthesizing low frequency voltages, $e_{A\,max}$ may be compared to the area under one half-cycle of the reference signal, A^{*}_{LF}. For sinusoidal reference signals this ratio is given as

$$\left| \frac{e_{A\,max}}{A^{*}_{LF}} \right| \leq \frac{\pi}{2} \frac{(1 + m)}{m} \frac{f_{LF}}{f_{HF}} \tag{4.4}$$

. Equation (4.4) shows that the lower order harmonic distortion in the synthesized voltage decreases as the modulation index and the frequency ratio are increased. In an ac link system, the modulation indices can be expected to be high when fixed amplitude voltages are synthesized because the link voltage can be adjusted to suit the individual converter needs. Variable voltage synthesis frequently used in motor control fortunately requires constant Volts/Hertz characteristics. In such converters, the low values of the modulation indices are compensated by correspondingly higher frequency differentials so that low-distortion synthesis can be realized over a wide range of amplitude change.

It should be noted that Pulse Density Modulation is inherently a discrete process. Thus, subharmonics and certain quantization noise are always present as part of the total distortion in the synthesized signal. However, amplitude of the subharmonic falls off rapidly (as in unsynchronized PWM [3]) as the frequency differential is increased. In the system under consideration frequency differentials are likely to be large for most types of synthesized signals. For these loads the subharmonics are not expected to be a serious concern.

4.2 PDM Synthesis of Three-Phase AC

4.2.1 Converter Power Circuit.

Figure 4.3 shows two basic circuit topologies for a three-phase PDM converter operating from a single- phase high frequency link. The major difference between the two circuits is that while the three-converter circuit (Fig. 4.3(a)) requires a transformer, the bridge circuit (Fig. 4.3(b)) can be operated without one. Three-converter circuit can be configured using half- or full brigde configuration. Besides the difference in the number of devices and the transformer rating, there is another more subtle difference between the use of half- and full bridge individual converters. This difference arises from the fundamental inability of a half-bridge configuration to apply a zero voltage at its output. A bridge circuit has the needed path for circulating the load current that is needed to ensure zero output voltage.

In order to establish feasibility and to determine some of the basic characteristics of a PDM type interface converter, the ac bridge configuration of Fig. 4.3(b) was selected for the initial investigation. Besides the advantage mentioned earlier of not always requiring a transformer, the configuration is easier to understand and apply due to its circuit equivalence to the popular dc link bridge converter. Fig. 4.4 illustrates this analogy by comparing the two bridge circuits. The DC link bridge converter (Fig. 4.4(a)) is a minimal power structure that transforms a single-phase voltage of a fixed frequency (in this case zero, i.e. dc) to three-phase voltages or current of controllable frequency and amplitude. A shunt filter (a large electrolytic capacitor) provides a low impedance path to t e harmonics in the current reflected back to the link by the switching action of the power circuit and thus, reduces the distortion (resulting ripple) of the link voltage. Once charged, the filter offers a very high impedance to the current of the link frequency (i.e. dc). The converter of Fig. 4.4(b) is, like the dc bridge, a minimal topology using six hybrid switches (but not necessarily the same number of devices due to the need for blocking voltages in both direction), which operates from a link of fixed frequency and regulated voltage and has a link side filter for circulating harmonic currents. One possible link filter configuration is a shunt connected LC tank circuit resonant at the frequency of the link. Once "charged", the tank circuit too offers a high impedance to the current of the link frequency and a lower impedance to currents of all other frequencies. The size of this tank circuit determines the amount of fluctuations ("ripple") in the link voltage much as it does for the dc link system.

4.2.2 Converter Power Switches.

Direct operation from an ac link requires that the power switches have bi-directional voltage blocking capability. Figure 4.5 shows some of the possible device arrangements that

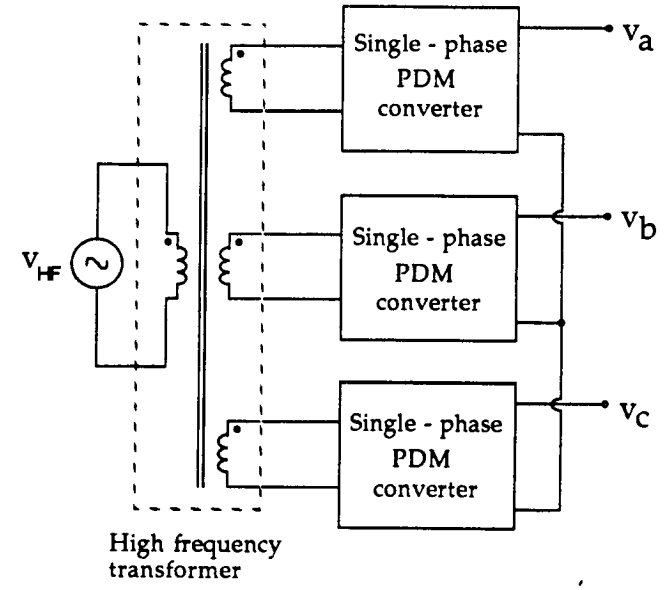

(a)

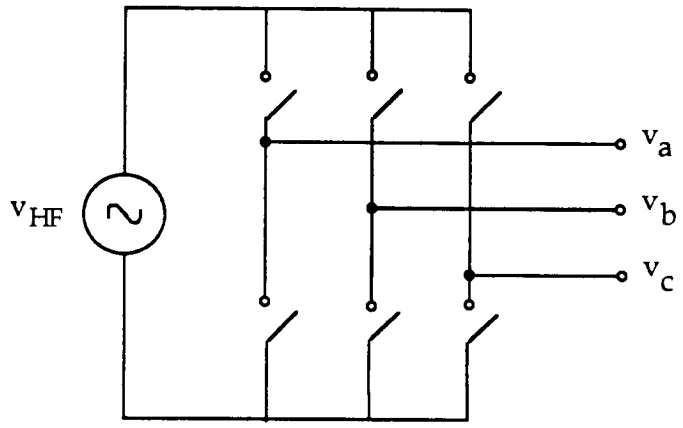

(b)

Figure 4.3: Power circuit for three-phase PDM converter. (a) Three-converter realization using a transformer. (b) Three-phase bridge.

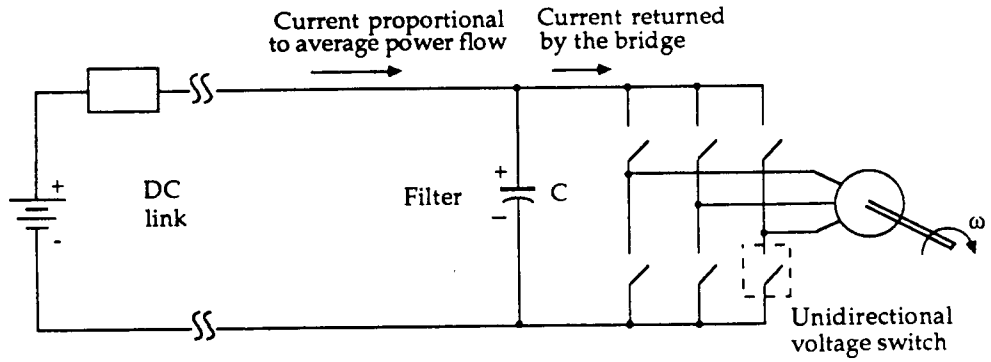

(a)

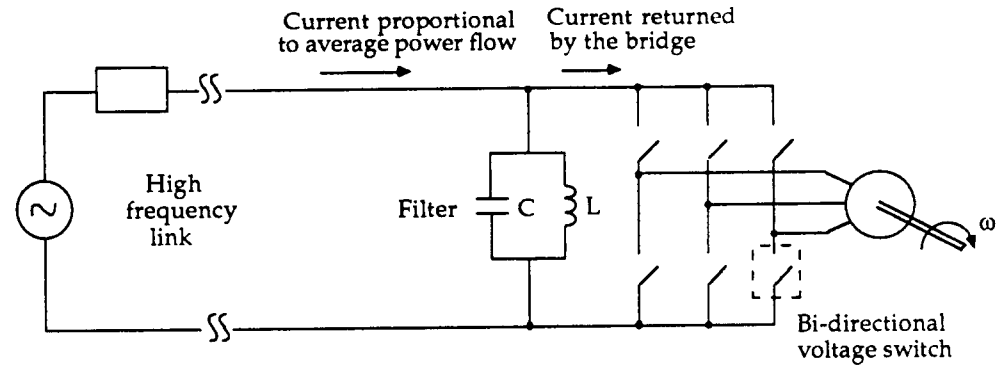

(b)

Figure 4.4: PDM bridge converter equivalence to the popular dc link bridge. (a) DC link bridge. (b) AC link bridge.

may be used to realize such a hybrid switch. The first group, represented by Fig. 4.5(a), uses devices with a built-in voltage blocking capability. Promising among this group of devices are the static induction thyristors [4] and fast (5 μs or less) GTO's [5]. In the second group, represented by Fig. 4.5(b) and 4.5(c), are the devices with no reverse blocking capability. Prominent in this group of devices are power darlingtons, power FET's, static induction transistors. MOS- IGT's or similar conductivity modulated switches being currently marketed belong to this group although devices with reverse blocking capability have been reported [6].

At first, it may appear that an ac bridge operating from a high frequency link would require a large number of very special devices making the power circuit complex and unreliable. This however need not be the case. In fact, the device capabilities needed for a PDM bridge operating from a link frequency in the neighborhood of 20 kHz are not markedly different from those needed in the present day PWM inverters operating at switching frequencies nearly one order of magnitude lower. This is because the switching frequencies of the PWM converters are limited essentially by the high losses and the voltage stresses generated as a result of "hard" switching from a dc link. The zero voltage switching used in PDM converters drastically reduces these stresses and allows the same devices to be used at higher frequency. Even the voltage rating of the devices, which in theory favors PWM by a factor of 1.5, should in actual practice be much closer because the safety factor for PDM devices can be made smaller as a result of the zero voltage switching and snubber action that does not involve overshoots. The number of devices required is not necessarily a problem because the same considerations (minimization of stray leakage, ease of manufacturing, reliability etc.) that have lead to the evolution of the present day hybrid switches for the PWM inverters (transistor- reverse diode or GTO- reverse diode, etc.) can be expected to eventually produce similar hybrid realizations suitable for operation from an ac link.

Although forced commutated devices have been discussed so far, it is entirely possible to use naturally commutated devices such as inverter grade thyristors to realize power switches for PDM converters. Automatic reversal of the ac link voltage offers the possibility of natural commutation of the devices. The difficulty arises with the need to establish circulating current of appropriate polarity to achieve turn-off of the conducting device because it makes the operation of the converter dependent on the power factor at the low-frequency end. The major difference in operation with naturally commutated devices occurs during intervals when the power flow is in the direction of the high-frequency link. For the duration of this interval, the circulating current of the correct polarity is established only if the incoming switch is fired in advance of the voltage reversal. The angle of advance is determined by the commutation overlap (likely to be small due to the presence of the resonant tank capacitor) and the turn-off time of the naturally commutated device. This advance firing increases distortion in the synthesized voltage, makes it more difficult to control distortion and frequency of the link voltage, and increases the switching losses in the converter. However, the performance in all these aspects is still likely to be far superior to that of a conventional

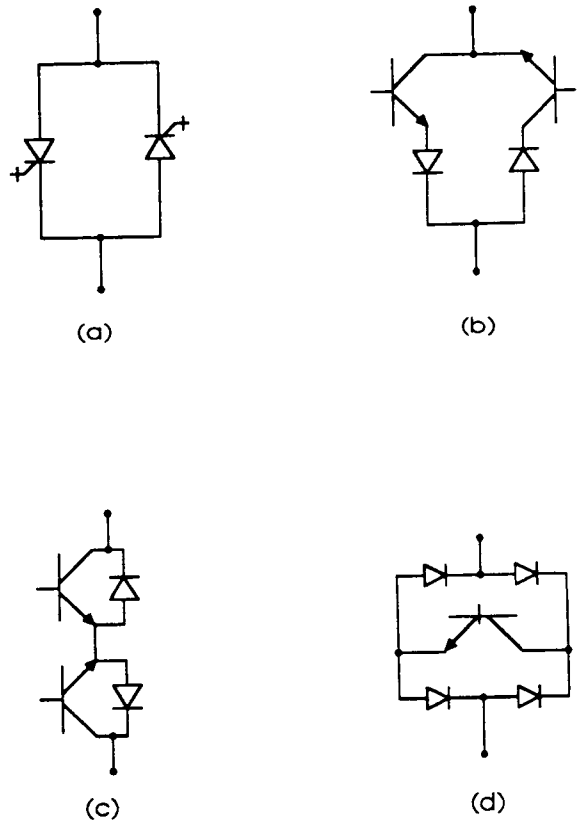

Figure 4.5: Realizations of the bi-directional switches (a) Using two reverse blocking devices such as GTOs and static induction thyristors etc. (b) and (c) Using two unidirectional voltage devices such as power darlingtons, IGTs, Power MOSFETs etc. (d) Using a single unidirectional voltage device.

phase angle controlled cycloconverter. When near unity power factor loads need to be supplied from the high-frequency link, use of naturally commutated PDM converter should be considered.

4.2.3 PDM Synthesis of a Balanced Set of Three-Phase Voltages.

Using the ac bridge power circuit shown in Fig. 4.3(b) and three independent AC-PDM controllers (one for each pole) a balanced set of pole voltages can be realized. For example, Fig. 4.6 shows a balanced set of sinusoidal voltages synthesized in this manner. A computer model of the converter andthe AC-PDM controller has been used to simulate these waveforms. Appendix C describes the development and verification of the computer model. Three phase-displaced reference signals having a frequency of 400 Hz and a peak amplitude corresponding to 163 V (i.e. 115 V rms per phase) were used. The simulated link frequency was selected as 20 kHz and the peak value of the link voltage was 500 V. Figure 4.7 shows the PDM bridge output waveforms when supplying a wye connected R-L load. The frequency of the synthesized signal in this case is 200 Hz. The modulation index is 76 percent. Near sinusoidal line current waveform indicates absence of any lower order harmonics in the synthesized voltage (this will be later confirmed in Chapter 5 when results from the laboratory breadboard are discussed). It can be observed that the link voltage, which had a nominal value of 450 V peak, now has a "ripple" due to circulation of the reflected current harmonics through the tank filter.

The maximum line voltage that can be synthesized from a given link voltage using the ac bridge circuit can be calculated using (4.2) and is given by

$$V_{l-l\,max} = \frac{\sqrt{3}\,V_{HF\,rms}}{\pi} \tag{4.5}$$

where $V_{l-l\,max}$ is the rms value of the fundamental line voltage and $V_{HF\,rms}$ is the rms value of the link voltage. Thus, the ratio of the two rms quantities is

$$\frac{V_{l-l\,max}}{V_{HF\,rms}} = \frac{\sqrt{3}}{\pi} \tag{4.6}$$

This ratio is approximately 0.55. To provide some basis for comparison, a similar ratio for dc link PWM inverters would have a value of $\sqrt{3}/2\sqrt{2} = 0.61$. The ratios change when the effect of dead times are included becoming still closer because dead times have smaller effect in the case of a sinusoidal link voltages.

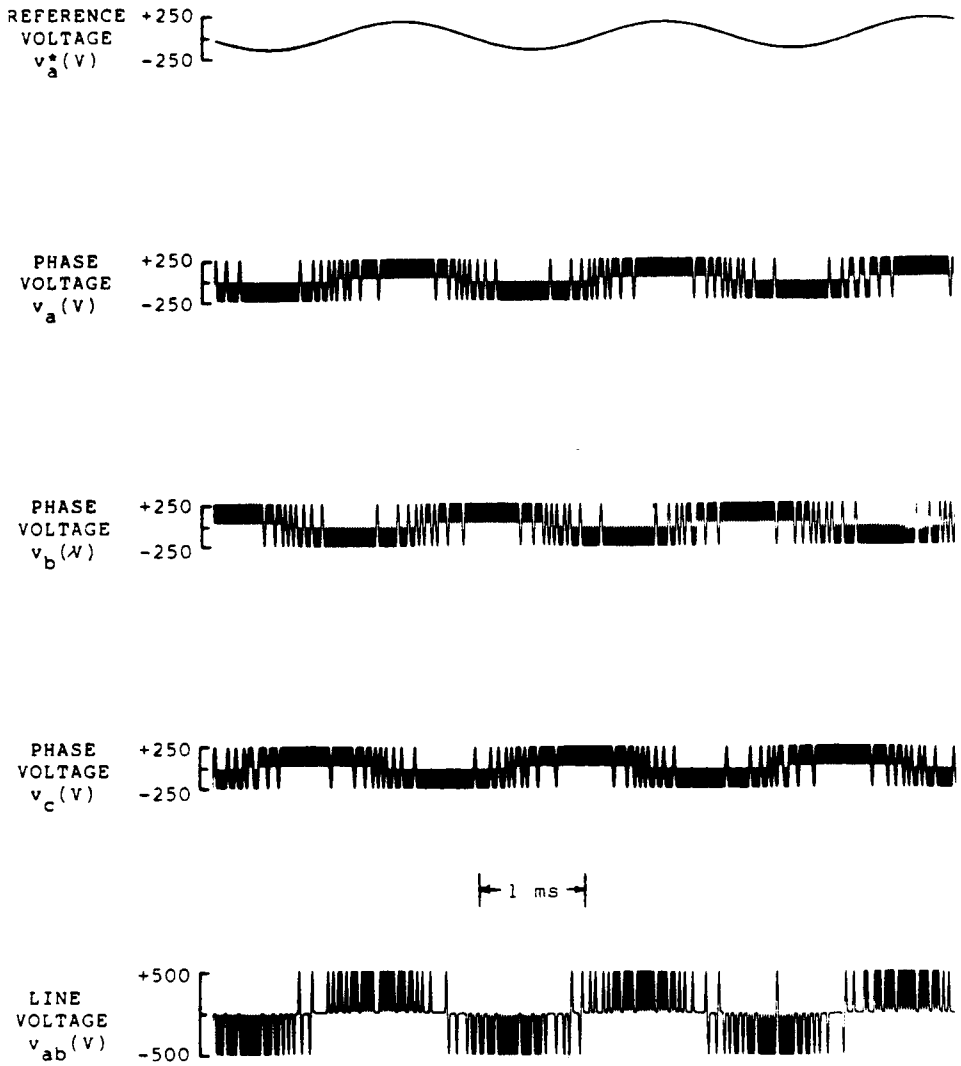

Figure 4.6: Synthesis of a balanced set of voltages having sinusoidal fundamental components. Fundamental frequency is 400 Hz with a modulation index of 0.9.

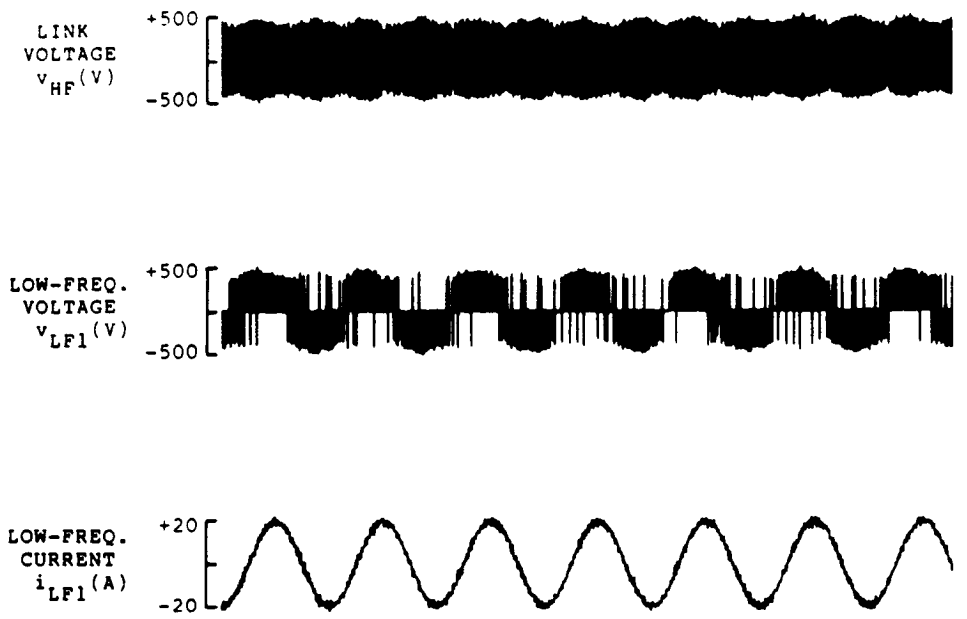

Figure 4.7: PDM bridge converter output waveforms when supplying a wye connected R-L load.

4.3 Interfacing of Induction Machines Using PDM Bridge Converter

It has been shown that the PDM bridge converter can be used to synthesize a balanced set of three-phase voltages from the high frequency link. Also, varying the frequency and the amplitude of the reference signal to the PDM converter has the effect of generating a nearly sinusoidal voltage supply of controllable frequency and amplitude independent of the power factor on the low frequency side. Earlier in Chap. 2.1 it was noted that a supply with such characteristics is adequate for operating an induction machine with either direction of power flow. The results of this Chapter clearly demonstrates this fact using computer models of the machine and the PDM Bridge converter.

The induction machine model which has been chosen to study machine behavior when operated from a converter supply is described in Appendix A. Since no specific machine is under consideration, a 400 Hz, 210 V three-phase machine having parameters typical of a machine in its class has been assumed for the purpose of this preliminary investigation. The parameters of the machine are given in Table 4.1. The machine model was first tried for simulating free-acceleration of the machine from a 110 V, 200 Hz (i.e. Volts/Hertz = 50 percent) sinusoidalsupply. Figure 4.8 shows a typical set of simulated waveforms. The line currents, speed and torque predicted by the model for this free acceleration test are typical of a machine of this class.

The same machine was then fed from the PDM bridge circuit. Appendix C describes the development of the model used for the PDM bridge. The converter output frequency was controlled so that the slip, the difference between the converter frequency and the actual rotor speed, corresponded to the amount and the direction of the desired power flow into the machine. Fig. 4.9 shows the block diagram of this slip controller. Figure 4.10 shows system waveforms as the slip frequency was controlled from zero to its rated value and then reduced steadily to its rated negative value. In the process, the power flow from the PDM converter went through a range of zero to full positive and then reversed to full negative at which point the machine was operating as a generator feeding power back to the high frequency link. These simulation results confirmed that:

1. There is no fundamental difficulty in having the proposed PDM converter feed an induction machine from a high frequency link with the machine operating either in motoring or generation.
2. Slip control strategy is adequate to cause the machine to change from motoring to generation or vice versa.
3. The synthesized voltages have no troublesome lower order harmonics since the re-

Rated power	7.5 HP
Rate voltage	210 V
Rated frequency	400 Hz
Rated speed	11200 rpm
Stator and rotor resistance	0.15 pu
Stator and rotor reactance	0.1 pu
Unsaturated magnetizing reactance	3 pu
Normalized inertia	0.2 s

Table 4.1: Parameters of 400 Hz., 210 V. Three Phase Induction Machine.

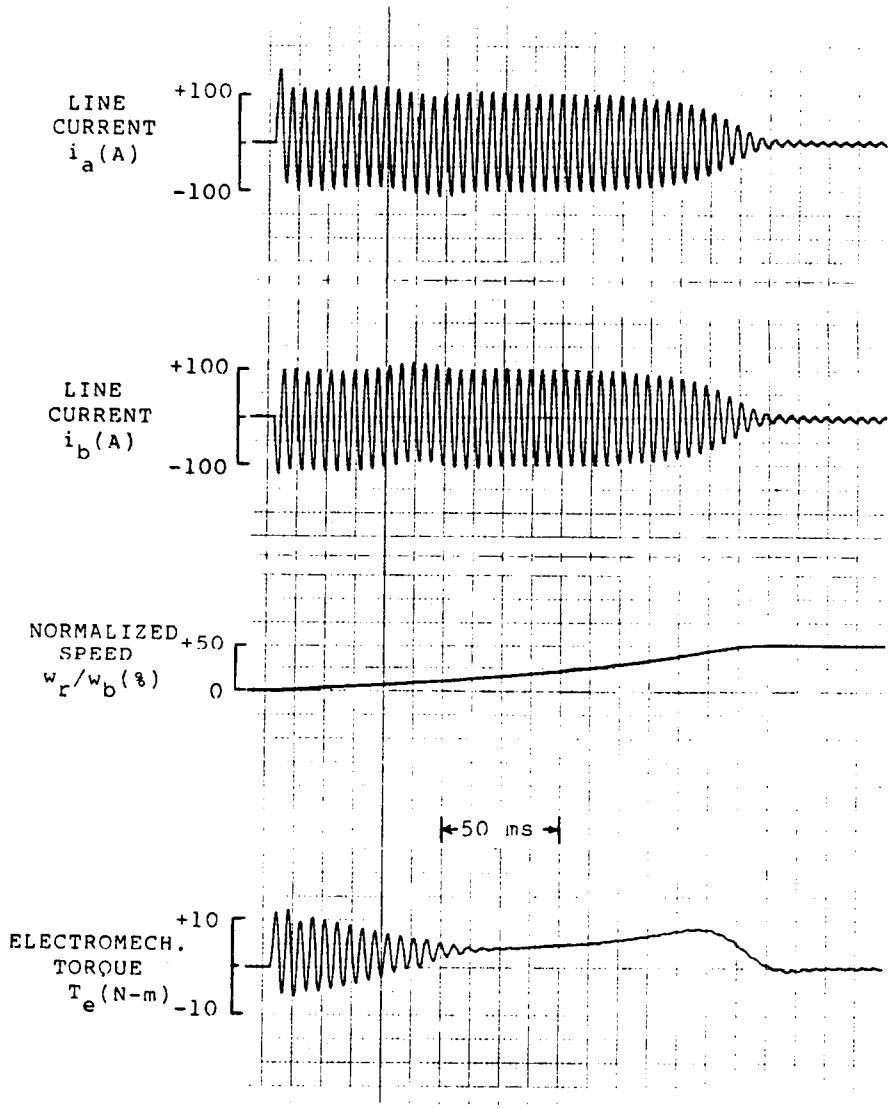

Figure 4.8: Simulated free acceleration of a 400 Hz induction machine. Machine parameters are given in Table 4.1.

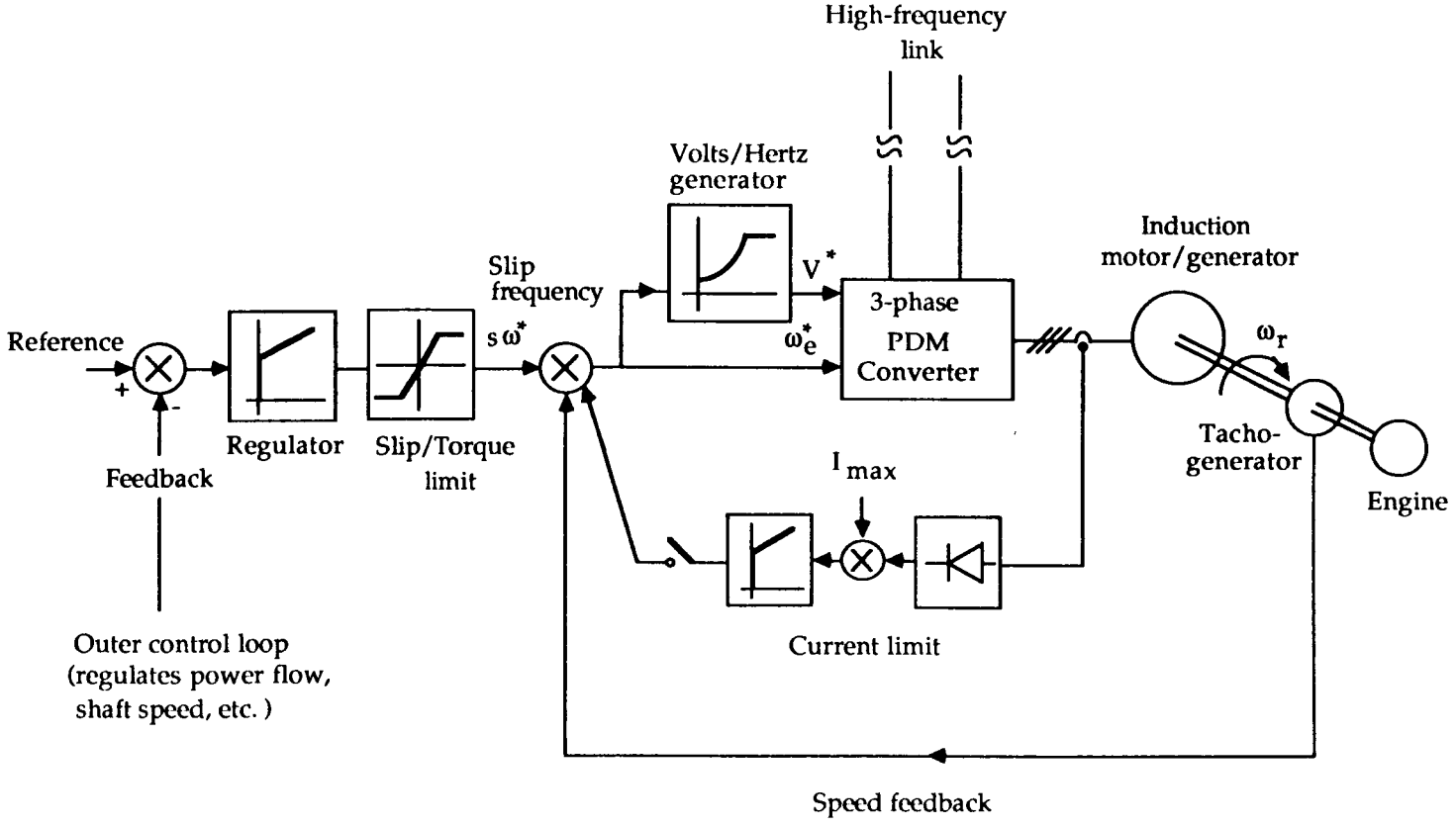

Figure 4.9: Block diagram of the slip controller.

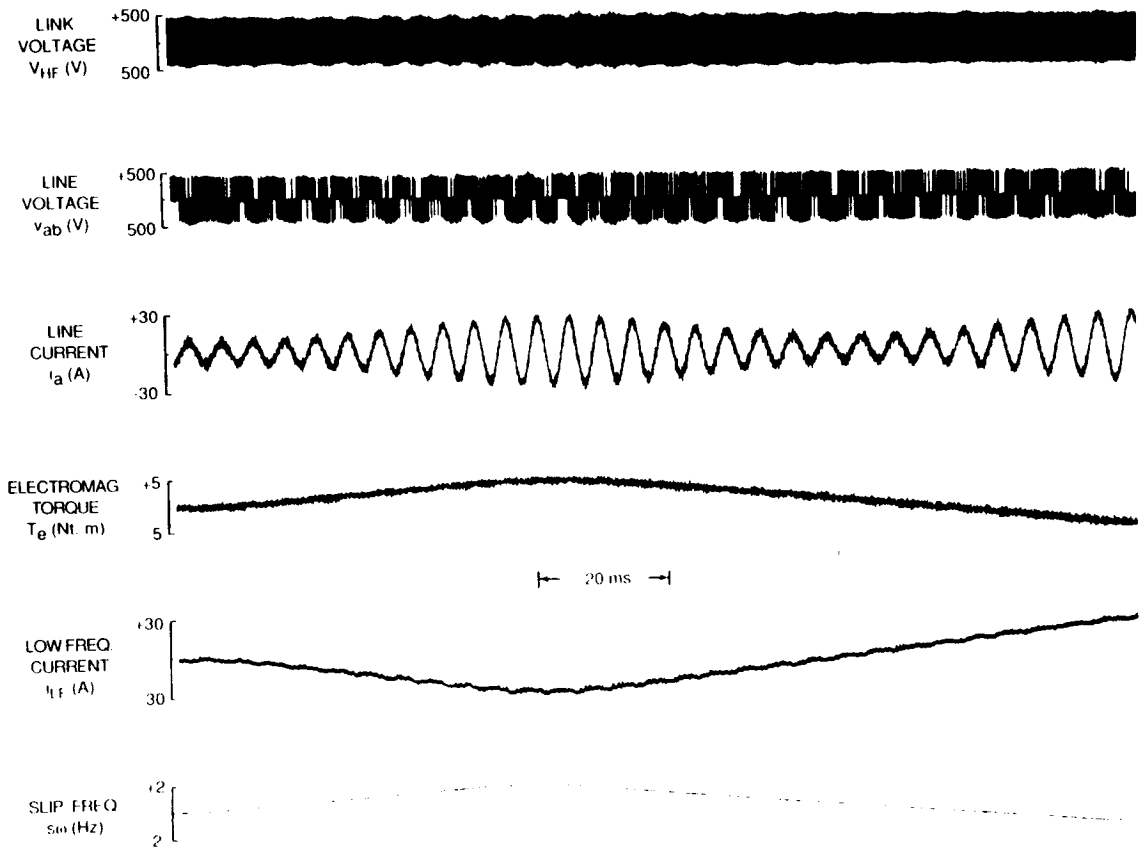

Figure 4.10: Induction machine - PDM converter system operation under both motoring and generation.

sulting line currents are nearly sinusoidal. Thus, no filters are needed between the PDM converter and the machine.

4. Frequency, amplitude or distortion of the link are not seriously affected even though the power factor at the low frequency end is undergoing a wide ranging change.
5. Actuators requiring quick and frequent torque reversals can be supplied through PDM converters.

4.4 Characteristics of PDM Converter as an Interface Converter

The work carried out in this investigation suggests the following favorable characteristics of the proposed PDM converter when used for interfacing of induction machines to a 20 kHz link.

- One-stage power processing.
- Low switching losses.
- Inherent bi-directional power flow capability.
- Low distortion synthesis to 1000 Hz.
- Flexible. Adaptable to voltage or current control and single- or three-phase machines.
- Capable of fast response needed for actuator control.
- Power circuit equivalence with the dc link bridge topology makes it easier to understand and apply.
- Control through simple to implement pulse-density-modulation scheme.

4.5 References

1. P. Espelage and B. K. Bose, *High-frequency link power conversion*, IEEE Trans. Ind. Appl., vol. IA-13, pp. 387-394, Sept./Oct. 1977.
2. P. K. Sood and T. A. Lipo, *Power Conversion distribution system using a resonant high-frequency ac link*, In Conf. Rec. 1986 Annu. Meet., IEEE Ind. Appl. Soc., pp. 533-541.

3. P. Wood, *Switching Power Converters.* New York: Van Nostrand Reinhold Company, 1981, Ch. 4, pp. 153.

4. J. Nishizawa et. al., *Low-loss high-speed switching devices, 2300-V, 150-A static induction thyristors*, IEEE Trans. Electron. Dev., vol. ED-32, pp. 882, 1985.

5. B. Thomas, D. Silber and H. Berg, *Progress in GTO's for industrial line inverter applications*, in Conf. Rec. 1985 IAS Annual Meeting, IEEE Ind. Appl. Soc., pp. 882-888.

6. H. Yilmaz et. al., *Comparison of the punch through and non-punch through IGT structures*, in Conf. Rec. 1985 IAS Annual Meeting, IEEE Ind. Appl. Soc., pp. 905-908.

Chapter 5

Experimental System

As part of this investigation a laboratory breadboard was proposed and built. The principal motivation for buiding a laboratory system was to experimentally verify the computer models used in this study and to demonstrate hardware feasibility of the proposed PDM interface converter. A secondary objective has been to provide a basis for a possible industrial type breadboard in the future.

5.1 Description of the Laboratory System

Figure 5.1 shows the block schematic of the laboratory breadboard as originally proposed. The breadboard consists of single-phase and a three- phase PDM converters connected through a single-phase 20 kHz sinusoidal voltage link. An exciter is connected to the high frequency link for the purpose of starting and maintaining the link voltage. In a system employing two (or more) PDM converters, the exciter is not required to participate in the primary power transfer regardless of the direction of the power flow. In fact, operation with the exciter entirely removed has been shown to be feasible as will be discussed under system considerations in Chapter 6. Due to the limitations of time and resources, it was agreed that initially, the portion of the system drawn with solid lines will be implemented in hardware. It was felt that hardware demonstration of motoring using single PDM experimental system along with the computer simulations of a two PDM system showing both motoring and generation operation would be adequate for establishing the feasibility of the proposed converter-machine interface.

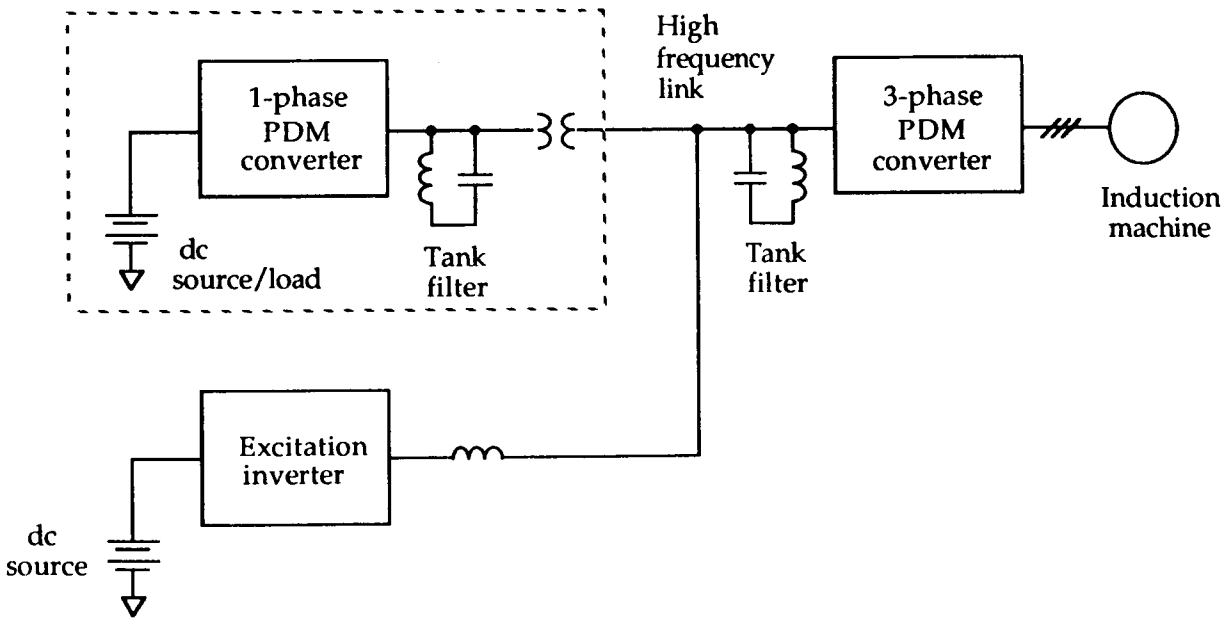

Figure 5.1: Block schematic of the laboratory breadboard as originally proposed. The portion implemented is drawn in unbroken lines.

5.1.1 Excitation Inverter.

In the laboratory system ultimately implemented, the excitation inverter provides the high-frequency power from which a PDM converter can operate to supply a three- phase load or an induction machine. The system was designed for 3- phase 200 V, 22 A output from the PDM converter with a maximum power capability of 5 kW. A parallel output series resonant (POSR) converter (Chapter 3) was selected for the excitation inverter because of its high efficiency and low distortion conversion of dc into a high frequency voltage. Figure 5.2 shows the power circuit used. Table 5.1 gives the component values used on the breadboard. The resonant frequency, as determined by inductor L and the resonant capacitor C, is 28.8 kHz. However, The effective resonant frequency for the split inductor configuration tends to be somewhat higher than the value determined by L and C because of the overlapping of SCR and diode conduction (mode III, Sec. 3.1). The nominal output frequency was selected to be 20 kHz. A frequency adjustment has been provided which allows the link frequency to be set within a range of 18 to 22 kHz. The subresonant operation was selected since it permits the use of naturally commutated devices. Asymmetrical SCRs with their short turn-off times have been used. Currents in the two legs of the bridge circuit were sensed using wide bandwith isolated current sensors. Converter control circuit uses these current signals to sense impeding commutation failures and prevents them by blocking the firing of the next pair of SCRs.

High frequency output of the POSR converter is connected through a series impedance to the LC tank filter at the input of the PDM converter. The purpose of the series impedance (currently an inductor, L_s) is to force the tank filter to handle most of the harmonic current reflected back by the PDM converter and thus require the POSR converter to deal mainly with the average power flow. A series resistor R_s is also brought in temporarily during the period that the link voltage is being first being built up. The resistor is shorted out by a relay after a delay selected to exceed the charge up time of link voltage.

The dc supply to the POSR converter was realized by rectifying the three-phase 60 Hz supply. If the adjustments in the dc voltage input to the POSR and hence, the high frequency link voltage are desired, a three phase variac (not shown) may be inserted between the supply and the rectifier input. Figure 5.3 shows the power circuit of the rectifier supply. The rectifier output has an active current limit with a foldback feature which safely shuts down the dc bus if excessive currents are sensed. For example, if the POSR converter were to suffer a shoot through (either because of commutation failure or due to a device or component related problem), the limiter would sense the abnormal current and turn-off the SCR's experiencing shoot-through by taking the bus current to zero. The fuses have been to provide a backup protection. Table 5.2 gives the values of the important components used in the breadboard dc supply.

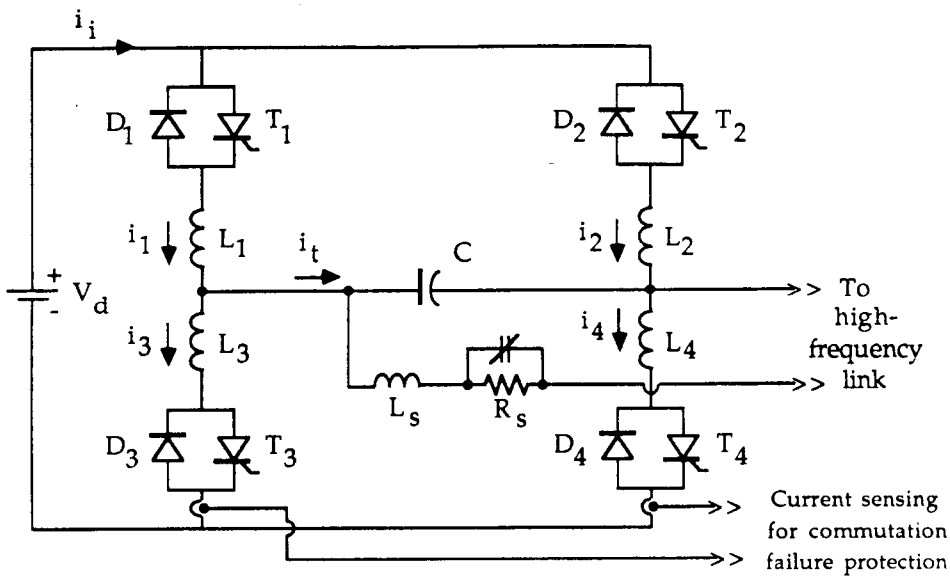

Figure 5.2: Power circuit of the breadboard POSR converter used to generate the High frequency link voltage. Component values are shown in Table 5.1

Component	Circuit Symbol	Key Specifications	Comments
Asymetrical SCRs	T1 - T4	40 A, 800 V, $t_q \leq 4\mu s$	Marconi ACR25U08L
Diodes	D1 - D4	63 A, 800 V, $t_{rr} = 0.2\ \mu s$	IR 40HFL80S02
Resonant inductors	L_1 - L_2 L_3 - L_4	33 μH, 46 A pk, 27 μH, 46 A pk	Litz wire, ferrite core Litz wire, ferrite core
Resonant capacitor	C	0.5 μF, 38 A, 2000 V pk	Two GE97F8522FC in series.
Series inductor	L_S	82 μH, 30 A	
Charging resistor	R_S	68 ohms, 50 W	
Relay		30 A, 230 V, SPDT	Magnacraft W199X-2
Current sensores		100 A, 1000:1, DC-100kHz	LEM LT 100-S
Snubber		100 ohms, 25 W 0.01 μF, 1600 VDC	 Sprague 715P series

Table 5.1: Component values of the breadboard converter.

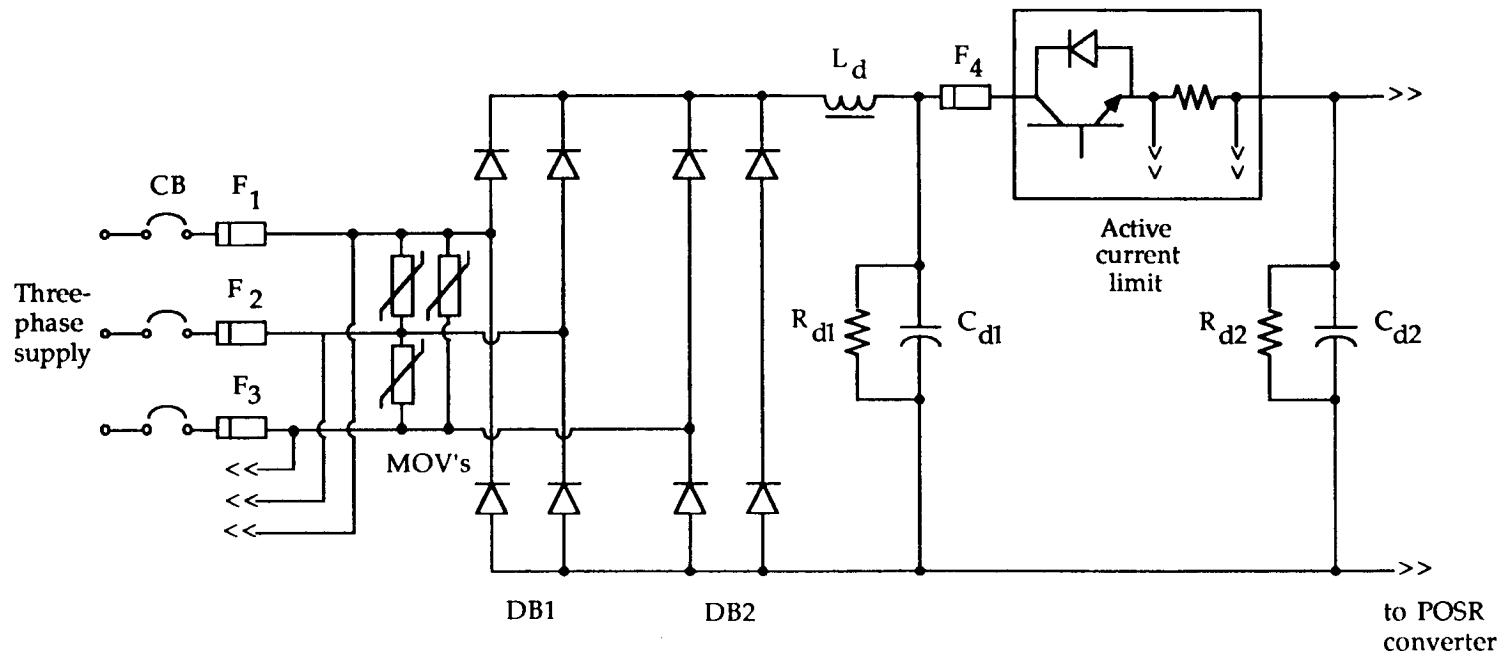

Figure 5.3: Power circuit of the rectifier supplying the POSR converter. Rectifier output has an active current protection. Component values are given in Table 5.2.

Component	Circuit Symbol	Key Specifications	Comments
Diode bridge	DB1, DB2	35 A, 600 V	Motorola MDA3506
Fuses	F1,F2,F3	20 A, 600 V	KAC 20
Choke	L_d	5 mH, 22.5 A	
Capacitor	C_d	2400 μF, 450 V	Two GE86F925TA
Current limiter	Q_{CL}	50 A, $V_{ceo(sus)} = 450$ V	GE D66DV6
Fuse	F4	20 A, 600 V	KAC 20
Sense resistor	R_{CL}	0.05 ohms, 50 W	Two RH-50
Capacitor	C_{d2}	200 μF, 300 V	

Table 5.2: Component values of the rectifier supply of Fig. 5.3.

5.1.2 Three-Phase PDM Converter.

Figure 5.4 shows the power circuit of the breadboard PDM converter. It converts the single-phase high frequency output of the POSR converter into low frequency three-phase voltages of controllable frequency and amplitude. Of the bi-directional switch realizations discussed in Sec. 4.4, the two-transistor inverse series connected configuration (Fig. 4.5 (c)) was selected because of the ready availability of the suitable power darlingtons. In addition, the majority of power darlingtons have internal reverse connected diodes which reduce the number of required power connections and thus, help minimize stray inductance in the circuit. Also, the common emmitter connection that results in this configuration is convenient when driving the darlingtons. (This realization is, however, somewhat sensitive to the the reverse recovery characteristics of the internal diodes. If the internal diodes are slow then large recovery currents occur at switching instances). Each bi-directional switch in the PDM power circuit has a capacitor and a MOS-varistor for snubbing and protection. The absence of series resistance in the snubber, made possible by the zero voltage turn-on of the switches, ensures losses snubbing action. Note that the snubber capacitors appear in parallel with the filter tank capacitor. Table 5.3 gives component values used in realization of the circuit of Fig. 5.4.

Like the electrolytic capacitor of a dc link system, the LC tank filter at link side of the PDM converter is designed to store a predetermined amount of energy. In order to minimize the losses associated with this energy storage it is necessary to design the tank circuit with as high a Q value as is practical. Thus, the tank capacitor should have a low dissipation factor while handling large currents at the tank resonant frequency. General Electric 97F85 series polypropylene film capacitors were used. Their performance with respect to both the current handling capability and the losses has been very satisfactory. Unlike the capacitor, the inductor has to be specially designed so that the various loss components (e.g. core losses, conduction losses and the eddy current losses in the conductors and fixtures) are optimized to produce a minimal total loss. Initially, an air-cored inductor wound with a litz wire was used to get started. Subsequently, an inductor with a ferrite core was used. Performance of these inductors is noted in Sec. 5.2.

5.1.3 PDM Converter Control.

The Area Comparison - Pulse Density Modulation (AC-PDM) scheme, described in Sec. 4.3, was used to control the low frequency output of the PDM converter. Three identical circuit channels were used to control each of the three poles of the bridge. Figure 5.5 shows block schematic of one of these channels. Reference signals for the three channels were identical in frequency and amplitude but were phase shifted with respect to each other by 120°. The feedback signals required for implementing AC-PDM control were obtained by

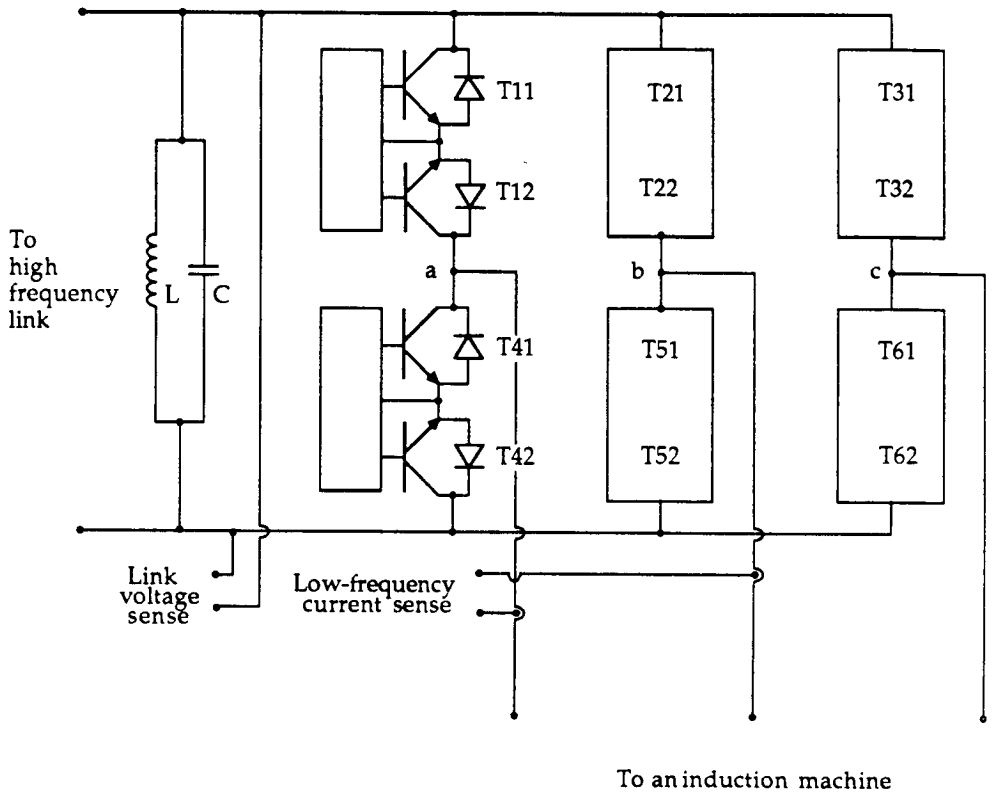

Figure 5.4: Breadboard realization of the three-phase PDM bridge. Component values are shown in Table 5.3.

Component	Circuit Symbol	Key Specifications	Comments
Power - darlingtons	T 11 - T 62	50 A, $V_{ceo(sus)}$ = 500, V_{cev} = 700 V, t_s = 5 μs	MJE 10016
Snubber capacitor	C 1 - C 6	0.047 μF, 1200 VDC	Sprague 715P series
Filter capacitor	C_T	3.0 μF, 1000 Vpk, 114 A	Three GE97F8522FC
Filter inductor	L_T	22.5 μH, 120 A	Litz wire, Ferrite core
Current sensors		100 A, 1000:1, DC-100kHz	LEM LT 100-S

Table 5.3: Component values of three-phase PDM bridge.

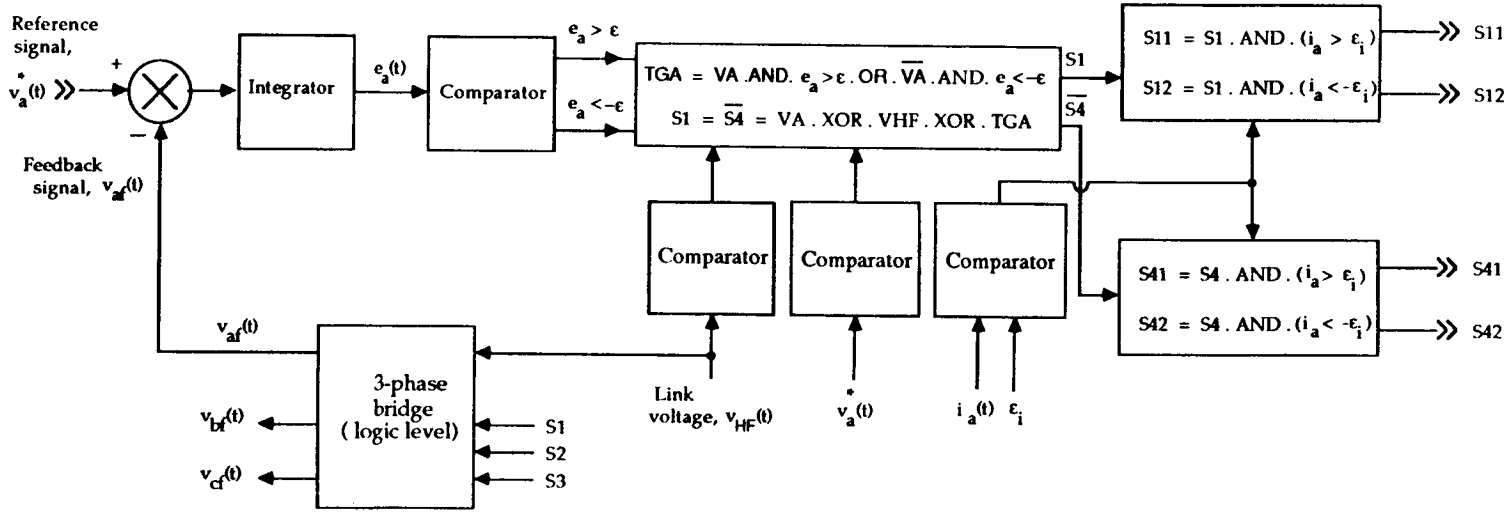

Figure 5.5: Block schematic showing implementation of one channel of the AC-PDM

sensing the link voltage with a signal transformer and applying to this isolated and scaled signal the same logic that fired the power circuit of the bridge. In this way, the difficult task of feeding back pole voltages of variable frequency and amplitude was avoided. Low frequency line currents were sensed in the usual manner. They were used for device selection, for sensing zero crossing of line currents at shut down of the converter, and to provide warning of the overcurrent condition in the lines.

5.2 Test Results and Discussions

The exciter and the tank filter portions of the system were first tested individually. The entire breadboard was then tested with a three-phase wye connected RL load at the output of the PDM converter. Finally, the system was operated with a three-phase induction machine.

5.2.1 Excitation Inverter.

The excitation inverter was disconnected from the rest of the system and was run first at no load and then with a resistive load. Table 5.4 shows the no load losses of the converter at different input voltage levels. The losses are proportional to a 3/2 power of the voltage. Table 5.5 gives the measurement results under resistive load conditions. Note that the converter losses do not change proprtionately with load. In fact, variations with load are quite small. This result is typical of POSR converters which operate with a large circulating current and thus, have poor efficiencies at light loads. As load is increased, the losses increase somewhat in the SCRs but decrease in diodes and the resonant inductors resulting in a net loss that is not significantly different from its corresponding no load value. The converter efficiency of 90% at partial load can be expected to increase to 95 to 96% at the full load value of 6 kW. Instrumentation limitations and the fact that the efficiency of the exciter has only a secondary role in the proposed power conversion system were the reasons for not verifying the converter full load efficiency. Figures 5.6 (no load) and 5.7 (with load) show typical circuit waveforms observed on the breadboard.

V_d (V)	I_d (A)	P_d (W)	v_{HF} (V rms)	v_{HF}/V_d	$(v_{HF})^{1.5}/V_d$	Comments
48.8	0.35	17.1	78.4	1.61	40.8	switching freq.
100.4	0.5	50.3	163.4	1.63	41.8	fixed at 19.3 kHz.
162.8	0.68	110.7	269.0	1.65	39.9	
200.0	0.75	150.0	325.0	1.63	39.1	with 230 V ac

Table 5.4: No load losses of excitation converter at different input voltage levels.

	V_d (V)	i_d (A)	P_d (kW)	v_{HF} (V rms)	i_{HF} (A rms)	P_{HF} (kW)	Efficiency (%)
1(1)	162.3	4.65	0.76	257.3	2.77	0.67	89.3
2(1)	161.8	7.35	1.19	240	4.76	1.07	89.6
3(2)	161.5	7.5	1.21	249	4.47	1.11	91.8

Notes 1. High frequency power measurements with Nicolet 4096.
2. High frequency power measurements with Yew 2533.

Table 5.5: Measured results under resistive load.

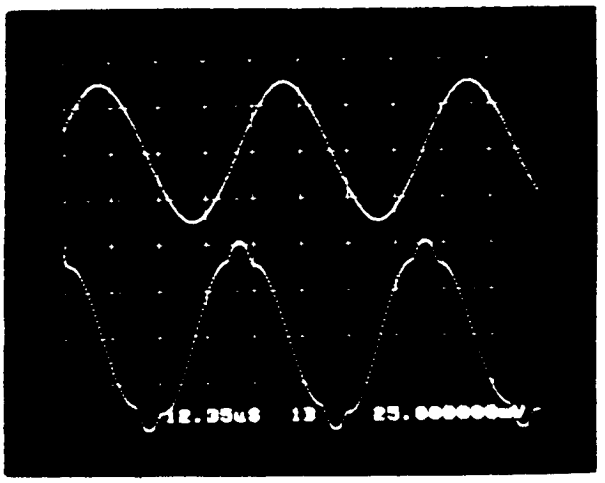

(a)

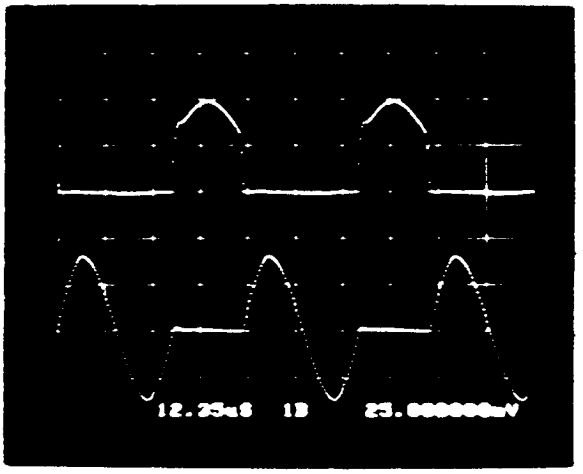

(b)

Figure 5.6: Typical waveforms observed on the breadboard POSR converter at no load. (a) Upper trace: Capacitor voltage, v_c; 250 V/div. Lower trace: Capacitor current, i_c; 12.5 A/div. (b) Upper trace: Switch voltage, v_{T4}; 125 V/div. Lower trace: Switch current, i_4; 12.5 A/div. Time scale: 12.35 μ s/div.

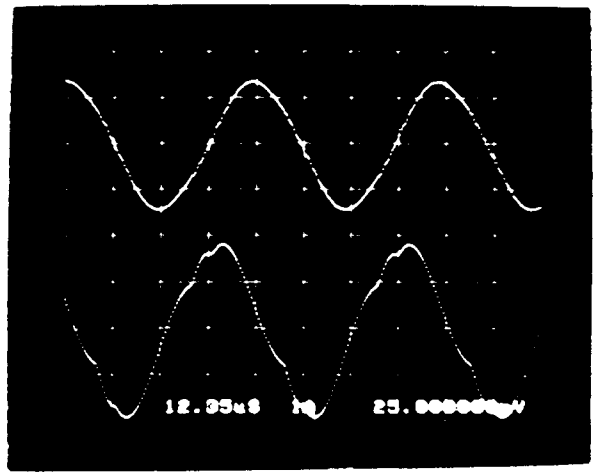

(a)

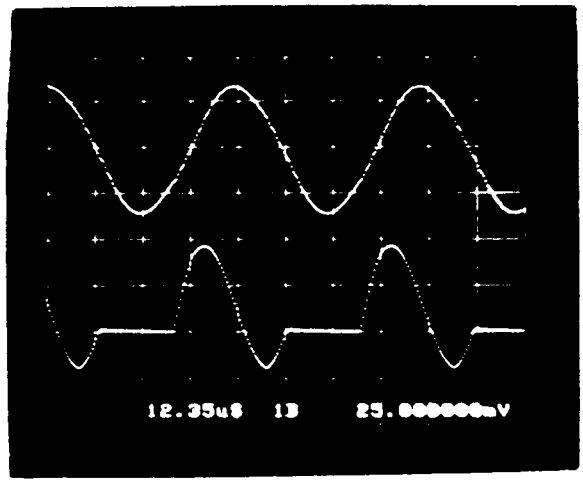

(b)

Figure 5.7: POSR converter waveforms with resistive load of 1.27 kW. (a) Upper trace: Capacitor voltage, v_c; 250 V/div. Lower trace: Capacitor current, i_c; 12.5 A/div. (b) Upper trace: Capacitor voltage, v_c; 250 V/div. Lower trace: Switch current, i_4; 12.5 A/div. Time scale: 12.35 μ s/div.

5.2.2 Tank Filter.

The POSR converter was next operated with the PDM converter. Converter itself was not fired initially so that only the tank filter loaded the POSR output. At start, tank filter has no stored energy. POSR circuit capabilities would be exceeded if the uncharged tank is suddenly switched to the POSR output or if the POSR converter is started with the filter present on its output. The problem is avoided by inserting a resistor, R_s in series with the POSR output and charging the tank circuit in a controlled manner as discussed earlier. Figure 5.8(a) shows this controlled charging of the filter tank circuit. A charging resistor of 68Ω was used for a duration of about $300ms$. Note that the actual charging time for this particular test was less than 2 ms. In this system, adjustment of the exciter switching frequency allows for fine tuning of the link frequency and the tank resonant frequency. However, experimental work has shown that circuit operation is not affected if the tank circuit is not perfectly tuned. Nonetheless, a significant detuning would cause reactive currents to flow from and to the filter even when the PDM converter is off. Figure 5.8(b) shows detailed waveforms of the link voltage and current after the link voltage build up has been completed. Note that the tank resonant frequency matches the link frequency in this case. As a result the current is nearly in phase and flows only to supply the losses in the tank circuit.

It is unfortunate that, wide bandwidth wattmeters needed for accurate and direct measurement of 20 kHz power were not available during this study. Instead, the losses in the tank circuit were measured using two independent methods. One method involved the use of Nicolet 4094 oscilloscope equiped with isolated, high-bandwidth voltage and current probes from which power measurements can be obtained using built in multiplying and averaging functions. The second method involved indirect measurement of these losses by measuring the POSR converter losses with and without the tank circuit on its output. This appears to be an adequate procedure considering that the losses in the POSR converter itself do not change significantly under load. Table 5.6 shows the measurement results when the air-cored inductor (measured Q of 81 at 133 V rms) was replaced with the inductor wound on the ferrite core. Although, losses in the inductor and the capacitor were not measured individually, very low dissipation factors specified for the capacitor and the lack of any noticable temperature rise in capacitor casings suggested that the majority of the losses occurred in the inductor which had a substantial temperature rise. The tank filter Q of 180 is very encouraging considering that little or no special efforts or materials have been used in realizing the LC tank circuit. These measurements show that there is no serious problem in realizing tank circuit Q's in the vicinity of 200. Since little or no special effors were required in achieving the measured tank circuit Q's of 180, it is reasonable to assume that with special efforts and materials Q's greater than 200 to 250 can be realized. Although it had a high Q, the design of this particular ferrite inductor was thermally compromised due to suitable cores not being available in time. Limits on the power dissipation have, in turn, limited the maximum voltage at which the link can be operated continuously to about 280

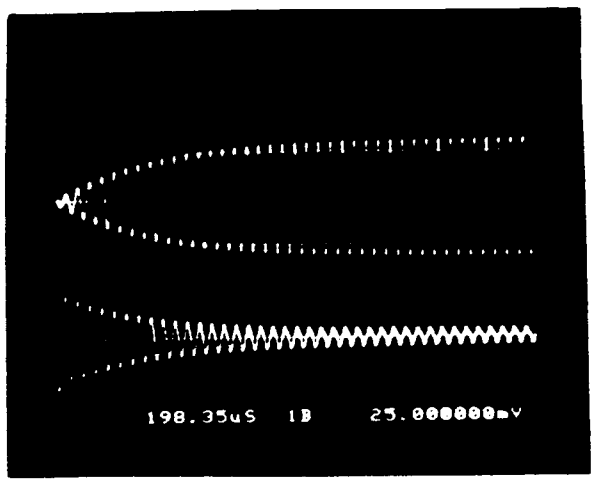

(a)

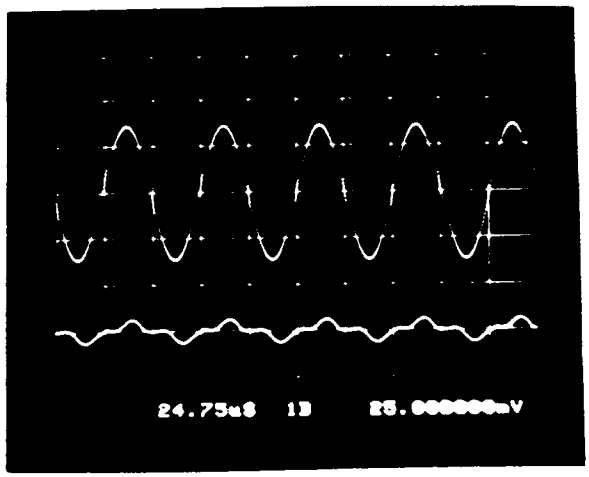

(b)

Figure 5.8: Controlled build up of the high frequency link voltage. (a) Link voltage and current during build up. Upper trace: Link voltage, v_{HF} ; 250 V/div. Lower trace: Link current, i_{HF} ; 5 A/div. Time scale: 198.35 μ s/div. (b) After build up has been completed. Upper trace: Link voltage, v_{HF} ; 250 V/div. Lower trace: Line current, i_{HF} ; 5 A/div. Time scale: 24.75 μ s/div.

			POSR measurements		Nicolet measurements	
V_d (V)	v_{HF} (V rms)	f_{HF} (kHz)	Loss,P_L (W)	Q	Loss,P_L (W)	Q
194.8	318.9	19.32	229.7	162.1	234	159.1
164.5	257.9	19.29	131.7	185.2	136	179.3
119.9	188.4	19.28	67.3	193.5	72.4	179.9
89.7	143.5	19.29	36.8	205.5	40.0	188.8
51.8	84.3	19.31	13.2	197.2	13.6	191.4

Table 5.6: Measurement results on tank filter Q using ferrite cored inductor.

V rms compared to its design value of 370 V rms.

5.3 PDM Converter

5.3.1 Pulse Density Modulation.

The performance of the AC-PDM scheme was tested by varying the frequency and amplitude over a wide range. For example, Fig. 5.9 shows line voltage waveform when the reference signal had a frequency of 400 Hz and the modulation index was near unity. The high frequency link voltage was 292 V rms at a frequency of 19.3 kHz. Corresponding harmonic spectrum is shown shown in Fig. 5.10(a). It is clear that the discrete nature of AC-PDM controller causes slow variations in the waveforms. As a result the harmonic spectrum changes from one sample to another. To obtain information more representative of a given operating point, a 10M- sample unsynchronized rms averaging was used. Note that well defined harmonics occur only as side bands of the switching frequency (38.6 kHz) which is twice the link frequency. The amplitude of these peaks is about one-third of the fundamental for this case. Such higher order harmonics pose no serious difficulty even if no filters are used since most loads, particularly machine loads, are unable to respond to such high frequencies.

Figure 5.10(b) demonstrates that distortion in the lower frequency range, a potential problem with electrical machine loads/supplies, is practically absent in the AC-PDM synthesis. The harmonic content over the medium frequencies depends on the relative amplitude of the output voltage to the link and the frequency of the reference signal. Note that there are no dominant peaks in the distortion which appears to be dispersed almost evenly over a braod range. As a result, the audible noise (such as the noise from a motor fed from PDm converter) is less bothersome than the tonal noise associated with PWM type waveforms. The dispersement of the distortion appears to be a result of free running of the synthesized frequency with respect to the link frequency and the feedback nature of the AC-PDM implementation.

Clearly, the controller capability to suppress the low-frequency distortion degrades the harmonic spectrum once the AC-PDM modulator begins to saturate. This result is illustrated by the line voltage spectrum when the controller is fully saturated and the line voltage is a quasi-square wave composed of rectified half-cycles of the link voltage, Fig. 5.11. An increase of $4/\pi$ in the fundamentalcomponent and the characteristic fifth, seventh, etc. harmonic components are observed as expected. Finally, Fig. 5.12(a) shows line voltage spectrum for the case of a low value of the modulation index. The frequency is 60 Hz and the modulation index has been reduced proportionately so that the frequency to amplitude

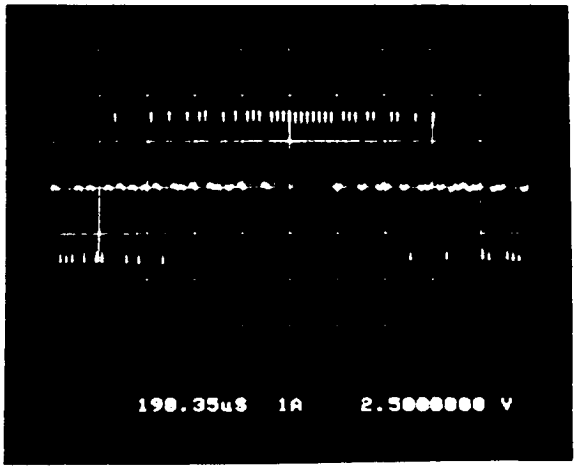

Figure 5.9: Line voltage waveform observed on breadboard PDM converter. Fundamental frequency is 400 Hz and the modulation index is unity. Voltage scale: 250 V/div. Time scale: 198.35 μ s/div.

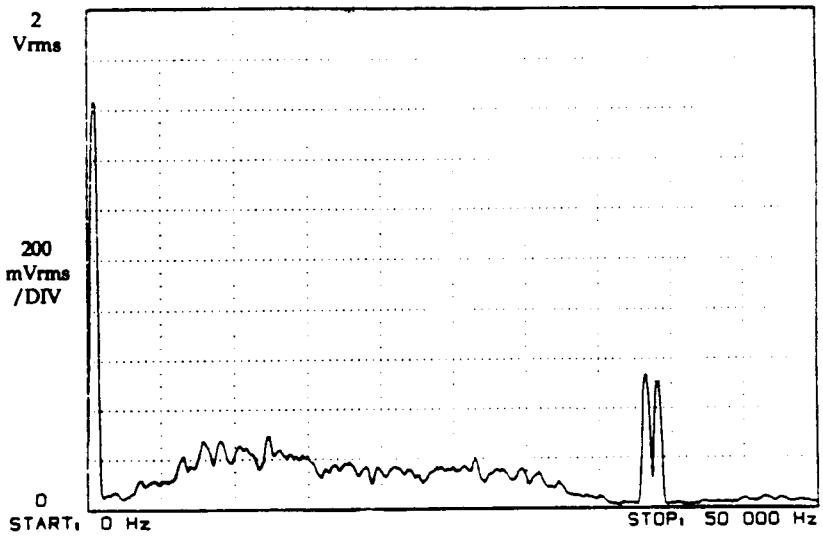

(a)

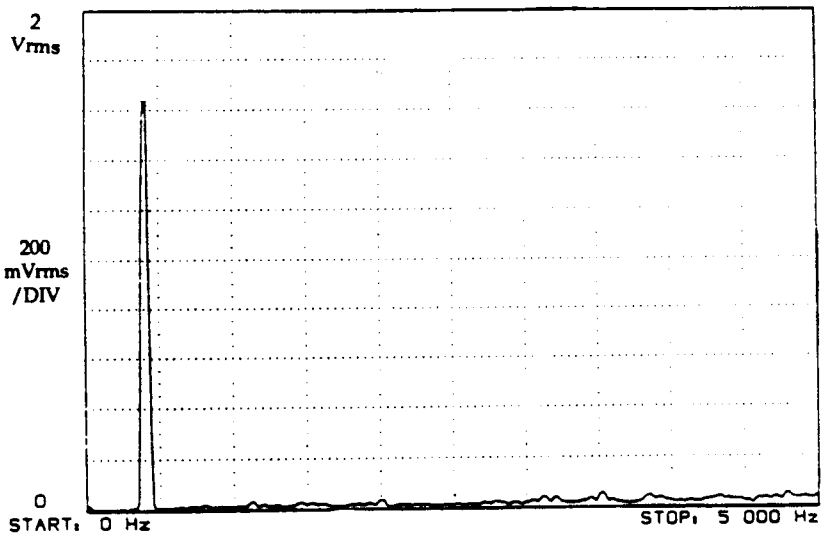

(b)

Figure 5.10: Harmonic spectra associated with the line voltage waveform of Fig. 5.9. Amplitude scale: 20 V/div. (a) Frequency range of 50 kHz. (b) Frequency range of 5 kHz.

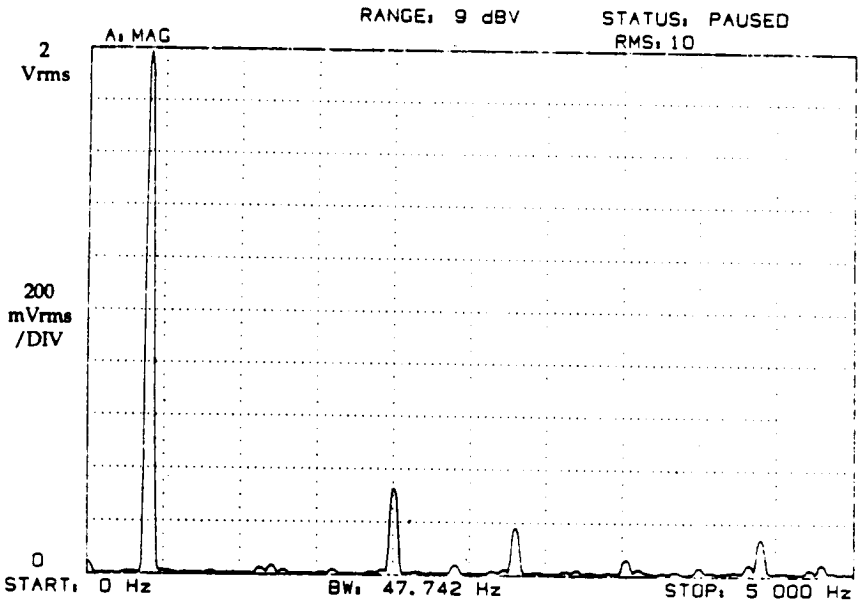

Figure 5.11: Line voltage spectrum with the controller in full saturation. Synthesized voltage is a quasi-square wave composed of rectified half-cycles of the link voltage. Amplitude scale: 20 V/div. Frequency scale: 500 Hz/div.

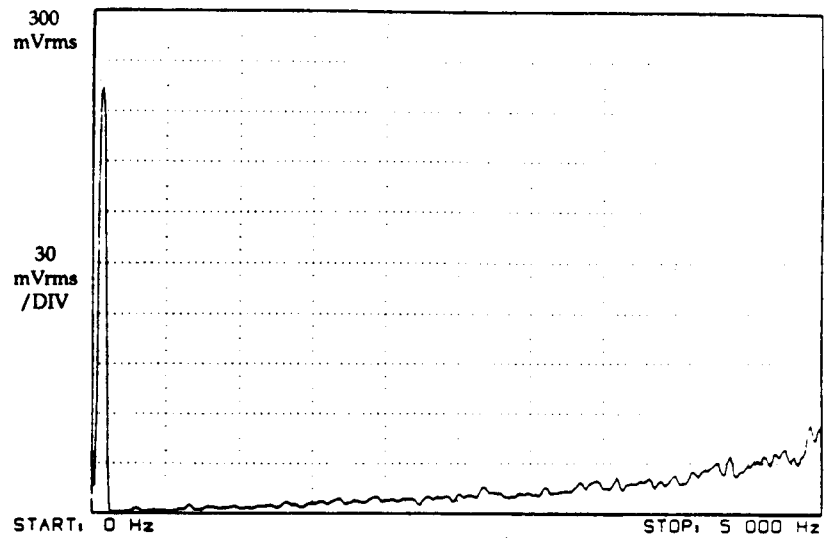

(a)

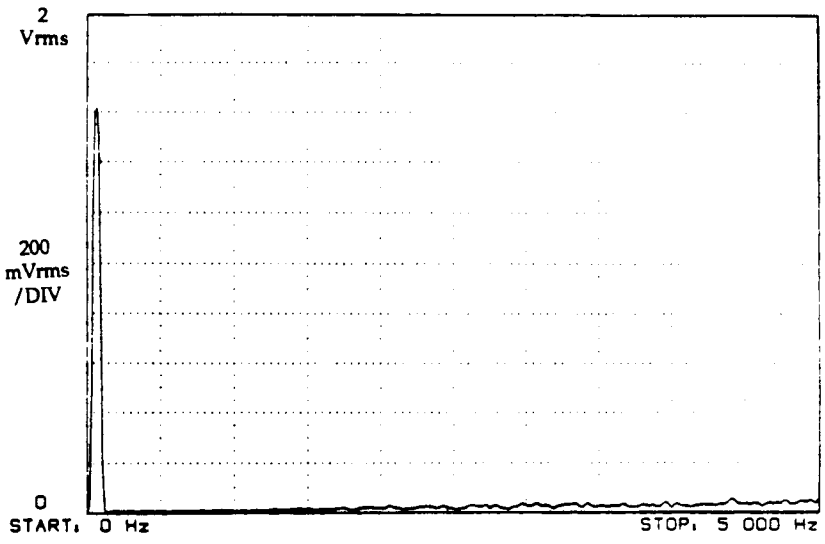

(b)

Figure 5.12: Spectra of the line voltage at 60 Hz. (a) Proportionately reduced modulation index. The volts/Hertz is the same as in Fig. 5.9. Amplitude scale: 3 V/div. Frequency scale: 500 Hz/div. (b) Modulation index of unity. Amplitude scale 20 V/div. Frequency scale: 500 Hz/div.

C-2

ratio is the same as in the synthesis of the 400 Hz signal. Figure 5.12(b) shows the spectrum when the modulation index is again increased to its full value of unity. It is apparent from this test data that the AC-PDM converters can synthesize low-frequency voltages having a wide range of frequencies and amplitudes with little or no lower order distortion being present.

5.3.2 Passive R-L load.

The system operation was then tested with the PDM converter supplying a wye connected R-L load in which the inductor was fixed but the resistance could be varied. Figure 5.13 shows a typical set of line voltage and current waveforms observed on the breadboard. Corresponding line voltage spectrum of Fig. 5.14 confirms that the AC-PDM controller continues to suppress lower order harmonics under load conditions. Figures 5.15 and to 5.16 show other key waveforms of the PDM converter.

For example, the waveform (Fig. 5.15(a)) of the current reflected by the bridge converter to the link is of considerable interest. Its harmonic spectrum (Fig. 5.15(b)) shows that the reflected current, which must depend on the PDM switching action, is rich in harmonics. Link voltage and current waveforms (Fig. 5.16(a)) show that the tank filter is able to handle the reflected current harmonics with acceptable levels of distortion in the link voltage.

The spectrum of the link side current (Fig. 5.16(b)) shows that as a result of the capability of the tank to circulate the harmonic currents, the link current spectrum is essentially of link frequency. It is clear therefore that the link has to deal primarily with the average power flow.

Figure 5.17 shows typical voltage and current waveforms observed across one converter switch. The waveforms demonstrate the zero voltage switching of the PDM converters. Small deviations from the ideal of zero voltage switching, however, still occur due to the variations in the storage times of the power switches. Capacitors connected directly across the switch (lossless snubbers) help minimize the effect of these deviations on the overall performance of the PDM converters. The currents flowing in the snubber capacitor cause the "ripple" superimposed on the device normal current. The sharp peaks are due to the relatively slow recovery of the internal diodes in the low cost Motorola power darlingtons used in the converter. Diodes with faster recovery or alternate bi-directional realizations in the manner of Fig. 4.5(a) or 4.5(b) should significantly reduce or eliminate these spikes.

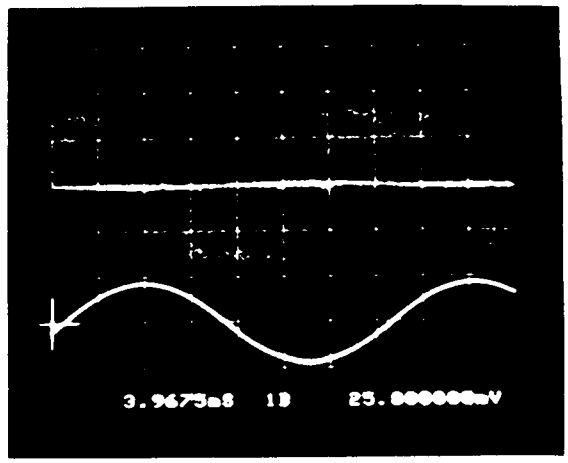

Figure 5.13: Typical set of line voltage and current waveforms observed on the breadboard with a wye connected R-L load. Upper trace: Line voltage, v_{ab} ; 250 V/div. Lower trace: Line current, i_a ; 12.5 A/div. Time scale: 3.9675 ms/div.

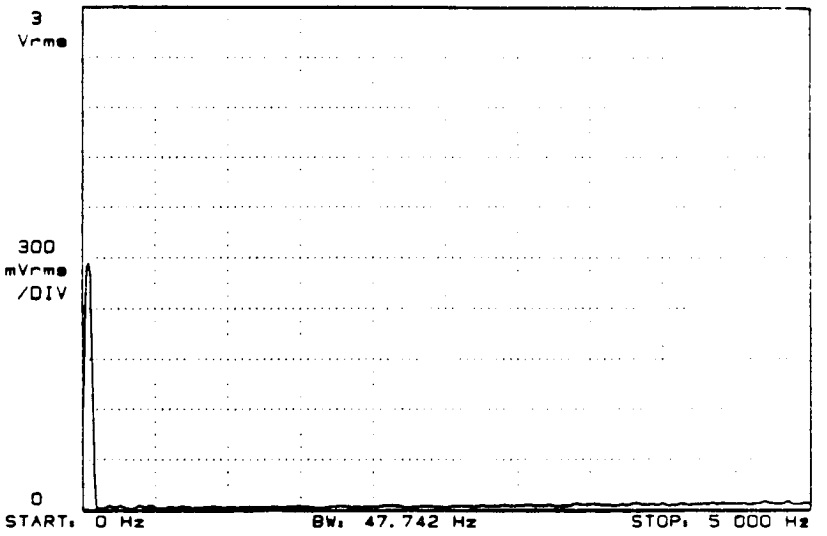

Figure 5.14: Frequency spectrum of line voltage waveform of Fig. 5.13. Amplitude scale: 30 V/div. Frequency scale: 500 Hz/div.

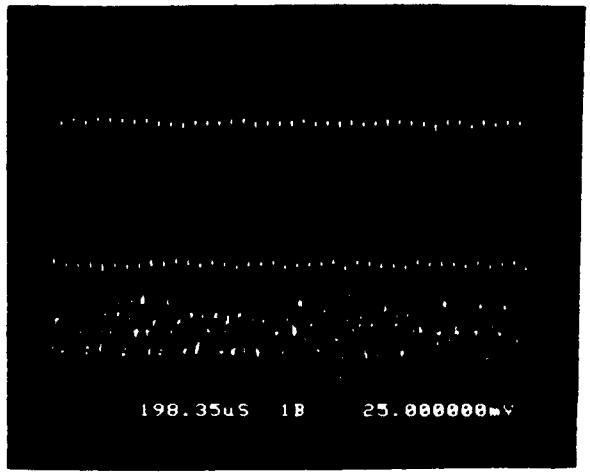

(a)

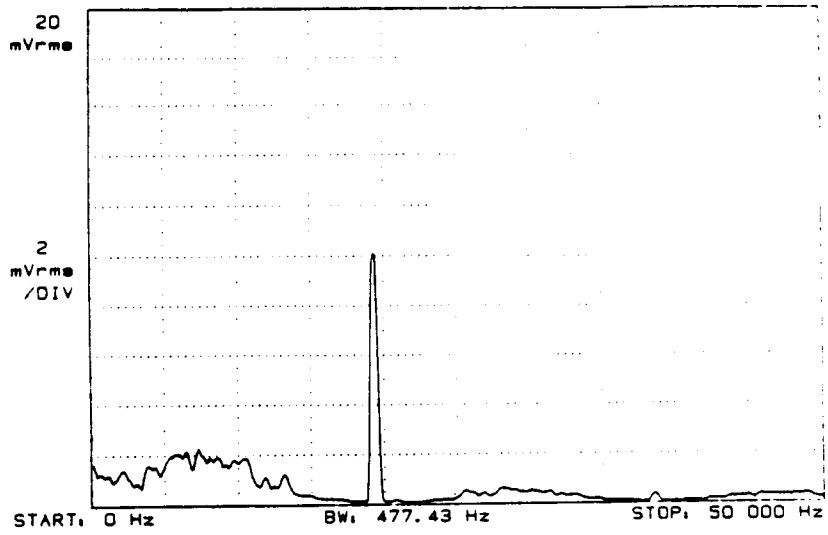

(b)

Figure 5.15: Current returned to the link by the PDM bridge converter. (a) Link voltage and returned current waveforms. Upper trace: Link voltage, v_{HF} ; 250 V/div. Lower trace: Returned current, i_I ; 12.5 A/div. Time scale: 198.35 μ s/div. (b) Spectrum of the returned link current, i_I. Amplitude: 10 A full scale. Frequency scale: 5 kHz/div.

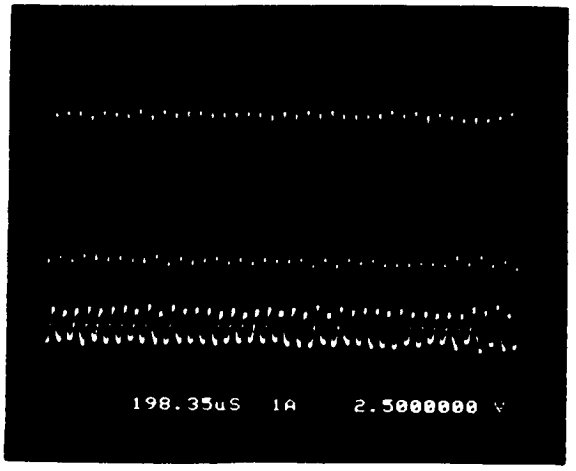

(a)

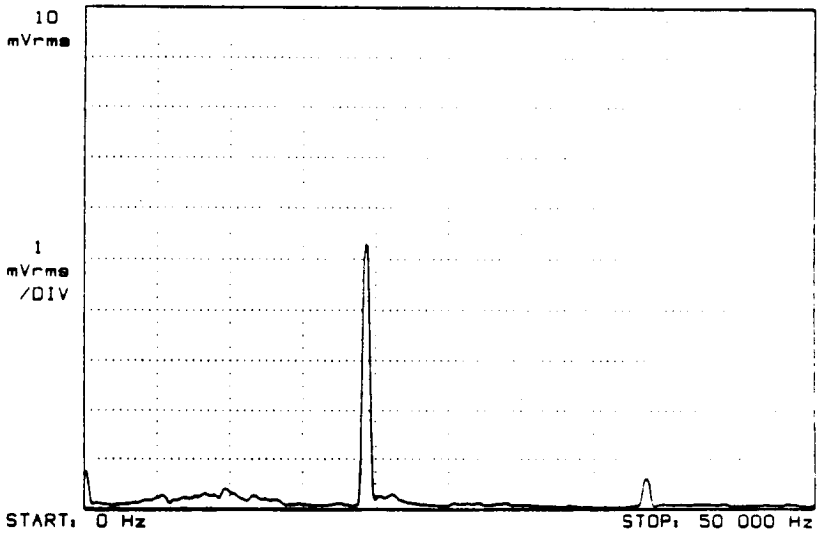

(b)

Figure 5.16: Filter action. (a) Link voltage and current waveforms under R-L load. Upper trace: Link voltage, v_{HF} ; 250 V/div. Lower trace: Line current, i_{HF} ; 12.5 A/div. Time scale: 298.35 μ s/div. (b) Spectrum of the link current, i_{HF} . Amplitude: 10 A full scale. Frequency scale: 5 kHz/div.

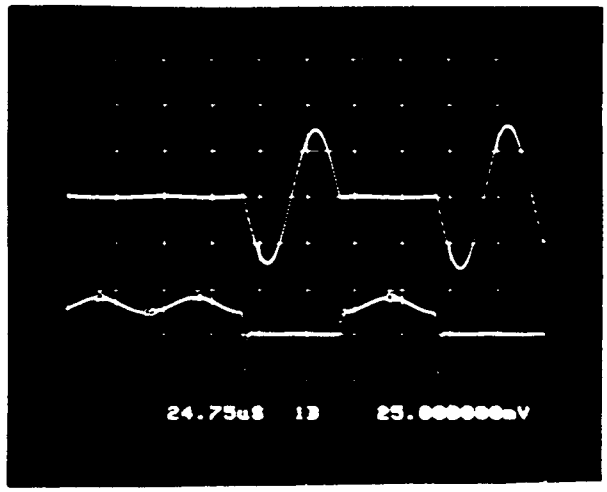

Figure 5.17: Typical voltage and current waveforms observed across one switch of the PDM converter. Upper trace: Switch voltage; 250 V/div. Lower trace: Switch current; 12.5 A/div. Time scale: 24.75 μ s/div.

5.3.3 Induction Machine Load.

Although the PDM converter is capable of full bi-directional power flow, the breadboard system as currently configured can only supply average power until the proposed second PDM converter can be added. In a two PDM converter breadboard, the machine can be operated either as a motor or a generator as was demonstrated in computer simulations of Sec. 4.5. If sustained or frequent generation is not needed, then the addition of a dynamic braking capability in the form of resistive dissipation of the energy received at the link might be an option. Since neither of these options has been implemeted on the breadboard yet, the machine was run simply as a motor to demonstrate basic feasibility.

In the lab the induction machine was fed from the PDM synthesizer which applied voltages having a fundamental component of controllable frequency and amplitude. As discussed in Chapter 2, such voltage fed operation of induction machine requires that voltage-to-frequency ratio of the impressed voltages be kept essentially constant so that the machine main flux remains unchanged as the machine speed is varied. This requirement was realized by making the frequency command to the PDM converter an independent variable determined by the desired machine speed and then deriving the voltage command is from a Volts/Hertz function generator which is designed to produce a constant main flux in the machine. Figure 5.18 shows how the Volts/Hertz function was implemented using two linear approximations. The lower segment represents a simple approximation of the boost needed to compensate for the stator resistive drop at low frequencies. Machine ratings (rated voltage, V_R and rated frequency, f_R) and the controller gains for voltage ($V_{l-l\,rms}/V_{pk}^*$ = 30.6) and frequency (f/V_f^* = 42.35 (Hz/V)) outputs determine the implementation for a given converter. For example, a 220 V, 60 Hz machine and a 200 V, 400 Hz machine would have slopes of 5 and 0.689 respectively in the PDM controller described in this Section.

In addition to these changes, a soft start feature and a current limit were added to the PDM controller for operation with the machine. The soft start is achieved by regulating the rate of increase of the frequency reference, V_f^* to a predetermined value. This has the effect of regulating the machine acceleration rate (within the capabilities of the machine and the power converter). Figure 5.19 shows line voltage and current waveforms during soft start of a 60 Hz, 220 V induction machine from a PDM bridge converter. Current limit provides a useful protection under overload conditions. It was implemented on the breadboard by comparing the magnitude of the line currents against a preset value. The controller allows adjustment of this preset value over a wide range.

Figure 5.20 shows a typical set of machine voltage and current waveforms when run from the PDM converter. Fig. 5.21 shows the associated spectra. As seen with passive loads, there are no lower order harmonics in the voltage waveform (Fig. 5.21(a)). The current spectrum (Fig. 5.21(b)) shows that a cage rotor induction machine does an excellent

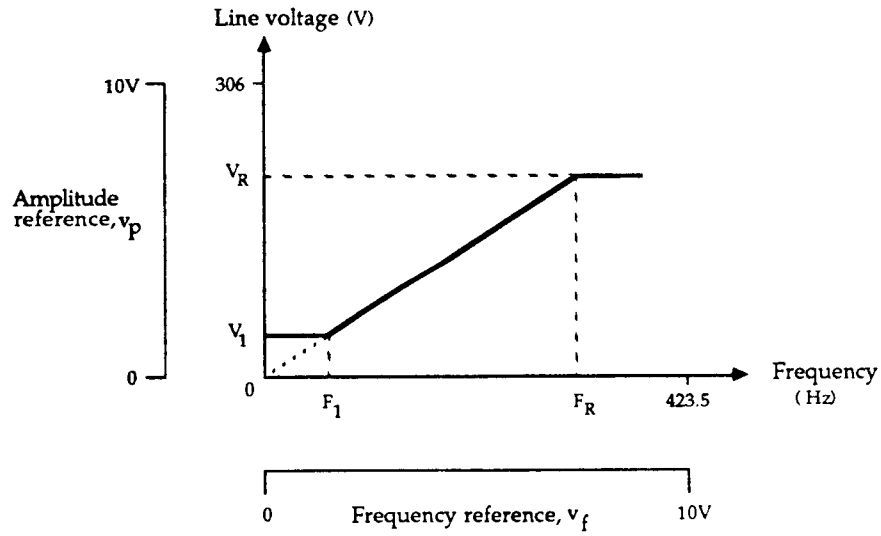

Figure 5.18: Approximation of the voltage-frequency function for constant machine flux.

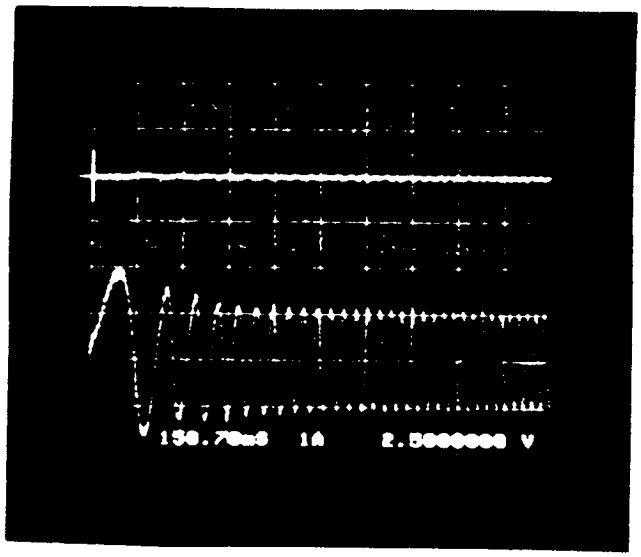

Figure 5.19: Line voltage and current waveforms during soft start of a 60 Hz, 220 V induction machine fed from a PDM converter. Upper trace: Line voltage, v_{ab}; 250 V/div. Lower trace: Line current, i_a; 5 A/div. Time scale: 158.7 ms/div.

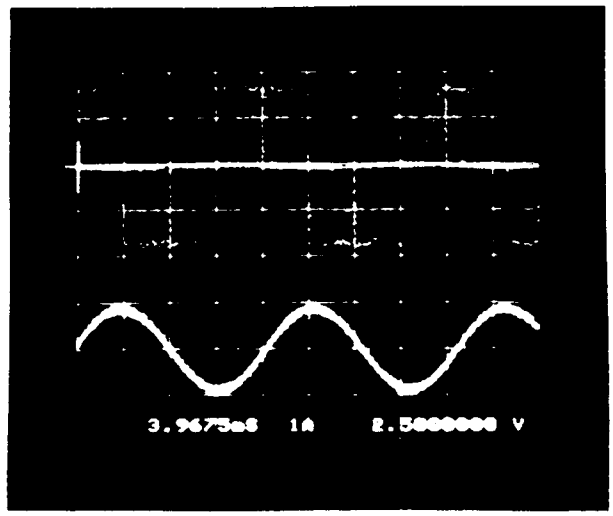

Figure 5.20: Typical set of machine voltage and current waveforms observed on the breadboard. Upper trace: Line voltage, v_{ab} ; 250 V/div. Lower trace: Line current, i_a ; 5 A/div. Time scale: 3.9675 ms/div.

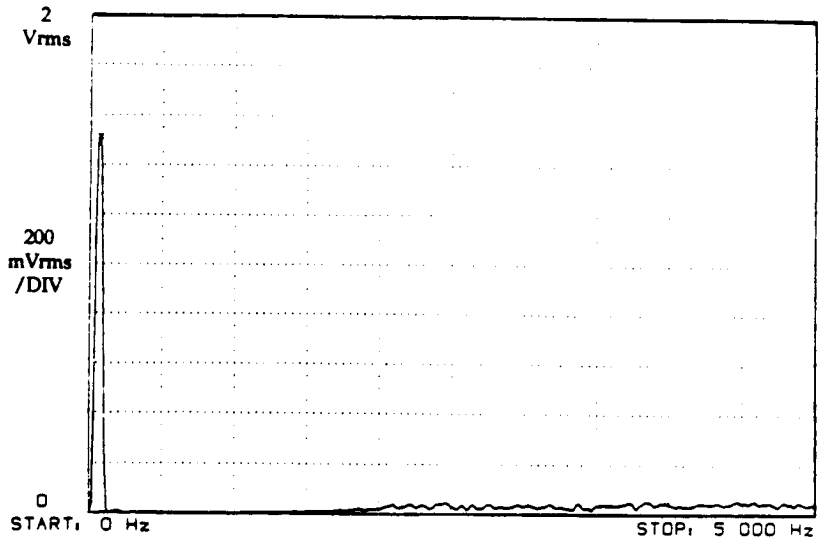

(a)

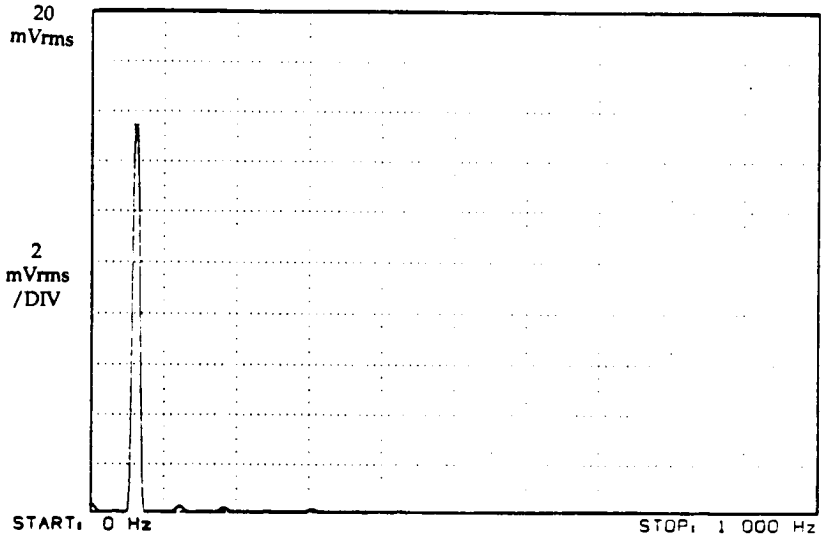

(b)

Figure 5.21: Spectra of the machine voltage and current. (a) Spectrum of the line voltage, v_{ab} . Amplitude scale: 20 V/div. Frequency scale: 500 Hz/div. (b) Spectrum of the line current, i_a Amplitude: 4 A full scale. Frequency scale: 100 Hz/div.

job of filtering the higher frequency harmonics so that these have a minimal influence upon torque production and the power flow in the machine.

If regeneration or dynamic braking capabilities are not present, shut down of the PDM converter poses a problem when load includes inductors or a machine with its back emf. With dc voltage link converters, reverse diodes and the link capacitor provide a sink for the uncoupled reactive energy of the load and therefore shut down involves simply turning off the main devices. Such a procedure in PDM converters may cause damage to the converter devices since no path remains available for the reactive energy in the load. The problem can be eliminated by providing an alternate path (e.g. a load side crowbar) in parallel to the PDM converter output. A more elegant and equally effective method for a three-phase PDM bridge is to detect low current condition in lines and then turn-off the associated poles of the bridge individually. The waveforms of Fig. 5.22 illustrate this safe shut down of the PDM bridge.

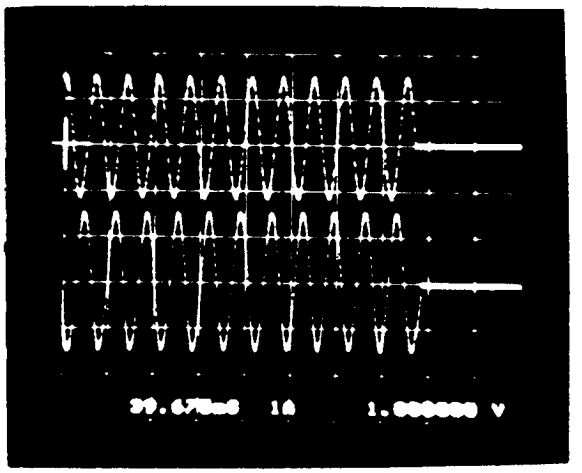

Figure 5.22: Line current waveforms showing safe shut down of the three-phase bridge converter. Upper trace: Line current, i_b ; 5 A/div. Lower trace: Line current, i_a ; 5 A/div.

Chapter 6

System Operation

This chapter discusses means by which a wide variety of loads and sources, in addition to induction machines, can be interfaced to the system high frequency link using PDM converter proposed in Chapter 4. This discussion suggests that a system configuration, based largely on the use of PDM converters is well suited to a distributed power conversion system. The remainder of this section discusses the operation of such PDM converters based system.

6.1 PDM Synthesis of Single Phase AC and DC

The PDM converter is inherently a versatile power converter configuration. Its power structure is made up of bi-directional switches thereby allowing maximum flexibility in power conversion. The control technique of area comparison - pulse density modulation (AC-PDM) proposed in Sec. 4.1 is also very general. It restricts only the frequency and amplitude of the synthesized signal relative to that of the link. Thus, PDM converters should be able interface single-phase sinusoidal ac or dc voltage or currents to the high frequency link.

6.1.1 PDM Synthesis of DC or Single-Phase AC Voltages.

A full bridge (Fig. 6.1), a transformer/half bridge (Fig. 6.2(a)) and a center tapped inductor/half bridge configuration (Fig. 6.2(b)) are basic power circuit topologies possible for the synthesis of dc or single-phase ac voltages. Besides well known differences in the num-

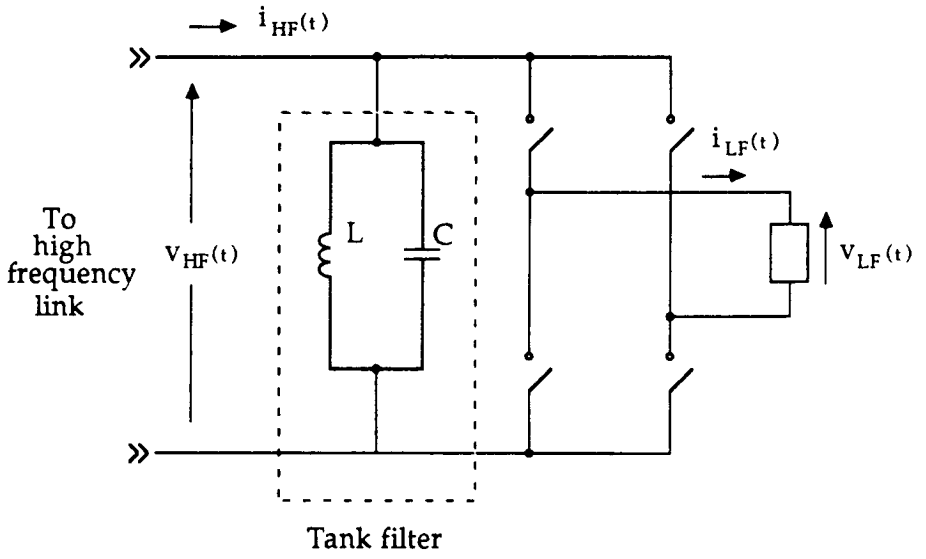

Figure 6.1: Full-bridge power circuit of a single-phase PDM converter.

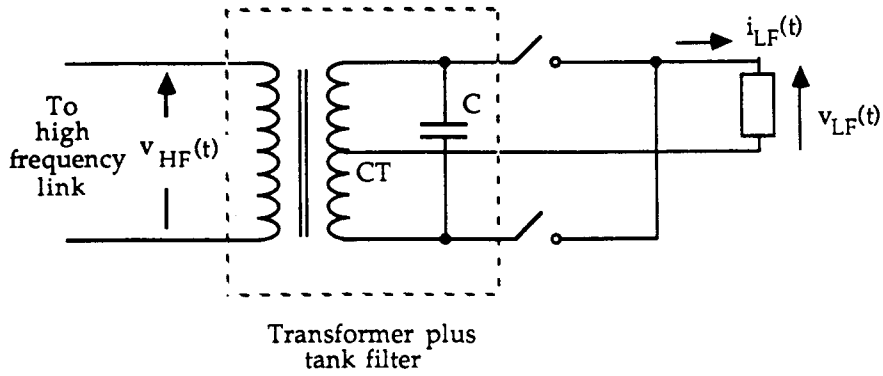

(a)

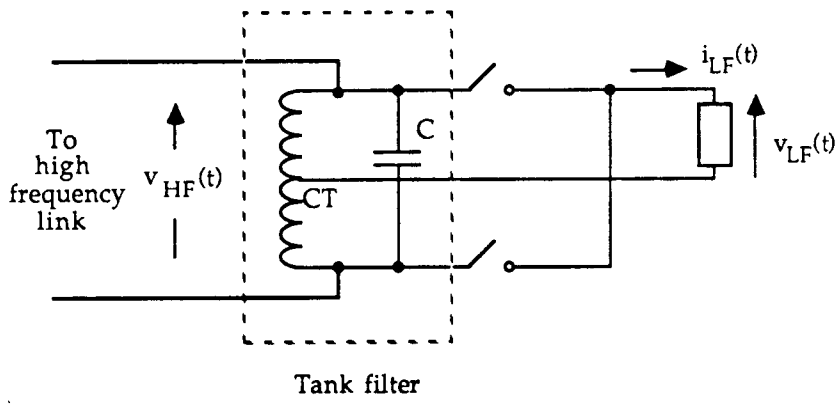

(b)

Figure 6.2: Alternate power circuits. (a) Center tapped transformer. (b) Center tapped inductor.

ber and voltage ratings of the required devices and the volt-amp ratings of the transformer secondary when a transformer is used, there is another important difference among these circuits when they are used for PDM type synthesis. This difference is best described by refering to the waveforms of Fig. 6.3. This figure illustrates several of the different ways in which a dc voltage may be synthesized using PDM type synthesis. The waveform of Fig. 6.3(a) is composed of combinations of all three of the voltage levels (i.e. zero, positive pulse and negative pulse) that are possible in the circuit. Such a waveform results when a full-bridge circuit is used with its two poles being controlled independently using two equal but out of phase reference signals. Note that this consititutes a direct adaptation of the three-phase PDM converter of Sec. 4.4. Figure 6.3(b) shows a PDM waveform composed of positive and negative pulses only. The pole voltage of the full-bridge or the output voltage of a half-bridge or center-tapped circuit always has this type of waveform. Figure 6.3(c) shows a third type of PDM waveform which is composed of zero levels together with levels that correspond to the instantaneous polarity of the reference signal. This type of waveform is sometimes called a commutated waveform and can be realized by direct synthesis of the line voltage in a single-phase bridge circuit using a single reference voltage corresponding to line voltage. Note that a bridge circuit can be made to generate any of these three types of waveforms. The other two topologies, on the other hand, can produce only the waveform of Fig. 6.3(b) because circuit paths needed to force a zero voltage interval on the output are not available in these circuits.

The waveforms of Fig. 6.3 differ not only in their harmonic content but also in the current they cause the converter to reflect back to the link. For a given load current, the commutated waveform (Fig. 6.3(c)) causes fewer reversals in the instantaneous power at the link. Further investigations of this aspect was not undertaken due to the limitations of time. It is desirable to do so in the future, however, since it may be helpful in reducing the size of the link side tank filter.

The waveforms of Fig. 6.4 are an example of the PDM synthesis of a single-phase ac voltage. In this figure a 120 V rms, 60 Hz voltage has been synthesized from a 300 V peak, 20 kHz link voltage using a full bridge power circuit. A single reference signal corresponding to the line voltage output was used. The commutated was obtained by constraining the synthesis to two levels (zero and the level corresponding to the instantaneous reference signal polarity). A dc voltage of either polarity can be synthesized by simply changing the reference signal to a dc voltage. The input-output voltage relationship of a full bridge PDM converter is

$$V_{LF\,max} = \frac{2V_{HF}}{\pi} \tag{6.1}$$

where $V_{LF\,max}$ is the maximum level of the dc signal or the peak value of the ac signal. Thus, the ratio of the output to link rms voltage for the case of full-bridge ac synthesis is

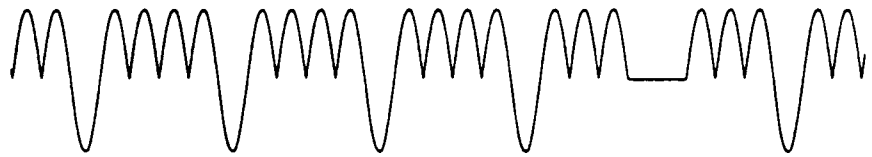

(a) Three-level (i.e. zero, positive and negative pulses).

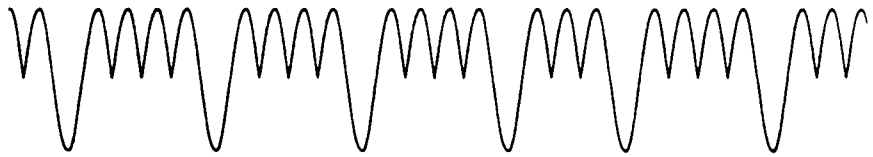

(b) Two level - without zero. (i.e. using positive and negative pulses).

(c) Two level - with zero (i.e. using positive and zero pulses when the reference signal is positive and negative and zero pulses when it is negative).

Figure 6.3: Waveforms types for PDM synthesis of a voltage.

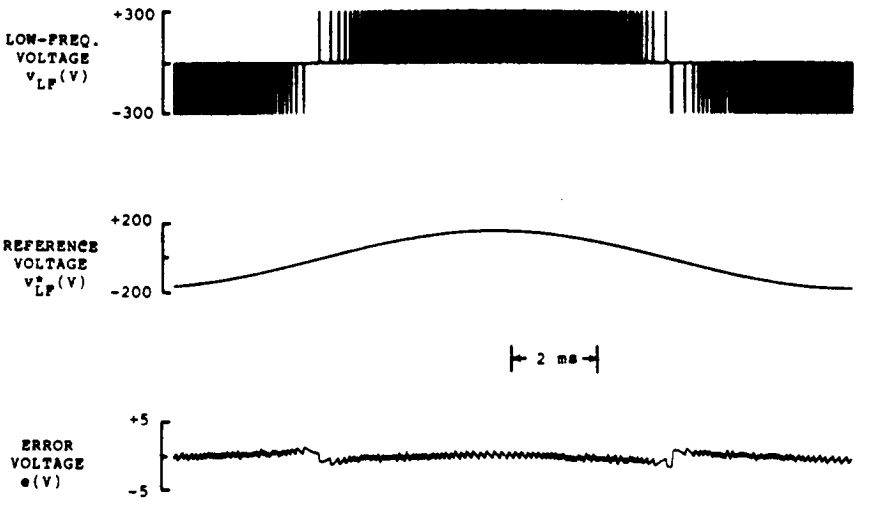

Figure 6.4: PDM synthesis of a 120 V rms, 60 Hz voltage using a full-bridge. Note that the waveform is the commutated type.

$$\frac{V_{LF\ rms}}{V_{HF\ rms}} = \frac{2}{\pi} \tag{6.2}$$

which is approximately 63.7 percent. Corresponding expressions for half-bridge circuit have been derived in Sec. 4.1.

6.1.2 PDM Synthesis of Single-Phase Currents.

If synthesis of dc or single-phase ac currents are desired rather than dc or ac voltages the same PDM converters can be used. However, the low-frequency current, instead of the voltage, must then be fed back to the AC-PDM controller. If low-frequency current is not smooth then it may be necessary to add a suitably sized inductor to limit the amount of ripple current. Figure 6.5 shows an example of dc current synthesized using a single-phase PDM bridge. In Fig. 6.5 the current reference signal was set to zero so that a zero current was synthesized feeding into a 115 V dc source. A 2 mH inductor was used to limit the current ripple. During synthesis, the polarity of the dc source was reversed to show the controller capability to automatically adjust to changing conditions at the low-frequency end. Note that the response to the step change in circuit voltage occured in one- half cycle of the high frequency link voltage. Figure 6.6 shows the circuit operation when this same converter was commanded to draw a current of 10 A from the 115 V dc source.

6.2 Proposed System Configuration

The demonstrated versatility of PDM control suggests a power conversion system configuration that uses only PDM converters to interface the majority of sources and the loads in the system to the high frequency link. PDM based system holds the promise of high efficiency, modularity, and a high degree of uniformity with significant improvements in controllability and reliability of the overall system.

6.2.1 Description of the System Configuration

As discussed in Chapter 1, a power conversion system based on a high frequency link is being considered for the forthcoming orbiting space station. Initial power requirements for the space station have been estimated at 75 kW level with modular growth to a level of 300 kw. Although the sources and loads may vary in type and number, this same basic configuration

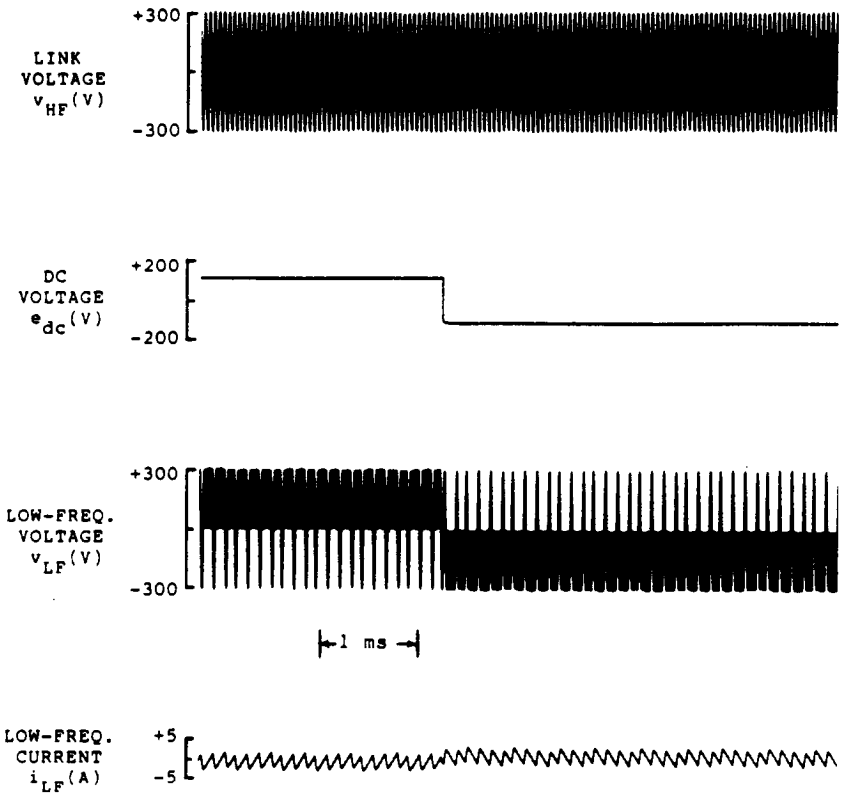

Figure 6.5: PDM synthesis of dc current into a dc source. Current command, i^*_{LF} was set to zero. e_{dc} = 115 V, L_d = 2 mH and V_{HF} = 300 V.

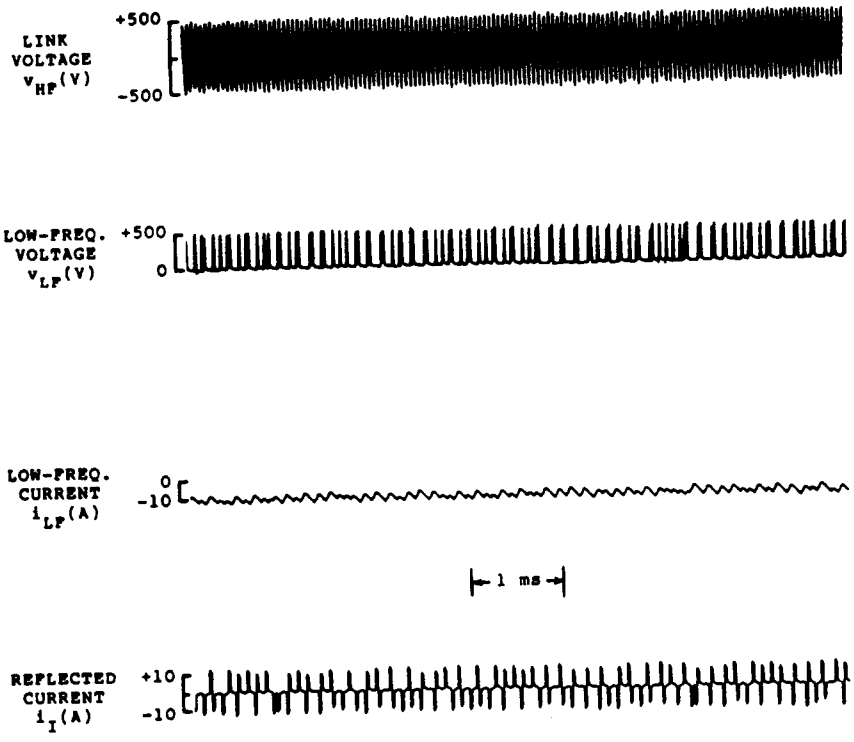

Figure 6.6: Waveforms for dc current synthesis with a current command of 10 A.

applies to other applications such as the secondary power system of the newer generation of transport aircraft, spacecraft 2000, recently proposed transatmospheric vehicle and other such systems requiring distributed power at multi-kilowatt levels. Figure 6.7 again shows a proposed implementation of such distributed power conversion systems using the PDM converters as the primary interface converter in the system.

The proposed configuration utilizes a single-phase 20 kHz sinusoidal voltage link. The single-phase link allows local circulation of reactive power associated with three-phase loads or sources through power converter switching action. This capability of power converters to circulate some of the reactive power associated with balanced three-phase loads means that the traditional assumption of better efficiency through three-phase distribution should not be applied automatically to power conversion distribution systems involving power converters. Use of a single-phase link also reduces the number of power devices, sensors and protection elements in the system. Redundancy is maintained by dividing the entire system power requirement among two or more identical systems. Power balance is maintained in the system at all times by matching the power received from the source(s) and the power delivered to the loads. It is possible to use a dedicated power converter to regulate high frequency link voltage from which the PDM converters can operate. However, this study has shown that if resonant tanks are used as ac filters then the link voltage can be built up and maintained without requiring a dedicated converter in the system for just this purpose.

This and other aspects of the system operation have been studied using the computer models that are described in Appendices A to C. In order to limit the size of system model and yet provide a good idea of the system operation a reduced system, shown in Fig. 6.8, has been simulated. The inductance L_l represents the combined estimated value of the inductance of the ac link together with the leakage inductance of one high frequency transformer.

6.2.2 System Operation and Control.

Since the operation of PDM converters depends on the availability of a high-frequency voltage at the link, a means of developing and regulating this link voltage is needed for satisfactory operation of the entire system. One method of achieving this task is to have a dedicated exciter in the system charge up the resonant tanks. The converters are operated with PDM control once the desired link voltage has been established. The exciter then regulates the link voltage but plays no role in the average power transfer in the system. Because of its role in regulating the link voltage, the exciter must share temporary energy storage with the resonant tank circuits. The sharing determines the nature of the link voltage regulation function of the exciter converter. For example, low values of energy circulation permit regulation of only the "average" value of the link voltage magnitude. A more active

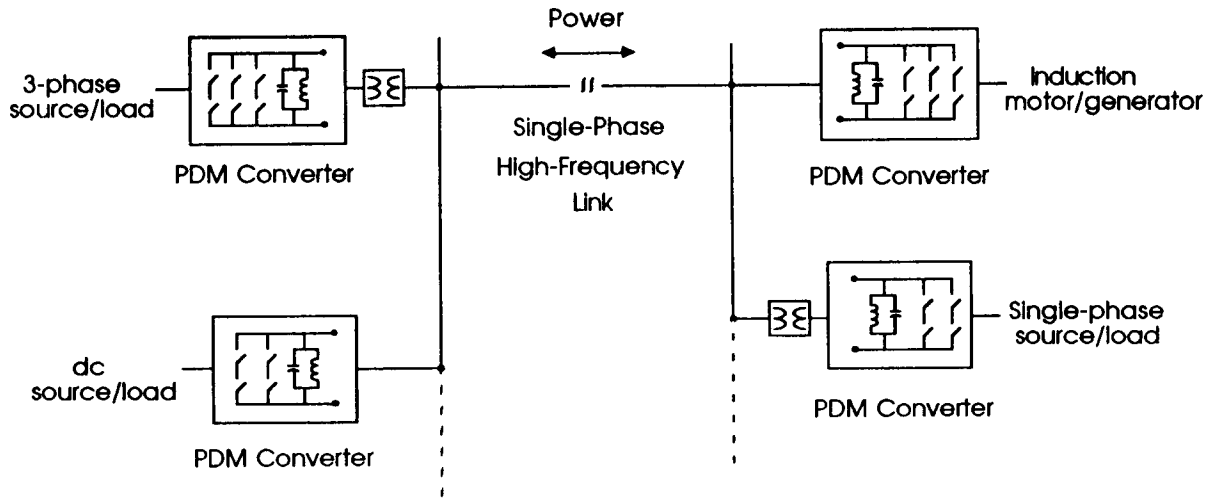

Figure 6.7: Proposed configuration of a high frequency link distributed power conversion system.

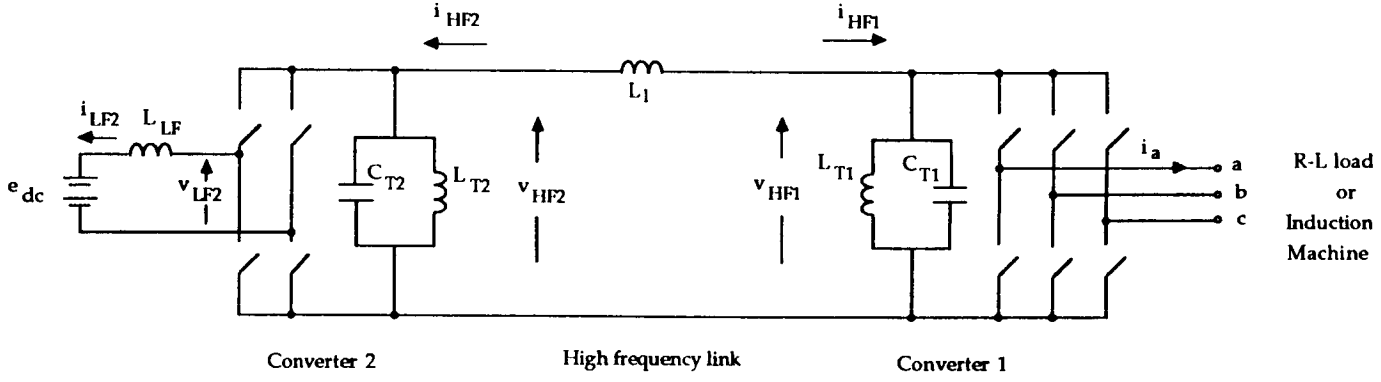

Figure 6.8: Reduced system configuration for modeling.

regulation (on a cycle-by-cycle basis) requires a temporary energy storage capacity in the exciter that is comparable to or larger than that of the tank filters. The energy storage in the exciter can be provided by a large electrolytic capacitor if a dc input exciter is used. Electrolytic capacitors are well suited to energy storage function due to their high energy storage densities, low losses and low cost. Exciter power circuit losses can be minimized by using resonant circuit topologies [1]. The Parallel Output Series Resonant (POSR) circuit of Chapter 3 is one example of such topologies.

The system described in Fig. 6.8 was first operated with a dedicated exciter. For this reduced system, average power flow balance is straight forward. The average power on the link side of converter #1 was monitored and used as an input to a closed loop controller #2. With this implementation the exciter supplied the tank losses and maintained the link voltage amplitude (averaged over several cycles) to near its nominal value. The generation of current reference of converter #2 was then modified to include the link voltage amplitude control. Figure 6.10 shows the performance of the voltage peak detector that is used to realize the added voltage regulation function. Figure 6.11 shows the modified controller where a voltage control loop has been added. Figure 6.12 shows the system waveforms with the exciter removed and the link voltage regulated by the modified controller of Fig. 6.11. These waveforms show that with minor modification of the controller, the system can be operated without an exciter.

6.2.3 Effects of PDM Converter Operation on the Link.

It is useful to again consider the waveforms of Figure 6.6. In particular, note the waveform of the current reflected back to the link. This waveform is typical of the reflected current waveforms observed in zero voltage switching PDM converters and illustrates several key high-frequency-end characteristics of such converters. First, the polarity changes in the reflected current always coincide with the zero crossings of the link voltage. Thus, the variable phase angle associated with a phase-angle-controlled cycloconverter is not present. However, the magnitude and the polarity (with respect to the link voltage) of the current vary as a function of the PDM switching and the instantaneous value of the low frequency end current. It is clear that a mechanism for temporary energy storage is required at the link side of the converter so that the instantaneous power swings can be accommodated and so that the current drawn from the link can be made to correspond to average power flow conditions. DC voltage link converters have similar requirements and is, in fact, the role of the dc link capacitor in such systems.

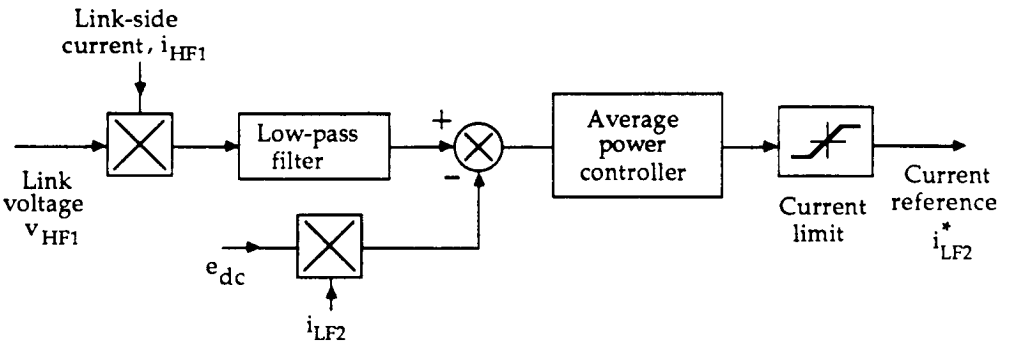

Figure 6.9: Controller for maintaining average power balance in the modeled system.

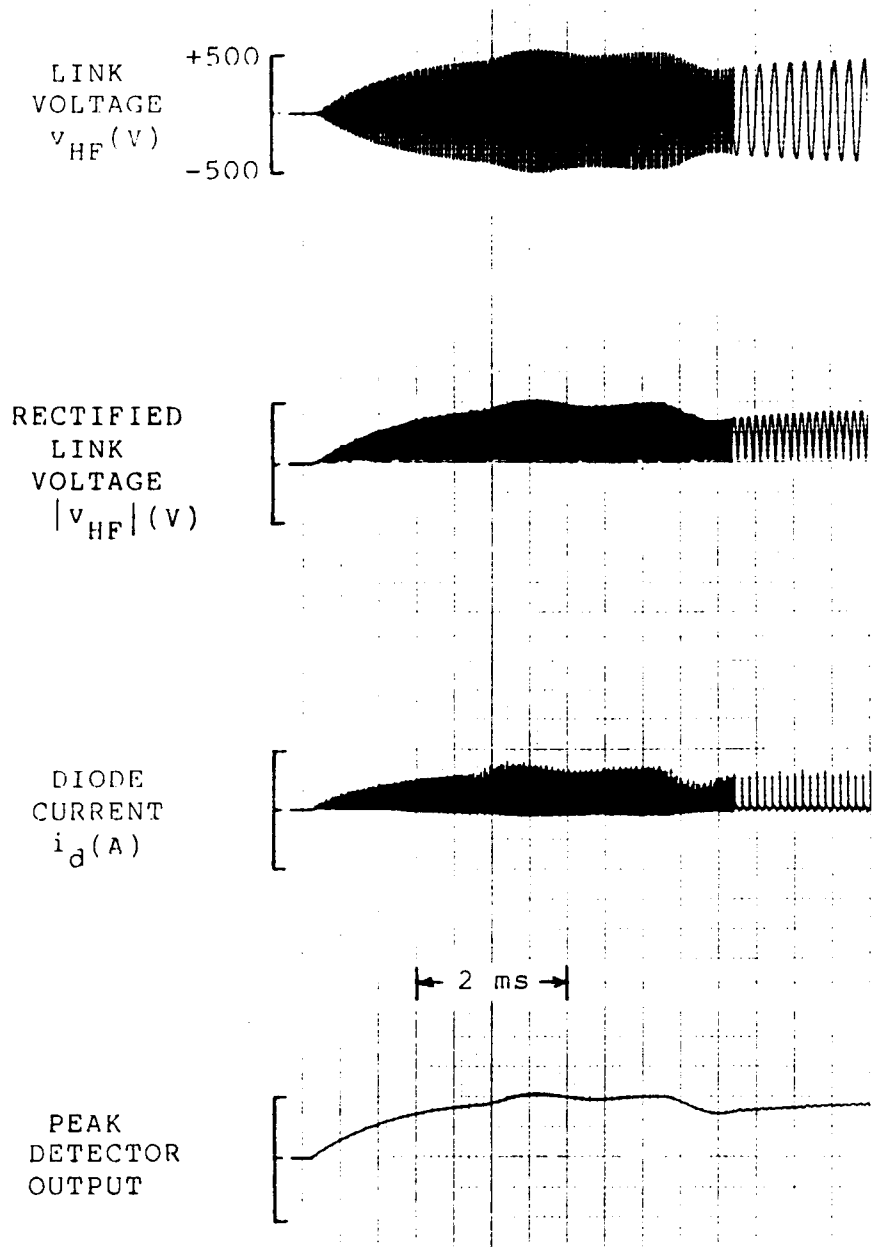

Figure 6.10: Waveforms showing the performance of the link peak voltage follower.

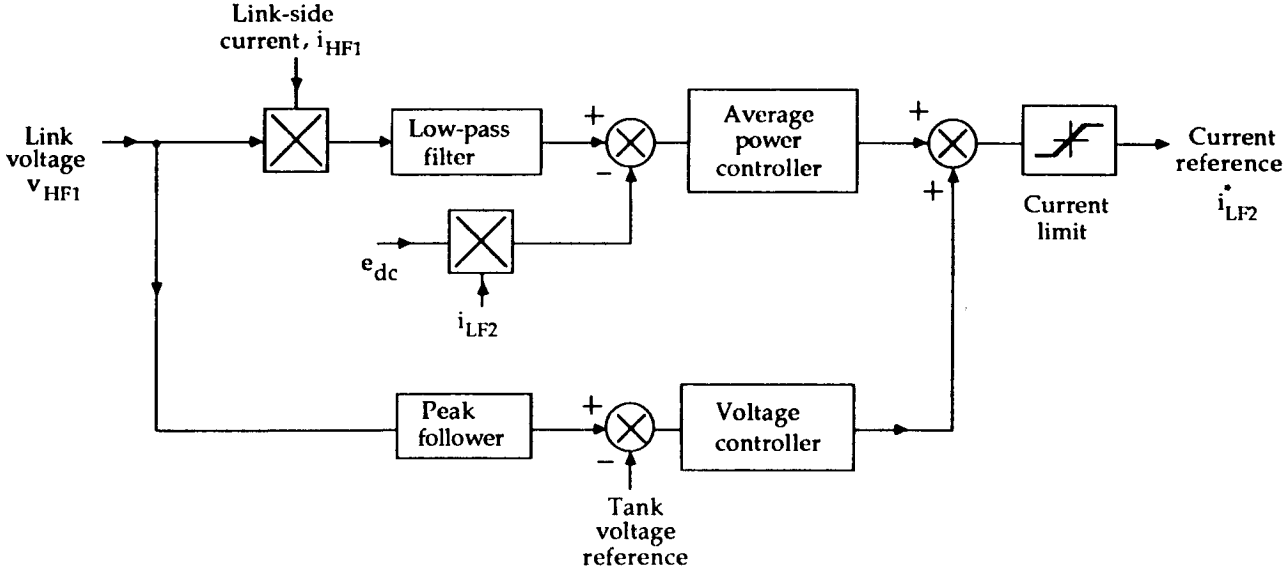

Figure 6.11: Block schematic of the modified link controller.

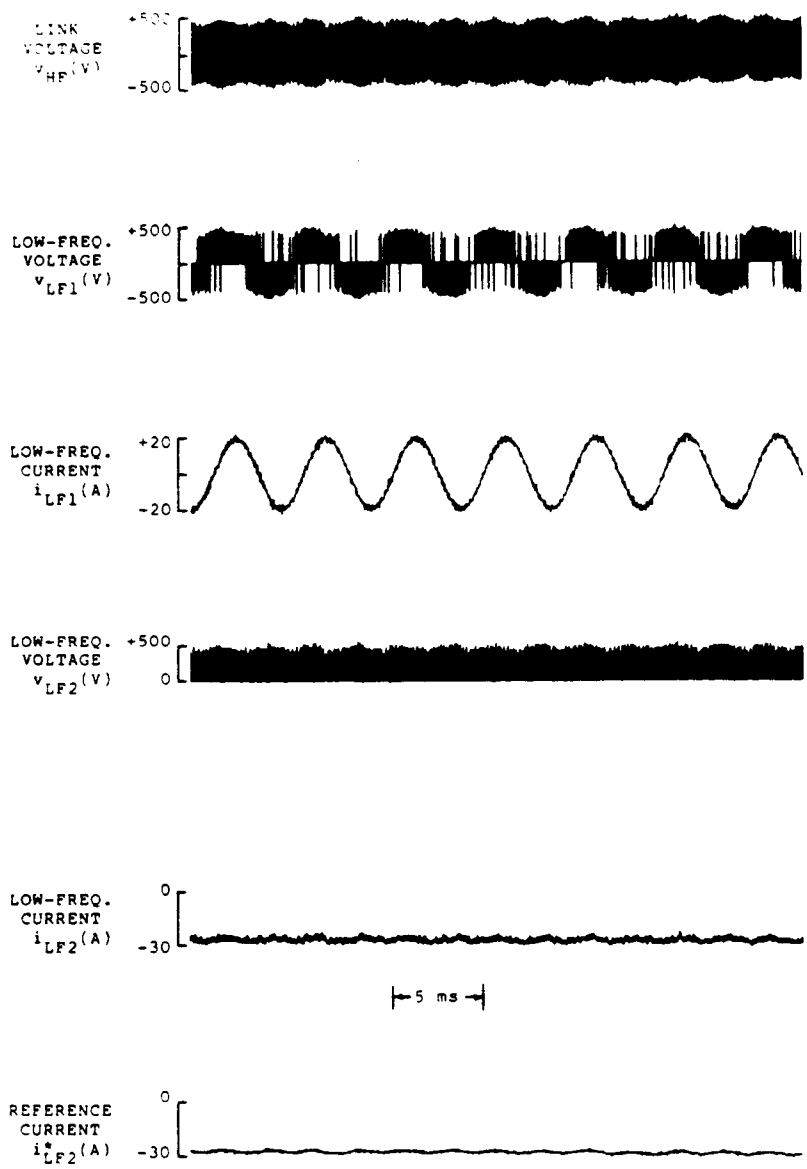

Figure 6.12: Waveforms showing system operation with the link controller of Fig. 6.11.

6.2.4 Link Filter.

A parallel connected LC tank circuit resonant at the frequency of the link plays the same role in an ac link system as the electrolytic capacitor in a dc link system. Once "charged", it offers high impedance to the currents of the link frequency and lower impedance to the currents of all other frequencies. By locating the capacitor of the tank circuit to close to the converter power circuit bus, the impedance seen by the high frequency components of the reflected currents is minimized so that they do not cause any significant distortion in the link voltage near its zero crossing points. The waveforms shown earlier in Fig. 6.6 were recorded with the presence of such a tank filter at the link side of the converter and demonstrate that a PDM converter is capable of handling the fast changing currents and the instantaneous power swings if a tank type filter is present on the ac side. It can be noted that the link voltage waveform and amplitude are still affected because of the desire to keep the the filter capacity small and minimize losses associated with the filter. How much filter capacity is adequate depends on such factors as the amount of "ripple" that can be tolerated on the link, the power circuit topology, the implementation of PDM technique (i.e.three- or two-level synthesis etc.), the number of PDM converters operating from the link, and the frequency characteristics of the link impedance, etc. It appears that a capacity of 3 to 5 times the peak low frequency current may be required if none of these factors are favorable. Investigation into alternate topologies and optimization of capacities of these filters is recommended as among the areas of further study.

6.3 Effect of the Link Voltage "Ripple".

While the resonant LC tank removes the large majority of the ripple in the ac link a small amount of ripple remains. In particular, note the link voltage "ripple" in the waveforms of Fig. 4.10 and again in Fig. 6.12. Note also, however, that the link voltage ripple has no noticable effect on the fundamental component of the low-frequency synthesized current as seen from the resulting current waveforms. Similar results were observed on the laboratory breadboard. This reduced sensitivity to the link voltage variations is a direct result of the feedback mechanism of the AC-PDM controller which automatically compensates for changes in link voltage amplitude. Of course, if the link voltage variations are allowed to become excessive the PDM controller may saturate and then the synthesis of the fundamental component will clearly be affected. Excessive link voltage variations may also increase distortion in the synthesized voltage, cause device voltage overratings and result in excessive currents to flow from and to the filter. If excessive voltage variations are present, then some auxillary means of limiting the voltage swings (such as active voltage clamps) may be needed.

6.4 System Start Up.

It has been demonstrated that the system can be operated without an exciter once the link voltage is available to run individual converters as the PDM converters. However, the question remains as to how the link voltage is established in the first place. This situation is not unlike a dc link system having PWM type bi-directional converters on each end. In that system, some means of charging up the link capacitor is needed before the PWM converters can operate. By analogy, controlled "charging" of the tank filters is needed in the ac link system before the PDM converters can be brought into their normal operation. This controlled charging can be achieved through the bi-directional power circuit of the converter connected to a source. If a converter in the system is already programmed for dc current operation (as converter #2 in Fig. 6.8) from a dc emf then the start up is straight forward. The waveforms of Fig. 6.13 demonstrate the link voltage build-up using converter #2. In particular, a current is built up in the low-frequency side inductor by shorting the low frequency end of the converter. As this current approaches a predetermined value the switches are made to operate normally thus causing energy to transfer from the inductor to the link resonant tanks. The transition to PDM converter operation with synthesis of just enough current needed to sustain this voltage is automatic for this type of current controlled converter.

If none of the converters in the system are connected to, or can be switched to a dc emf, it may still be possible to start up the tanks from a low-frequency ac emf since at least, one source in the system is assumed. Hence, the slow changing emf amplitudes together with the bi-directional devices in the system can be viewed as simply an approximation of a dc emf supply. This aspect of system start up, however, needs to be studied further.

6.5 Characteristics of the Proposed System.

A power conversion system based on a high frequency (20 kHz) sinusoidal voltage link can be expected to have the following favorable characteristics. The features that can be attributed directly to the proposed PDM based configuration have been highlighted by the use of italics.

1. Flexibility of adjusting link voltage to meet diverse needs.
2. *Well suited to a modular system design.*
3. *High system efficiency due to one-step zero-voltage-switching power conversion.*

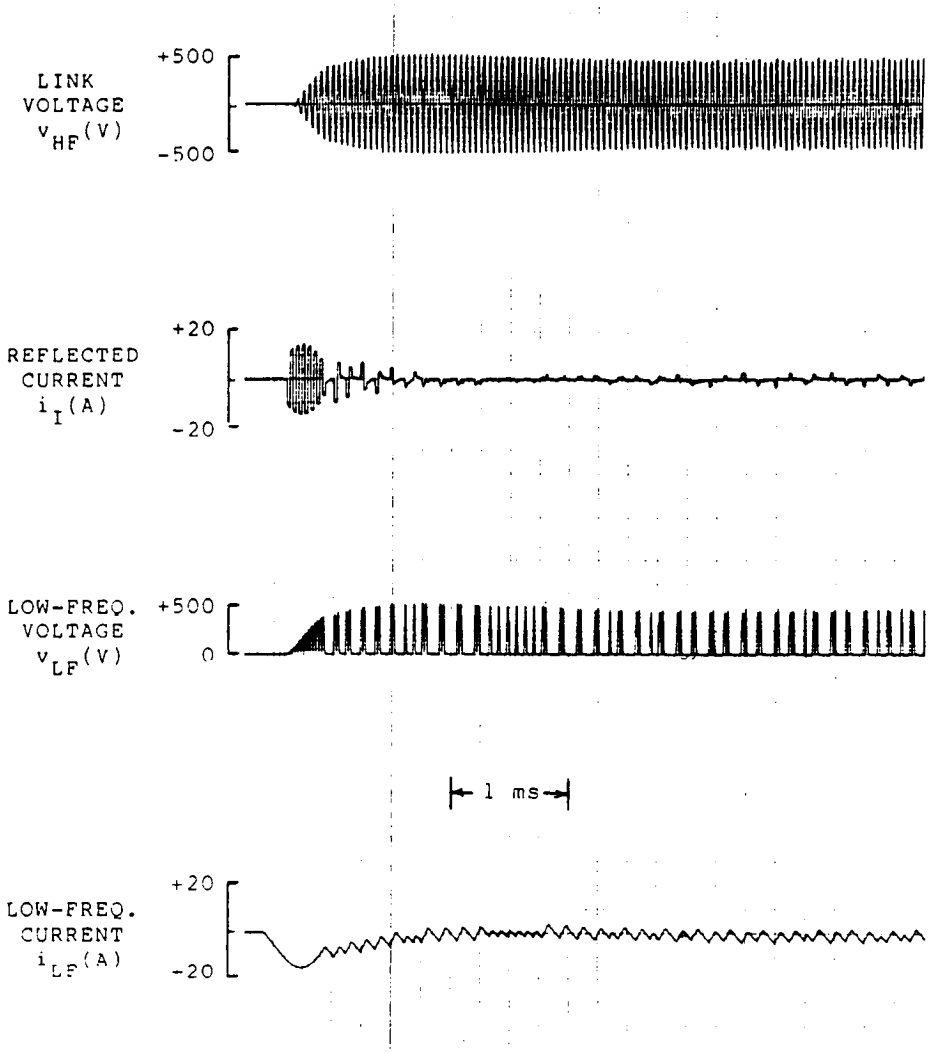

Figure 6.13: Waveforms showing link voltage build-up in the modeled system using converter #2.

4. *High degree of system uniformity that increases system reliability.*
5. Easy isolation of grounds for safety and for the reduction of electrical noise and crosstalk.
6. Easy and fast isolation of a faulty converter module.
7. Reduced system size and weight.
8. Added safety because of the energy limited characteristics and better human sensitivity at higher frequencies.
9. Faster system response.
10. Elimination of audible noise associated with the link frequency. *Reduction in audible noise associated with low frequencies synthesized with PDM.*
11. Accepts and delivers energy at low-frequencies but shifts the interference to higher frequencies.

6.6 References

1. R. L. Steigerwald, *High-frequency resonant transistor dc-dc converters*, IEEE Trans. Ind. Elect., vol. IE-31, pp. 181-191, May 1984.

Chapter 7

Conclusions and Suggestions for Further Work

7.1 Conclusions

In this report a static power conversion system based on a high-frequency voltage link has been proposed. The system uses a single-phase 20 kHz sinusoidal voltage link for power conversion and temporary energy storage. Choice of a high frequency ac link permits the use of link side trasformers for voltage matching, to operate section(s) of the system at higher (or lower) voltage levels, and to obtain electrical isolation for safety or noise suppression purposes without compromising system size and weight. Zero voltage switching pulse-density-modulated (PDM) converters have been proposed for one-step interfacing of system sources and load to the link. Zero voltage switching prevents high switching losses, excessive device stresses during switching, or high values of dv/dt's in the generated waveforms but allows benefits of high speed switching such as high converter bandwidths, high maximum frequencies in generated waveforms, reduction of low frequency distortion, fast and easy isolation of faulty converters, and others. Thus, the combination of ac link power distribution and high speed switching gives the proposed system a unique set of system characteristics which are summarized below.

- A modular, utility type system capable of handling a wide variety of loads/sources having wide ranging voltage level requirements.
- Easy isolation of grounds for safety and/or noise reduction and isolation.
- High system efficiency due to one-step zero-voltage-switching power conversion.

- A high degree of uniformity and somewhat increased reliability in the system due to the use of one basic type of interface converter.
- Easy and fast isolation of a faulty converter module.
- A very compact and light weight system.
- Added safety because of the energy limited characteristics and reduced human sensitivity to the 20 kHz link frequency.
- Faster system response.
- Elimination of audible noise associated with the link frequency. Reduction in audible noise associated with low frequencies synthesized with PDM.
- Capability to accept and deliver power at low-frequencies but relagate interference to higher frequencies.

This research has shown that zero-voltage switching permits power converters to operate directly off a high frequency link without incurring high switching losses or excessive device stresses. Theoretical and experimental work have both demonstrated that pulse-density-modulation is a very effective technique for providing zero-voltage switching converters with a control over frequency, amplitude and the waveshape of the fundamental component. As a result, a whole class of power converters are possible that can interface dc or ac, single- or three-phase, voltage or current type loads/sources to the link with one-step power conversion and with inherent capability of bi-directional power flow. Operation of a three-phase bridge PDM converter with a three-phase induction machine has demonstrated that:

- A PDM converter operating directly from a high frequency link is able to control induction machine in both motoring or generation mode.
- Machine voltage or currents do not have troublesome lower order harmonics. Adequate filtering of the high frequency ripple caused by the PDM converter is done by the machine itself. Thus, no filters are needed between the PDM converter output and the machine.
- With adequate filters on the ac link side, frequency, amplitude or the waveshape of the link voltage is not adversely affected with machine operation.
- Quick and frequent torque reversals needed for actuator control appear to be achievable without any difficulty.

Computer studies and the data from the breadboard have helped identify the following salient characteristics of the proposed PDM converters.

- One-stage power processing.
- Low switching losses.
- Inherent bi-directional power flow capability.
- Low distortion synthesis to 1000 Hz (from a 20 kHz or higher frequency link).
- Adaptable to voltage or current control and single- or three-phase loads/sources.
- Capability of fast response needed for actuator control.
- Power circuit equivalence with the dc link bridge topology resulting in a system which is easier to understand and apply.
- Control through simple to implement pulse-density-modulation scheme.

7.2 Suggestions for Further Work

Flexibility and scope of the proposed high frequency link configuration is such that considerable opportunities exist for further work in this area. Some of the promising areas have been identified below.

7.2.1 Active Energy Storage in the Link.

It has been shown that POSR converter can be used for temporary energy storage in the system. Further work is needed to evaluate the effectiveness (in terms of cost, losses, voltage swings on the link, etc) of this and other circuit topolgies for active energy storage with or without additional passive energy storage (such as LC tanks) in the system.

7.2.2 Alternate PDM Circuit Topologies.

Alternate power circuits for PDM converter should be studied and compared with the strategies identified and studied in this research. For example, a three-converter topology (Fig.

5.1(a)) was identified for three phase PDM converters. It remains necessary to determine if this topology would produce smaller variations of the instantaneous power on the link side of the converter or has other features which are superior to the bridge PDM circuit that has been studied thus far.

7.2.3 Study of Switching Strategies.

The study of the switching strategies for zero voltage converters initiated in this research should be continued. In particular, the pulse-density-modulation technique needs to be examined further in order to fully understand the characteristics of this type of controller. In addition, alternate implementations of PDM (as illustrated in Fig. 5.11) need to be characterized for their effect on the variations of instantaneous power at the link side of the converter. The objective should ultimately be to minimize the overall requirements of temporary energy storage in the system.

7.2.4 Alternate Filter Configurations.

A parallel tank circuit tuned to the link frequency has been shown to be an effective filter topology for PDM converters. However, further work is needed to investigate if alternate topologies (for example, with an additional series branch on the link side) are capable of better performance (measured in terms of reduced circulating current, increased decoupling, etc.)

7.2.5 Application to Dedicated Power Conversion Systems.

Applications identified in Chapter 1 should be studied in greater detail. In particular, application of the proposed high frequency link approach to specific power conversion functions should studied further with industrial applications in mind. Such reduced order systems are easier to implement and afford optimizations specific to the system to be incorporated. Of particular promise are areas of uniterruptable power supplies and alternate energy power generation.

7.2.6 Further Experimental Work.

As planned, the laboratory system should be expanded to include a second PDM converter. This capability would allow full bi-directional power flow capability in the system. This capability that has already been shown to be feasible in the computer simulations carried out as a part of the work reported herein. The expanded breadboard can then be used for experimental verification of induction machine operation with fast, bi-directional control of torque as needed for actuator type applications. Sustained reverse power operation as required for interfacing induction generators to the link should also be experimentally demonstrated. Experimental system can be used for development of suitable control strategies in each case. Characterization of power devices and other power components required in high frequency link systems is another area suitable for experimental work.

Chapter 8

Selected Bibliography

This bibliography is organized by broad subject categories relevant to this report. Within these categories, the listings are in alphabetical order. A reference that discusses more than on subject category is classified on the basis of its primary topic of discussion and listed under the category that represent the best fit.

A. AC Link Distributed Power Systems

[A.1] P. M. Espelage and B. K. Bose, *High-frequency link power conversion*, IEEE Trans. Ind. Appl., vol. IA-13. pp. 387-394, Sept./Oct. 1977.

[A.2] L. Gyugyi and F. Cibulka, *The high-frequency base converter - A new approach to static high-power conversion*, IEEE Trans. Ind. Appl., vol. IA-15, pp. 420-429, July/Aug. 1979.

[A.3] I.G. Hansen, *Description of a 20 kilohertz power distribution system*, 21st Intersociety Energy Conversion Engineering Conference (IECEC), San Diego, Aug., 1986.

[A.4] T. A. Lipo and P. K. Sood, *Study of the generator/motor operation of induction machines in a high frequency link space power system*, NASA report. Contract no. NAG3-631, Sept. 1986.

[A.5] J. Mildice and L. Wappes, *Resonant ac power system proof-of- concept*, NASA CR-175069, 1986.

[A.6] P. K. Sood and T. A. Lipo, *Power conversion distribution system using a resonant high-frequency ac link*, Conf. Rec. 1986 Annu. Meet. IEEE Ind. Appl. Soc., pp. 533-541.

B. Dedicated High Frequency link Systems

[B.1] H. Huisman and S. W. H. de Haan, *A dc to 3-phase series resonant converter with low harmonic distortion*, IEEE Trans. Ind. Electron., vol. IE-32, pp. 142-149, May 1985.

[B.2] J. B. Klaasens, *DC to AC series-resonant converter system with high internal frequency generating synthesized waveforms for multikilowatt power levels*, in Conf. Rec. IEEE Power Electronics Specialists Conf., Gaithersburg, MD, June 1984.

[B.3] R. Myers and R. D. Peck, *200-kHz power FET technology in new modular power supplies*, Hewlett-Packard Journal, pp. 3-10, August 1981.

[B.4] V. T. Ranganathan, P. D. Ziogas and V. R. Stefanovic, *A dc-ac power conversion technique using twin resonant high-frequency links*, IEEE Trans. Ind. Appl., vol. IA-19, pp. 393-400, May/June 1983.

[B.5] V. T. Ranganathan, P. D. Ziogas and V. R. Stefanovic, *Performance characteristics of high frequency links under forward and regenerative power flow conditions*, Conf. Rec. 1983 IEEE Ind. Appl. Soc. Annual Meeting, pp. 831-837.

[B.6] F. C. Schwartz, *An improved method of resonant current pulse modulation for power converters*, IEEE Trans. Ind. Electron. Cont. Inst., vol. IECI-23, pp. 133-141, May 1976.

[B.7] F. C. Schwartz, *A double sided cycloconverter*, IEEE Trans. Ind. Electron. Cont. Inst., vol. IECI-28, pp. 282-291, November 1981.

[B.8] F. C. Schwartz and W. L. F. U. A. Moize de Chateleux, *A multikilowatt polyphase ac/dc converter with reversible power flow and without passive low-frequency filter*, IEEE Trans. Ind. Electron. Cont. Inst., vol. IECI-28, pp. 273-281, November 1981.

C. High Frequency Converters

[C.1] D. M. Divan, *The resonant dc link converter - a new concept in static power conversion*, Conf. Rec. 1986 Annu. Meet. IEEE Ind. Appl. Soc., pp. 648-655.

[C.2] J. G. Kassakian, *A new current mode sine wave inverter*, IEEE Trans. Ind. Appl., vol. IA-18, pp. 273-278, May/June 1982.

[C.3] J. G. Kassakian, A. F. Goldgerg and D. R. Moretti, *A comparative evaluation of series and parallel structures for high frequency transistor inverters*, in Conf. Rec. 1982 Annual Meeting IEEE Power Electronics Specialist's Conf., pp. 20-26.

[C.4] R. J. King and T. A. Stuart, *Modelling the full-bridge series resonant converter*, IEEE Trans. Aerosp. Electron. Syst., vol. AES-18, pp. 449-459, July 1982.

[C.5] K. H. Liu and F. C. Lee, *Zero voltage switching technique in DC/DC converters*, in Conf. Rec. 1986 Annual Meeting IEEE Power Electronics Specialist's Conf., pp. 58-70.

[C.6] N. Mapham, *An SCR inverter with good regulation and sine-wave output*, IEEE Trans. Ind. Gen. Appl., vol. IGA-3, pp. 176-187, Mar./Apr. 1967.

[C.7] T. Natarajan, *An evaluation of inverter topologies for high power spacecraft*, 21st Intersociety Energy Conversion Engineering Conference (IECEC), San Diego, Aug., 1986.

[C.8] B. R. Pelly, *Latest developments in static high frequency power sources for induction heating*, IEEE Trans. Ind. Electron. Contr. Instrum., vol. IECI-17, pp. 297-312, June 1970.

[C.9] S. D. T. Robertson and K. M. Hebbar, *A variable low frequency inverter using thyristors*, IEEE Trans. Ind. Gen. Appl., vol. IGA-4, pp. 501-507, Sept./Oct. 1968.

[C.10] R. R. Robson and D. J. Hancock, *A 10 kW series resonant converter design, transistor characterisation and base drive optimization*, in Conf. Rec. 1982 Power Elect. Spec. Conf. (PESC-82), pp. 33-44.

[C.11] P. Savary, M. Nakaoka and T. Maruhashi, *Resonant vector control base high frequency inverters*, in Conf. Rec. 1985 Annual Meeting IEEE Power Electronics Specialist's Conf., pp. 204-213.

[C.12] P. K. Sood and T. A. Lipo, *A versatile power converter for high frequency link systems*, to be published in Conf. Proc. of forthcoming IEEE Appl. Power Elect. Conf. (APEC'87), March 1987.

[C.13] R. L. Steigerwald, *High-frequency resonant transistor dc-dc converters*, IEEE Trans. Ind. Elect., vol. IE-31, pp. 181-191, May 1984.

[C.14] V. Vorperian and S. Cuk, *Small signal analysis of resonant converters*, Conf. Rec. 14th Annual IEEE Power Electronics Specialists Conference, PESC 1983.

[C.15] P. D. Ziogas, V. T. Ranganathan and V. R. Stefanovic, *A four-quadrant current regulated converter with a high-frequency link*, IEEE Trans. Ind. Appl., vol. IA-18. pp. 499-506, Sept./Oct. 1982.

D. Modulation Techniques

[D.1] M. Boost and P. D. Ziogas, *State of the art PWM techniques: a critical evaluation*, in Conf. Rec. 1986 Annual IEEE Power Electronics Specialist's Conference, pp. 425-433.

[D.2] S. W. H. De Haan, *A new integral pulse module for the series-resonant converter*, IEEE Trans. Ind. Elect., vol. IE-31, pp. 255-262, Aug. 1984.

[D.3] M. A. Rahman, J. E. Quaicoe and M. A. Choudhury, *An optimum delta modulation strategy for inverter operation*, in Conf. Rec. 1986 Annual IEEE Power Electronics Specialist's Conference, pp. 410-416.

[D.4] H. R. Schindler, *Delta modulation*, IEEE Spectrum, vol. 7, pp. 69-78, Oct. 1970.

[D.5] F. C. Schwarz, *An improved method of resonant current pulse modulation of power coverters*, IEEE Trans. Ind. Electron. Contr. Instrum., vol. IECI-23, pp. 133-141, May 1976.

[D.6] R. Steele, *Delta Modulation Systems*, New York: Halsted Press, 1975. .bibitem[D.7] P. Wood, *Switching power converters*. New York : Van Nostrand Reinhold Company, 1981.

[D.8] P. D. Ziogas, *The delta modulation technique in static PWM inverters*, IEEE Trans. Ind. Appl., vol IA-17, pp. 199-204, March/April 1981.

E. Power Devices for High-Power High-Frequency Switching

[E.1] W. Bosterling et al, *Asymetrical thyristors for switching frquencies above 20 kHz*, in Conf. Rec. 1986 Annual Meeting IEEE Ind. Appl. Soc., pp. 362-365.

[E.2] M. M. Jovanovic, F. C. Lee and D. Y. Chen, *Characterization of high-power BJTs for motor-drive applications*, in Conf. Rec. 1986 Annual IEEE Power Electronics Specialist's Conference, pp. 413-419.

[E.3] K. Muraoka et. al., *Characteristics of the high speed SI thyristor and its application at the 60 kHz, 100 kW and the efficiency of more than 90% inverter*, in Conf. Rec. 1986 Annual IEEE Power Electronics Specialist's Conference, pp. 94-103.

[E.4] J. Nishizawa et. al., *Low-loss high-speed switching devices, 2300-V 150-A static induction thyristors*, IEEE Trans. Electron Devices, vol. ED-32, pp.882, 1985.

[E.5] B. Thomas, D. Silber and H. Berg, *Progress in GTO's for industrial line inverter applications*, in Conf. Rec. 1985 Annual Meeting IEEE Ind. Appl. Soc., pp. 882-888.

[E.6] W. F. Wirth, *High speed, snubberless operation of GTO's using a new gate drive technique*, in Conf. Rec. 1986 Annual IEEE Power Electronics Specialist's Conference, pp. 453-457.

[E.7] H. Yilmaz et. al., *Comparison of the punch through and non-punch through IGT structures*, Conf. Rec. 1985 Annual Meeting IEEE Ind. Appl. Soc., pp. 905-908.

F. Components of High Frequency Link System

[F.1] M. R. Patel, *High frequency power distribution system*, NASA CR-175071, April 1986.

[F.2] R. L. Steigerwald and R. E. Tompkins, *A comparison of high frequency link schemes for interfacing a dc source to a utility grid*, in Conf. Rec. 1982 Annual Meeting IEEE Ind. Appl. Soc., pp. 759-766.

[F.3] J. P. Welsh, *Design and development of multi-Kilowatt power electronic transformer*, NASA CR-168082, 1983.

G. Application of High Frequency Power Distribution

[G.1] A. F. Forestieri and C. R. Baraona, *Space station power system*, IEEE Trans. Aero. and Elect. Sys., vol. AES-20, pp. 666-670, Nov. 1984.

[G.2] I. G. Hansen and F. J. Wolff, *20 kilohertz space station power system*, Conf. Rec. 19th Annul. Electronics and Aerospace Conf., Washington, D.C., Sept. 1986.

[G.3] I.G. Hansen and G.R. Sundberg, *Space station 20-kHz power management and distribution system*, 1986 Power Electronics Specialist's Conference, Vancouver, Canada, June 23-27, 1986.

[G.4] W. W. Howison and G. W. Zumwalt, *Electroninc/electric technology benefit study*, NASA CR-165890, 1982.

[G.5] A. C. Hoffman, I. G. Hansen, R. F. Beach, et. al., *Advanced secondary power system for transport aircraft*, NASA technical paper 2463, 1985.

[G.6] R. R. Rice, *Space Station Power System Selection*, 21st Intersociety Energy Conversion Engineering Conference (IECEC), San Diego, CA, Aug., 1986.

Appendix A

An Induction Machine Model with Saturable Main Flux

When induction machines are operated from power converters, it is often necessary to study behavior of the machine under transient and variable speed conditions so that converter-machine interactions can be studied adequately. Differential equations which describe the machine behavior under these dynamic conditions involve time-varying coefficients due to the relative motion of the rotor with respect to the stator. Fortunately, this problem can be resolved by transforming both the stator and rotor variables to a common reference frame. These transformed equations, called Stanely's equations, form the basis of induction machine modelling.

Machine models based on Stanely's equations have been developed and used for many years. However, saturation of the main flux in the machine is often neglected in the development of these models. This is a good compromise when the main flux saturation is known to be small or a minimal model is desired even at the cost of some accuracy. If the induction machine is to be operated as a generator then incorporating the main flux saturation is generally desirable. This is because for a given terminal voltage, the machine operates with higher levels of main flux when operating as a generator. In addition, if the generator operation is of self-excited type then the conventional model with unsaturable main flux cannnot be used at all.

This appendix describes the development and verification of a model for an induction machine which incorporates the saturation of the main flux. A simple modification allows this general model to be reduced to the special case of the conventional model with unsaturable main flux.

A.1 Development of the Model

The starting point for deriving a machine model are the machine equations transformed to an orthogonal $d-q-n$ reference frame, rotating at an unspecified angular speed ω, the so called *arbitrary reference frame*. The transformation of the machine equations from their phase variable form (with rotor position dependent inductances) to this generalized reference frame has been adequately described in the literature, e.g. [1]. The transformation used is summarized by the following matrix representation.

$$f_{qdn} = [\,T(\theta)\,]\, f_{abc} \tag{A.1}$$

where

$$[\,T(\theta)\,] = \frac{2}{3}\begin{bmatrix} \cos(\theta) & \cos(\theta - 2\pi/3) & \cos(\theta + 2\pi/3) \\ \sin(\theta) & \sin(\theta - 2\pi/3) & \sin(\theta + 2\pi/3) \\ 1/\sqrt{2} & 1/\sqrt{2} & 1/\sqrt{2} \end{bmatrix} \tag{A.2}$$

and $\theta = \int \omega\ dt + \theta_0$. The vector f represents voltage, current or flux quantities.

The transformed equations are of the form

$$v_{qs} = r_s i_{qs} + p\lambda_{qs} + \omega\lambda_{ds} \tag{A.3}$$

$$v_{ds} = r_s i_{ds} + p\lambda_{ds} - \omega\lambda_{qs} \tag{A.4}$$

$$v_{ns} = r_s i_{ns} + p\lambda_{ns} \tag{A.5}$$

$$v'_{qr} = r'_r i'_{qr} + p\lambda'_{qr} + (\omega - \omega_r)\lambda'_{dr} \tag{A.6}$$

$$v'_{dr} = r'_r i'_{dr} + p\lambda_{dr} - (\omega - \omega_r)\lambda'_{qr} \tag{A.7}$$

$$v'_{nr} = r'_r \beta i'_{nr} + p\lambda'_{nr} \tag{A.8}$$

where $p = d/dt$, ω_r is the rotor speed, ω is the angular speed of the rotating $d-q$ axes and the primes denote rotor quantities referred to stator. The flux linkages above are related to currents in the following manner

$$\lambda_{qs} = L_{ls} i_{qs} + \lambda_{mq} \tag{A.9}$$

$$\lambda_{ds} = L_{ls} i_{ds} + \lambda_{md} \tag{A.10}$$

$$\lambda_{ns} = L_{ls} i_{ns} \tag{A.11}$$

$$\lambda'_{qr} = L'_{lr} i'_{qr} + \lambda_{mq} \tag{A.12}$$

$$\lambda'_{dr} = L'_{lr} i'_{dr} + \lambda_{md} \tag{A.13}$$

$$\lambda'_{nr} = L'_{lr} i'_{nr} \tag{A.14}$$

$$\lambda_{mq} = L_m (i_{qs} + i'_{qr}) \tag{A.15}$$

$$\lambda_{md} = L_m (i_{ds} + i'_{dr}) \tag{A.16}$$

where L_{dm} is the magnetizing inductance which in general is flux dependent. Equations (A.8) to (A.12) can be rewritten to express currents in terms of the flux linkages. For example

$$i_{qs} = \frac{(\lambda_{qs} - \lambda_{mq})}{L_{ls}} \tag{A.17}$$

Using (A.16) and similar expressions for the other current terms, currents can be eliminated from (A.2) to (A.7). The resulting equations are written in terms of reactances and modified flux linkages, e.g. $X_{ls} = \omega_b L_{ls}$ and $\psi_{qs} = \omega_b \lambda_{qs}$ where ω_b is the base angular speed of the system. Note that the modified flux linkages have units of voltage.

$$v_{qs} = \frac{r_s}{X_{ls}} (\psi_{qs} - \psi_{mq}) + \frac{p}{\omega_b} \psi_{qs} + \frac{\omega}{\omega_b} \psi_{ds} \tag{A.18}$$

$$v_{ds} = \frac{r_s}{X_{ls}} (\psi_{ds} - \psi_{md}) + \frac{p}{\omega_b} \psi_{ds} - \frac{\omega}{\omega_b} \psi_{qs} \tag{A.19}$$

$$v_{ns} = \frac{r_s}{X_{ls}} \psi_{ns} + \frac{p}{\omega_b} \psi_{ns} \tag{A.20}$$

$$v'_{qr} = \frac{r'_r}{X'_{lr}} (\psi'_{qr} - \psi_{mq}) + \frac{p}{\omega_b} \psi_{qr'} + \frac{(\omega - \omega_r)}{\omega_b} \psi'_{dr} \tag{A.21}$$

$$v'_{dr} = \frac{r'_r}{X'_{lr}} (\psi'_{dr} - \psi_{md}) + \frac{p}{\omega_b} \psi'_{dr} - \frac{(\omega - \omega_r)}{\omega_b} \psi'_{qr} \tag{A.22}$$

$$v'_{nr} = \frac{r'_r}{X'_{lr}} \psi'_{nr} + \frac{p}{\omega_b} \psi'_{nr} \tag{A.23}$$

When (A.17) to (A.22) are specialized to a stationary reference frame, i.e. $\omega = 0$, and rewritten in integral form suitable for analog simulation, they take the form

$$\psi_{qs} = \int [\omega_b v_{qs} - \frac{\omega_b r_s}{X_{ls}} (\psi_{qs} - \psi_{mq})] \, dt \tag{A.24}$$

$$\psi_{ds} = \int [\omega_b v_{ds} - \frac{\omega_b r_s}{X_{ls}} (\psi_{ds} - \psi_{md})] \, dt \tag{A.25}$$

$$\psi_{ns} = \int [\omega_b v_{ns} - \frac{\omega_b r_s}{X_{ls}} \psi_{ns}] \, dt \tag{A.26}$$

$$\psi'_{qr} = \int [\omega_b v'_{qr} - \frac{\omega_b r'_r}{X'_{lr}} (\psi'_{qr} - \psi_{mq}) + \omega_r \psi'_{dr}] \, dt \tag{A.27}$$

$$\psi'_{dr} = \int [\omega_b v'_{dr} - \frac{\omega_b r'_r}{X'_{lr}} (\psi'_{dr} - \psi_{md}) - \omega_r \psi'_{qr}] \, dt \tag{A.28}$$

$$\psi'_{nr} = \int [\omega_b v'_{nr} - \frac{\omega_b r'_r}{X'_{lr}} \psi'_{nr}] \, dt \tag{A.29}$$

The per unit shaft speed ω_r / ω_b may be treated as an independent variable in case of generator operation. Motor operation, however, requires the solution of the following equations

$$\frac{\omega_r}{\omega_b} = \frac{1}{J\omega_b}\int (T_e - T_l)\, dt \tag{A.30}$$

$$T_e = (\frac{3p}{4\omega_b})(\psi_{ds}i_{qs} - \psi_{qs}i_{ds}) \tag{A.31}$$

The quantities T_e and T_l are the electromegnetic and load torque respectively. J is the inertia associted with the shaft.

The voltages in (A.23) to (A.28) may either be specified *a priori* as in the case of motor operation or generator operation with impressed voltages, e.g. line excited or converter excited generator or it may come from an generator exciter model. This leaves the air-gap flux components, ψ_{mq} and ψ_{md} to be determined in order to solve (A.23) to (A.28). Lipo and Consoli [A.2] have shown a method for calculating the instantaneous values of these flux components using the air-gap saturation characteristics of the machine. The method utilizes a flux dependent saturation function defined as

$$K_m(\hat{\psi}_m) = \frac{(\hat{\psi}_m - \psi_m)}{\hat{\psi}_m} \tag{A.32}$$

where ψ_m and $\hat{\psi}_m$ are the total air-gap flux linkages in the machine with and without saturation.

Figure A.1 illustrates the method used by Lipo and Consoli for obtaining the saturation function K_m from experimentally determined machine terminal characteristics at no load. First, the air-gap characteristics are derived from the terminal characteristics by accounting for the stator leakage drop. The linear portion of this curve determines the unsaturated value of the magnetizing reactance, $\hat{X}_m$. Then for each value of the unsaturated flux linkage, $\hat{\psi}_m = \hat{X}_m i$ the saturation function is computed using (A.2) and plotted against $\hat{\psi}_m$ as shown. The deviation from the linear characteristics, indicated by a nonzero value of K_m, is seen both at the high and very low flux levels. The saturation function can be modelled using curve fitting techniques. When only analog components are available, a limited number of linear segments may be used to approximate K_m. Also, if the excitation build up mechanism is not under study, then further simplification is achieved by ignoring the low flux values of K_m. Figure A.2 shows an implementation using analog components that approximates the saturation function in the high flux region using two linear segments.

To use the saturation function in the calculation of the actual values of flux components assume, first, that their unsaturated values are known. Then the total unsaturated value of the air-gap flux is given as

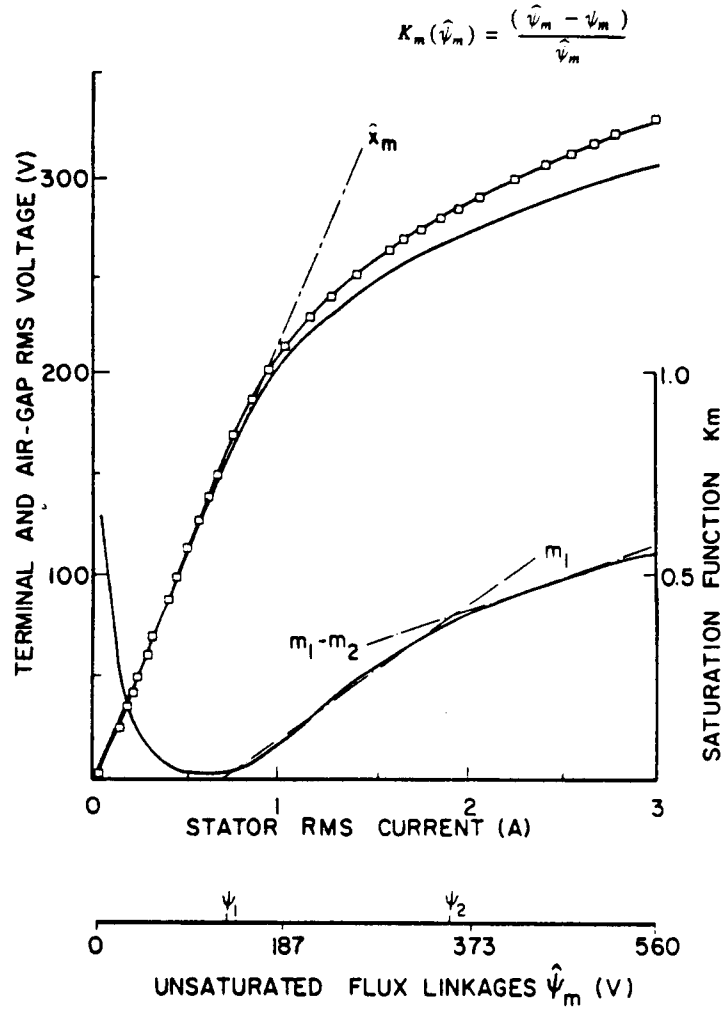

Figure A.1: Derivation of the saturation function $K_m(\hat{\psi}_m)$ from the no load terminal characteristics of the machine.

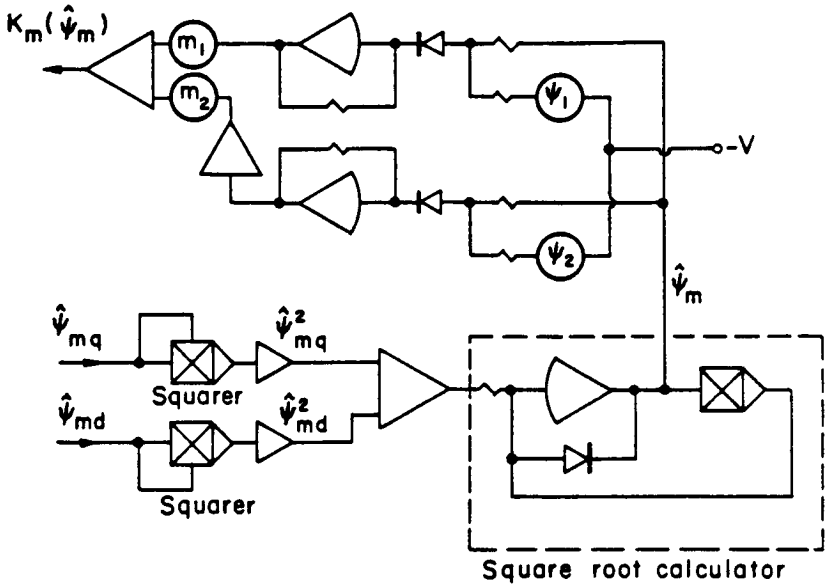

Figure A.2: Two-segment analog approximation of the saturation function in the high flux region.

$$\hat{\psi}_m = \sqrt{\hat{\psi}_{mq}^2 + \hat{\psi}_{md}^2} \tag{A.33}$$

Since K_m is known as a function of $\hat{\psi}_m$ then

$$\Delta\psi_{mq} = \hat{\psi}_{mq} - \psi_{mq} = K_m(\hat{\psi}_m)\,\hat{\psi}_{mq} \tag{A.34}$$

then

$$\psi_{mq} = \hat{\psi}_{mq} - \Delta\psi_{mq} \tag{A.35}$$

This form of (A.33) and (A.34) is particularly convenient for hybrid computer simulation. Similarly for the $d-$ axis

$$\Delta\psi_{md} = \hat{\psi}_{md} - \psi_{md} = K_m(\hat{\psi}_m)\,\hat{\psi}_{md} \tag{A.36}$$

$$\psi_{md} = \hat{\psi}_{md} - \Delta\psi_{md} \tag{A.37}$$

Expressions for the unsaturated values of the flux components, assumed above as known, can now be derived as follows. By definition

$$\hat{\psi}_{mq} = \hat{X}_m(\, i_{qs} + i'_{qr}\,) \tag{A.38}$$

But from (A.16) and (A.34)

$$i_{qs} = \frac{\psi_{qs} - (\,\hat{\psi}_{mq} - \Delta\psi_{mq}\,)}{X_{ls}} \tag{A.39}$$

and similarly

$$i'_{qr} = \frac{\psi'_{qr} - (\,\hat{\psi}_{mq} - \Delta\psi_{mq}\,)}{X'_{lr}} \tag{A.40}$$

substituting for currents in (A.37) and rearranging

$$\psi_{mq} = \frac{\tilde{X}}{X_{ls}} \psi_{qs} + \frac{\tilde{X}}{X'_{lr}} \psi'_{qr} + \tilde{X} \left(\frac{1}{X_{ls}} + \frac{1}{X'_{lr}} \right) \Delta\psi_{mq} \tag{A.41}$$

Similarly for the $d-$axis

$$\psi_{md} = \frac{\tilde{X}}{X_{ls}} \psi_{ds} + \frac{\tilde{X}}{X'_{lr}} \psi'_{dr} + \tilde{X} \left(\frac{1}{X_{ls}} + \frac{1}{X'_{lr}} \right) \Delta\psi_{md} \tag{A.42}$$

where

$$\frac{1}{\tilde{X}} = \left(\frac{1}{\hat{X}_m} + \frac{1}{X_{ls}} + \frac{1}{X'_{lr}} \right)$$

Figure A.3 shows the resulting simulation diagram for the induction generator. A squirrel cage rotor has been assumed. Therefore, the rotor voltages v'_{qr}, v'_{dr} and v'_{nr} and the rotor neutral current i'_{nr} are all zero.

For comparison, Fig. A.4 shows the conventional machine model with unsaturable main flux. Note that the general model of Fig. A.3 operates as a conventional model by the simple modification of forcing the saturation function K_m to zero.

A.2 Verification of the model.

Because the operation as a self-excited generator relies on the nonlinear characteristics of the air-gap flux to establish an operating point, it provides an excellent means of verifying the model. Fig. A.5(a) shows the machine with a fixed capacitor excitation. Parallel resistors represent core losses as well as any external load. Figure A.5(b) shows the additional equations in simulation form required to obtain the stator voltages from stator current. Figure A.6 compares the simulated and experimental results. Self-excitation process is started by placing an initial charge on the capacitors. The model has been successfully used in the study of a new technique of excitation control in stand alone induction generators [A.3].

A.3 References

1. P. C. Krause and C. H. Thomas, *Simulation of symmetrical induction machinery*, IEEE Trans. on Power App. and Sys., vol. PAS-84, pp. 1038-1053, Nov., 1965.

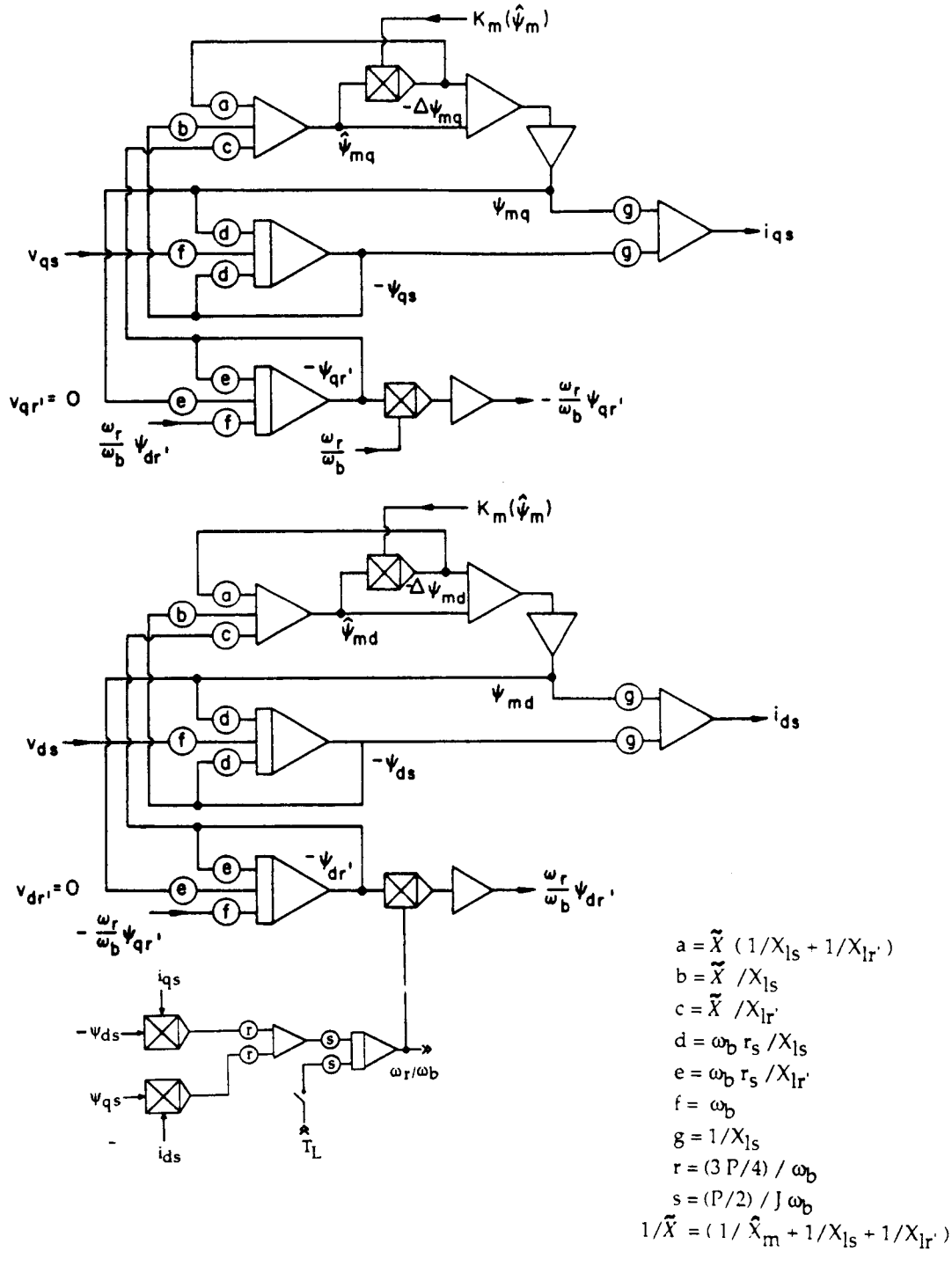

Figure A.3: Induction machine model with main flux saturation.

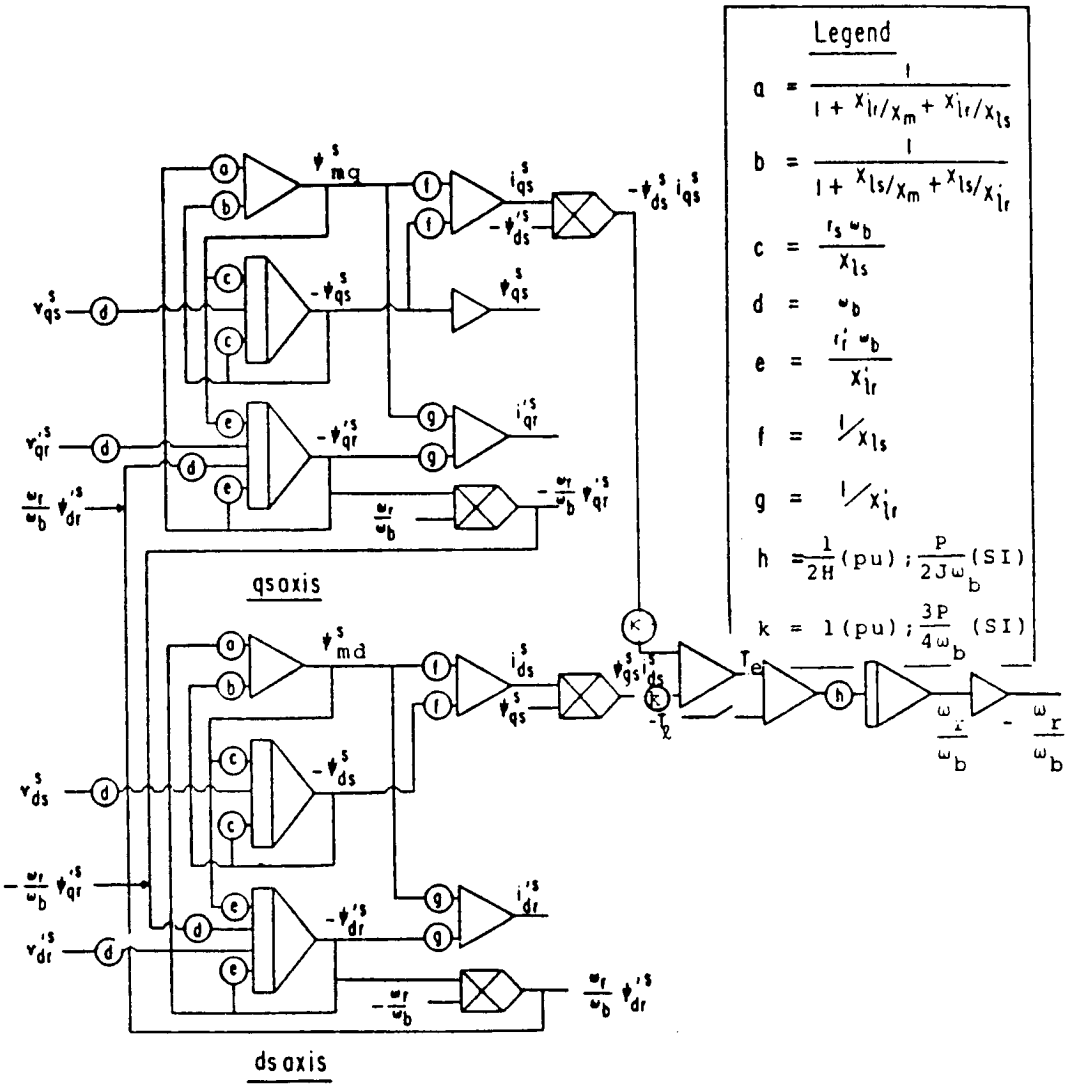

Figure A.4: Induction machine model with no iron saturation

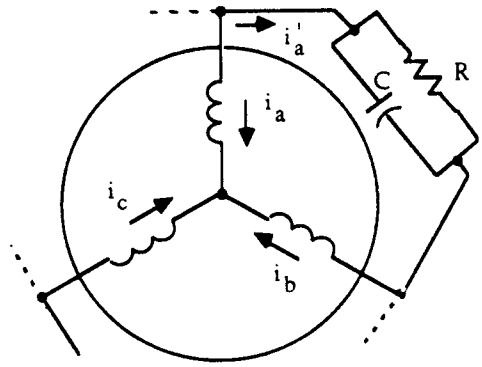

(a)

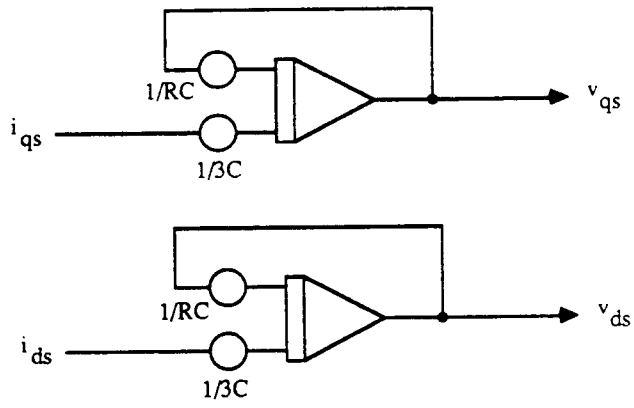

(b)

Figure A.5: Operation as a capacitor excited generator for verification of the model. (a) Circuit, (b) Model.

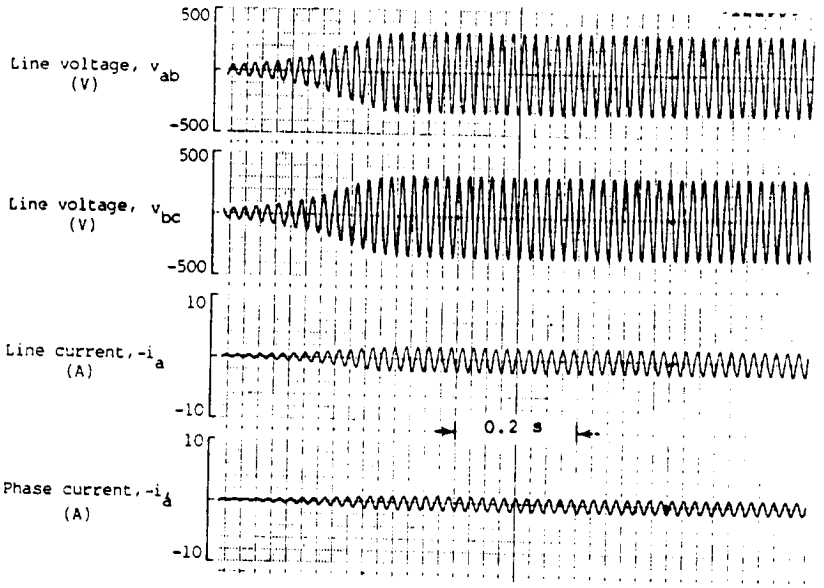

(a)

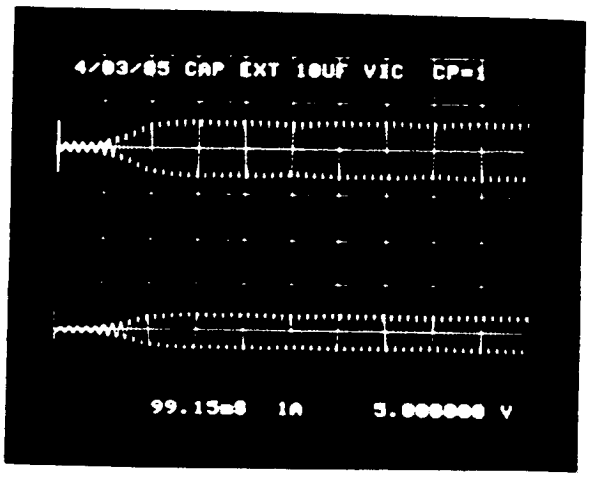

(b)

Figure A.6: Waveforms as a capacitor-excited generator. (a) Simulated Waveforms. (b) Waveforms from a laboratory model. Upper trace: Line voltage; 500 V/div. Lower trace: Line current; 5 A/div.

2. T. A. Lipo and A. Consoli, *Modeling and simulation of induction motors with saturable leakage reactances*, IEEE Trans. Ind. Appl., vol. IA-20, pp. 180-189, Jan./Feb. 1984.

3. P. K. Sood, Habib Rehaoulia, D.W. Novotny and T. A. Lipo, *A pulse-width controlled three-switch exciter for induction generators*, in Conf. Rec. 20th Annul. Meet. of the IEEE Ind. Appl. Soc., pp. 653-661, Oct. 1985.

Appendix B

Modelling the Parallel Output Series Resonant (POSR) Converter

This appendix describes the development and verification of a hybrid computer model of the single-phase bridge configuration of a parallel output-series-resonant (POSR) converter. The circuit topologies and the basic operation of the POSR converter were discussed in Chapter 3.

B.1 Development of the Model

The developed model has been specialized to subresonant operation (i.e. $f_o/f_r < 1.0$) for which the circuit permits natural commutation of its switches. Super resonant operation (i.e. $f_o/f_r > 1.0$) or operation with discontinuous capacitor current have not been considered al though it is possible to generalize the model to include these conditions. The power switches have been modeled so that the circuit can be operated with both a dc and a low frequency ac input voltage.

B.1.1 Power Circuit.

Figure B.1 shows the detailed power circuit of the bridge POR converter prepared for simulation. Switches S_1 to S_4 are naturally commutated bi-directional switches that can carry current in both direction and block voltages of either polarity. This is a representation of a reverse connected pair of thyristor that would be normally required if operation from a

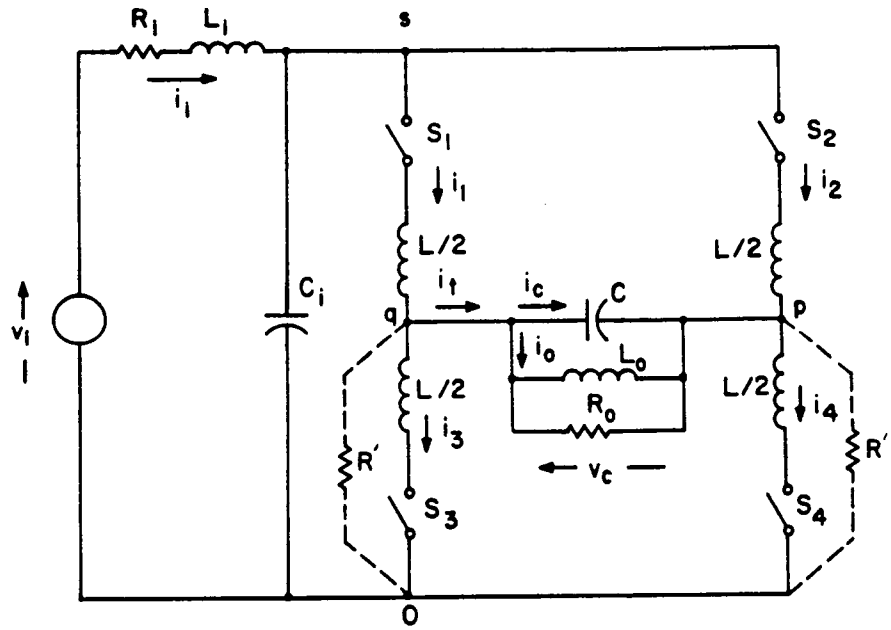

Figure B.1: Power circuit of the POSR converter prepared for simulation.

low-frequency ac voltage is desired. If the input voltage is dc, then a thyristor-reverse diode combination is adequate since the switch has to block voltage in only one direction.

A source impedance R_i, L_i and an input decoupling capacitor C_i have been included to represent the general case of nonnegligible source impedance and its decoupling through a parallel input capacitor. When the operation is from a dc source, these component are not important to the circuit operation and can be deleted from the model through an easy modification. Inductance L_o represents the magnetizing inductance of the output transformer that may be needed for voltage matching or input/output isolation. L_o should normally be an order of maginitude larger than the value of the resonant inductance L. When L_o is not present in the circuit, it can be also be removed from the model by forcing the gain of the corresponding amplifier to zero. The load and circuit losses are represented together by the parallel resistor, R_p. Finally, the resistors shown in dotted lines and labelled R' are used to help solve the node equations. They are of such high value as not to significantly alter the operation of the circuit. If this assumption becomes difficult to justify, then the resistors should be returned to a fictitious center point in the supply instead of point "o" in Fig. B.1 in order to minimize assymetry in the predicted results.

B.1.2 Modeling of the bi-directional switch.

In this split inductor configuration of the POSR converter, an inductor is physically present in series with each switch. Figure B.2 shows how this switch inductor combination can be modeled on a hybrid computer. The voltage across the combination is integrated for as long as the switch remains closed to yield the current through the branch. The switch is commanded closed with signal G representing the gating pulse to the SCR. The integrator is disabled (i.e. switch opened) when the integrated current goes through its second zero crossing which is characterisitc of the assumed subresonant operation. This modification in the normal implementation of the naturally commutated devices reduces the total number of components required for simulating one bridge circuit. This permits simultaneously simulation of three such bridge converters needed for studying the operation from a three-phase low frequency source. When operating from an ac input, the initial conduction through the switch may be in either direction. Therefore, detection of the second zero crossing must be independent of the direction of the initial conduction. Figure B.2 (b) shows a logic scheme that reliably detects the second zero crossing of the current for both the forward initial conduction (B.2 (c)) and the reverse initial conduction (B.2 (d)).

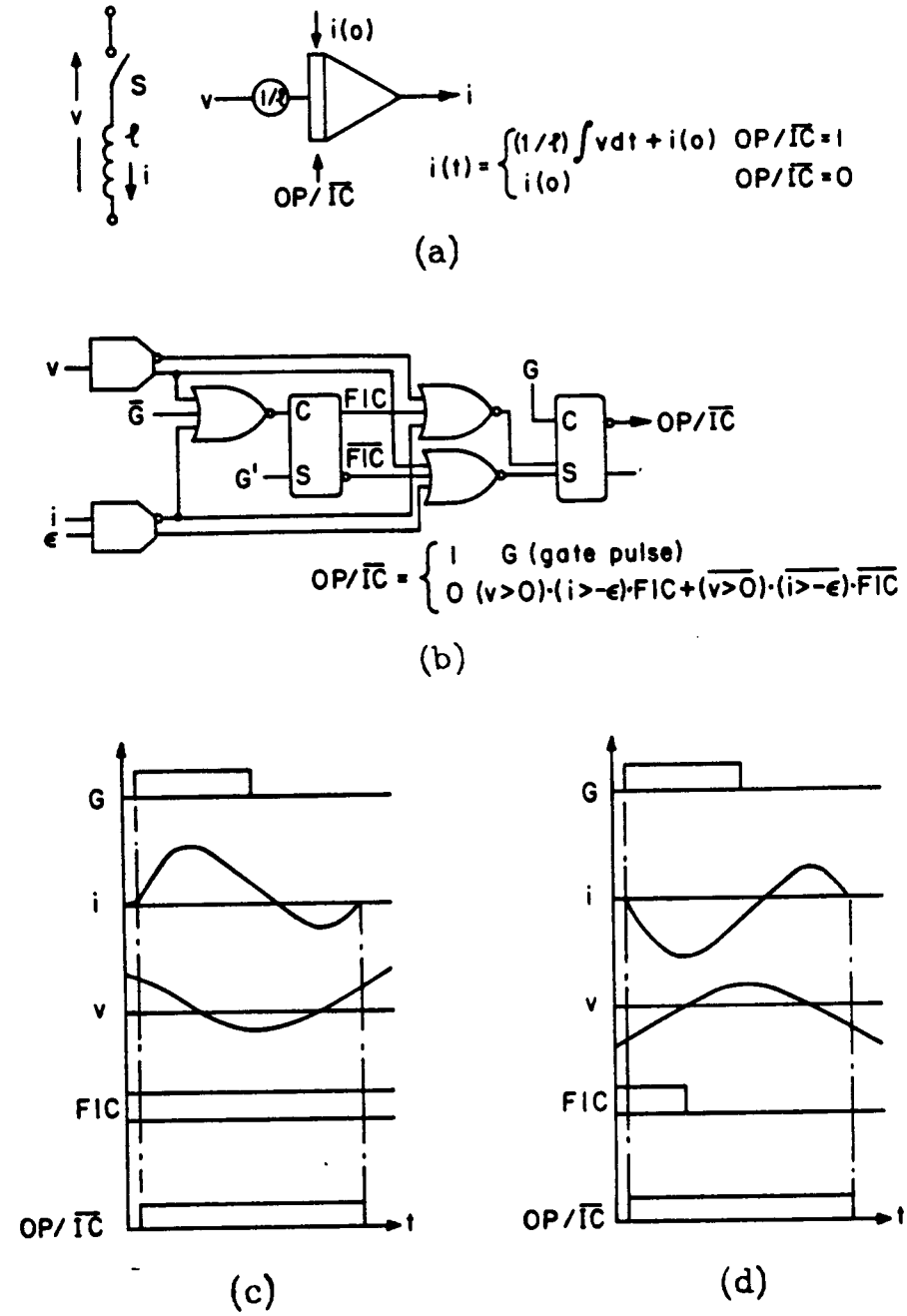

Figure B.2: Modeling of the POSR converter bi-directional switch. (a) A controlled integrator representation of the switch-inductance combination. (b) Integrator control logic. (c) Forward initial conduction. (d) Reverse initial condition.

B.2 Circuit Equations.

The circuit equations to be solved are
Switch Currents.

$$i_1 = \begin{cases} \frac{2}{L}\int v_{sq}\,dt & S_1 ON \\ 0 & S_1 OFF \end{cases} \tag{B.1}$$

$$i_2 = \begin{cases} \frac{2}{L}\int v_{sp}\,dt & S_1 ON \\ 0 & S_1 OFF \end{cases} \tag{B.2}$$

$$i_3 = \begin{cases} \frac{2}{L}\int v_{qo}\,dt & S_1 ON \\ 0 & S_1 OFF \end{cases} \tag{B.3}$$

$$i_4 = \begin{cases} \frac{2}{L}\int v_{po}\,dt & S_1 ON \\ 0 & S_1 OFF \end{cases} \tag{B.4}$$

Low Frequency End
Input Port

$$i_i = \frac{1}{L_i}\int [\,(v_i - v_{so}) - i_i R_i\,]\,dt \tag{B.5}$$

$$v_{so} = \begin{cases} \frac{1}{C_i}\int (i_i - i_1 - i_2)\,dt & \\ v_i & \text{if } R_i,\ L_i \text{ and } C_i \text{ removed} \end{cases} \tag{B.6}$$

HF Output Port

$$i_o = \frac{1}{L_o}\int v_o\,dt - \frac{v_c}{R_p} \tag{B.7}$$

$$i_c = (i_4 + \frac{v_{po}}{R} - i_2 - i_o) \tag{B.8}$$

$$v_o = v_c = \frac{1}{C}\int i_c \, dt \tag{B.9}$$

Voltage Relations

$$v_{qo} = R(i_1 - i_3 - i_c - i_o) \tag{B.10}$$

$$v_{sq} = v_{so} - v_{qo} \tag{B.11}$$

$$v_{po} = v_{qo} - v_c \tag{B.12}$$

$$v_{sp} = v_{qo} - v_{po} \tag{B.13}$$

Voltage across the switches are obtained from the voltages of the switch- inductance combinations derived above. For example, the voltage across S_1 is given by

$$v_{S1} = \begin{cases} v_{sq} & S_1 OFF \\ 0 & S_1 ON \end{cases} \tag{B.14}$$

Figure B.3 shows the resulting circuit model in analog simulation form.

B.2.1 Gating Signals.

A possible scheme for generating the gating signals for the POSR converter model is shown in Fig. B.4(a). Figure B.4(b) shows the associated waveforms. Six signals, phase displaced by sixty degrees of the output cycle, are generated. Any two that are phase shifted by 180 deg can be used to gate one bridge converter. Thus, up to three single-phase converters can be gated using the scheme which permits modeling of the three-converter three-phase configuration of Fig. 3.11.

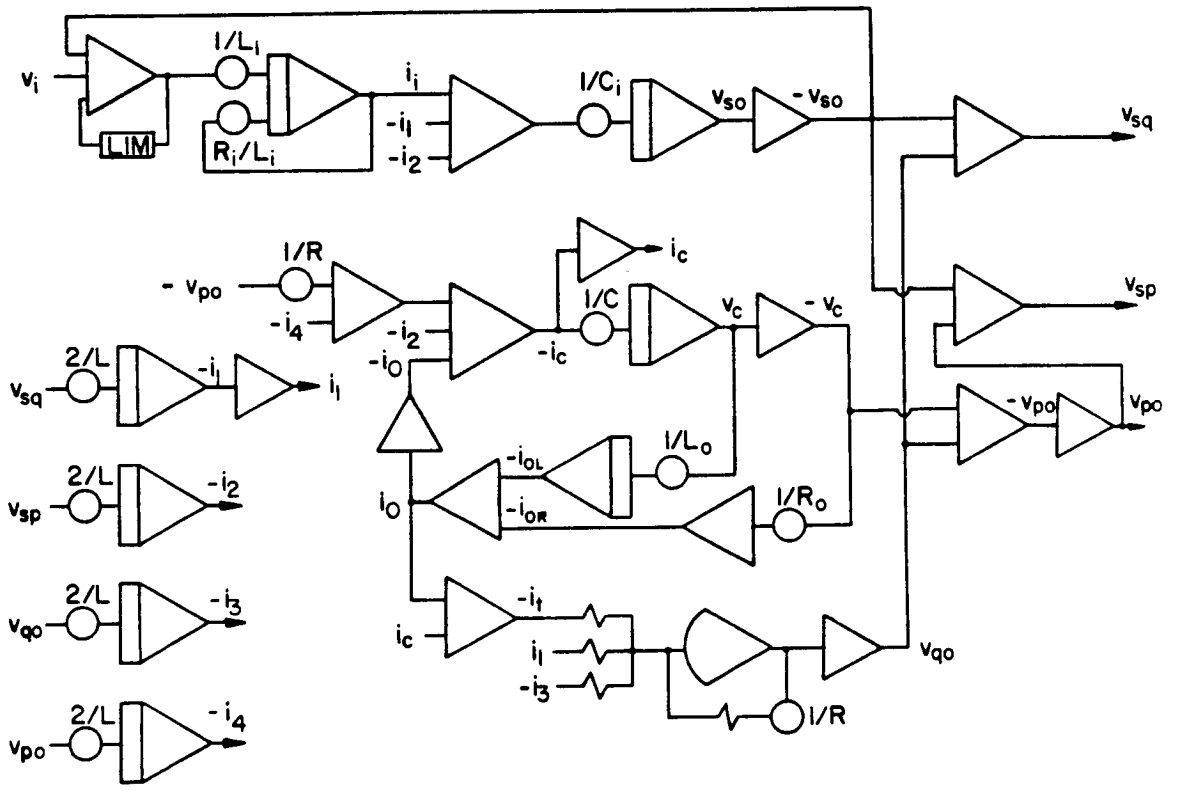

Figure B.3: Hybrid computer model of the POSR converter.

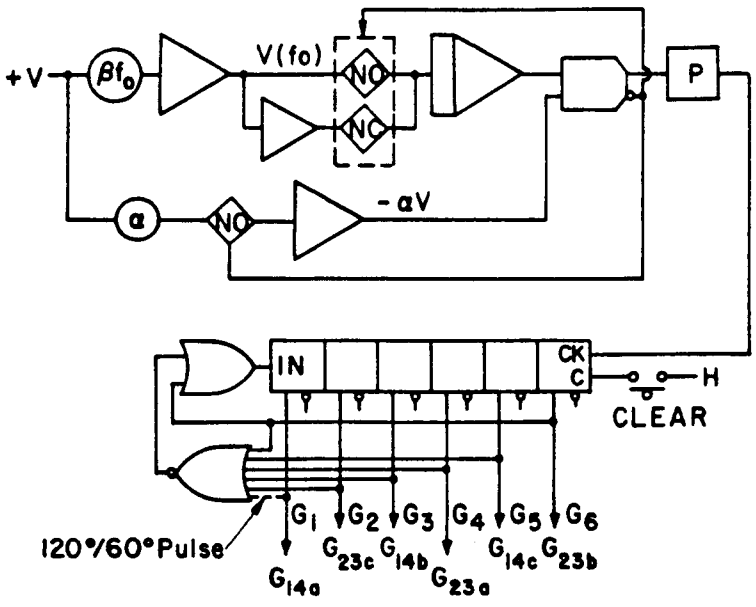

(a)

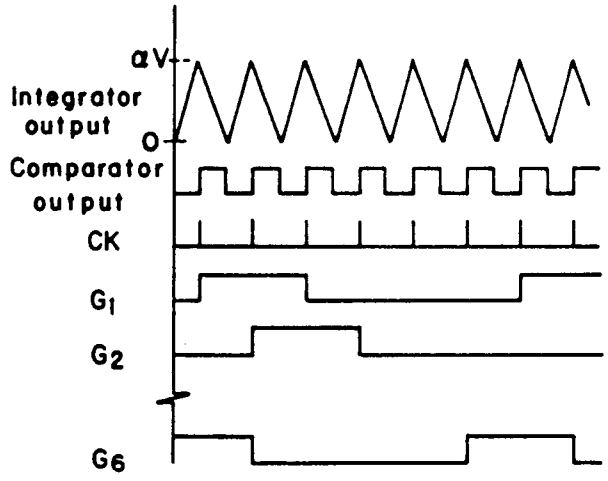

(b)

Figure B.4: Scheme for generating the gating signals. (a) Hybrid computer realization. (b) Associated waveforms.

B.3 Verification of the Model

Results predicted by model compare favorably with the experimental data obtained from our own breadboard and the data made available by General Dynamics - Convair division from their similar POSR breadboard. For example, Figure B.5 and B.6 show a set of circuit waveforms from the GDC breadboard run from a stiff 90 V dc source and switched at a frequency of 20 kHz. Figures B.7 (no load) and B.8 (1.6 kW load) show the corresponding waveforms predicted by the model. For this simulation run, input impedance and the decoupling capacitor were omitted and circuit parameters of $C = 1.5\,\mu F$, $L = 24\,\mu H$, $L/L_o = 20$ were used to match the circuit components used on the GDC breadboard.

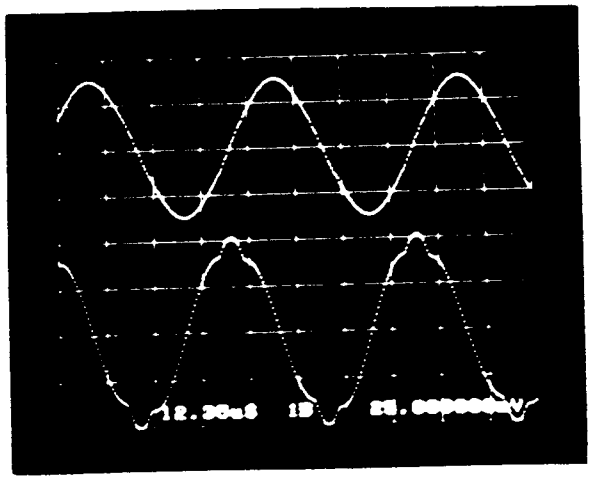

(a)

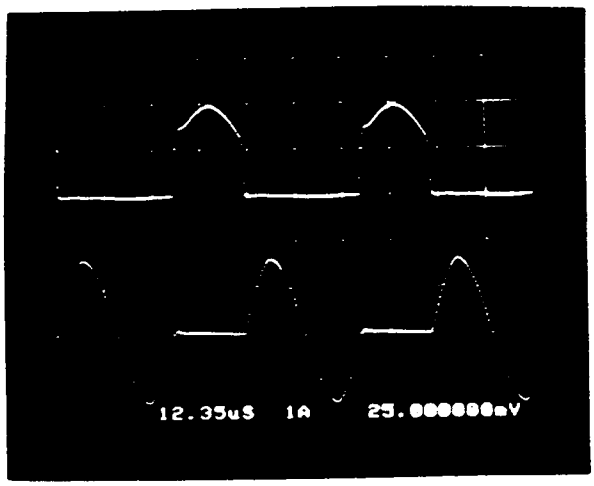

(b)

Figure B.5: Experimental waveforms observed at no load. (a) Upper trace: Capacitor voltage, v_c; 250 V/div. Lower trace: Capacitor current, i_c ; 12.5 A/div. (b) Upper trace: Switch voltage, v_{T4}; 125 V/div. Lower trace: Switch current, i_4; 12.5 A/div.

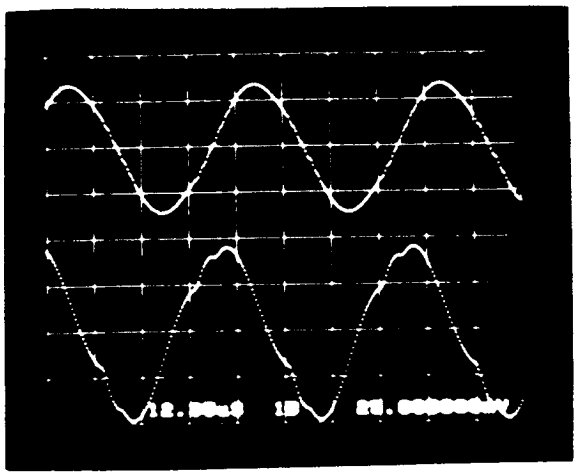

(a)

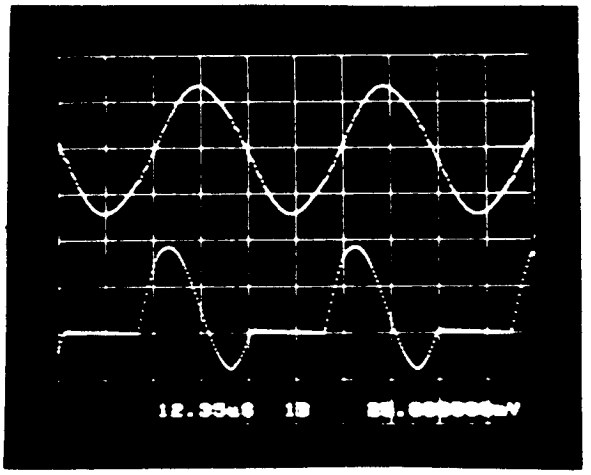

(b)

Figure B.6: Experimental waveforms observed with resistive load of just over 1.2 kW. (a) Upper trace: Capacitor voltage, v_c; 250 V/div. Lower trace: Capacitor current, i_c ; 12.5 A/div. (b) Upper trace: Capacitor voltage, v_c; 250 V/div. Lower trace: Switch current, i_4; 12.5 A/div.

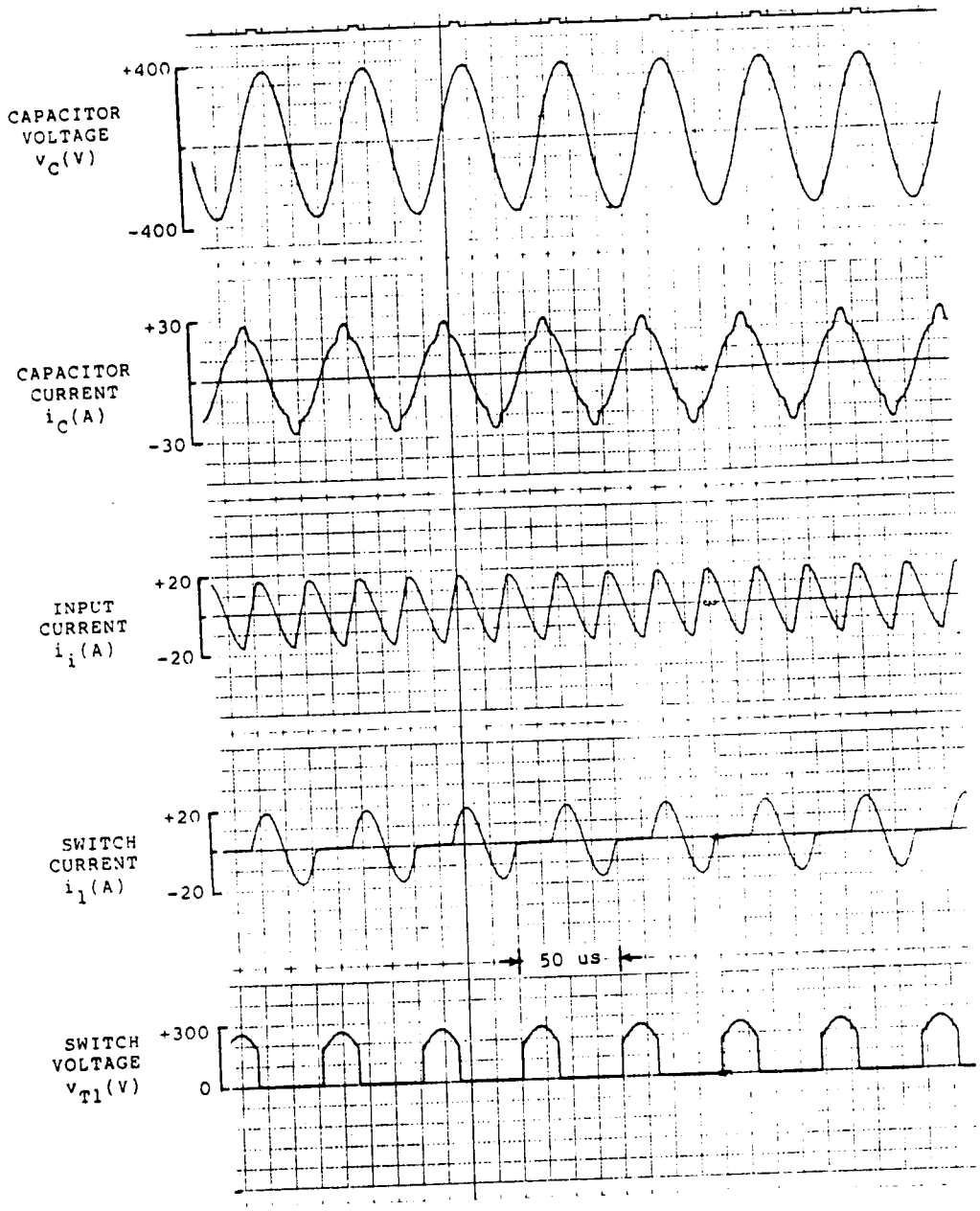

Figure B.7: Corresponding no load waveforms predicted by the POSR model.

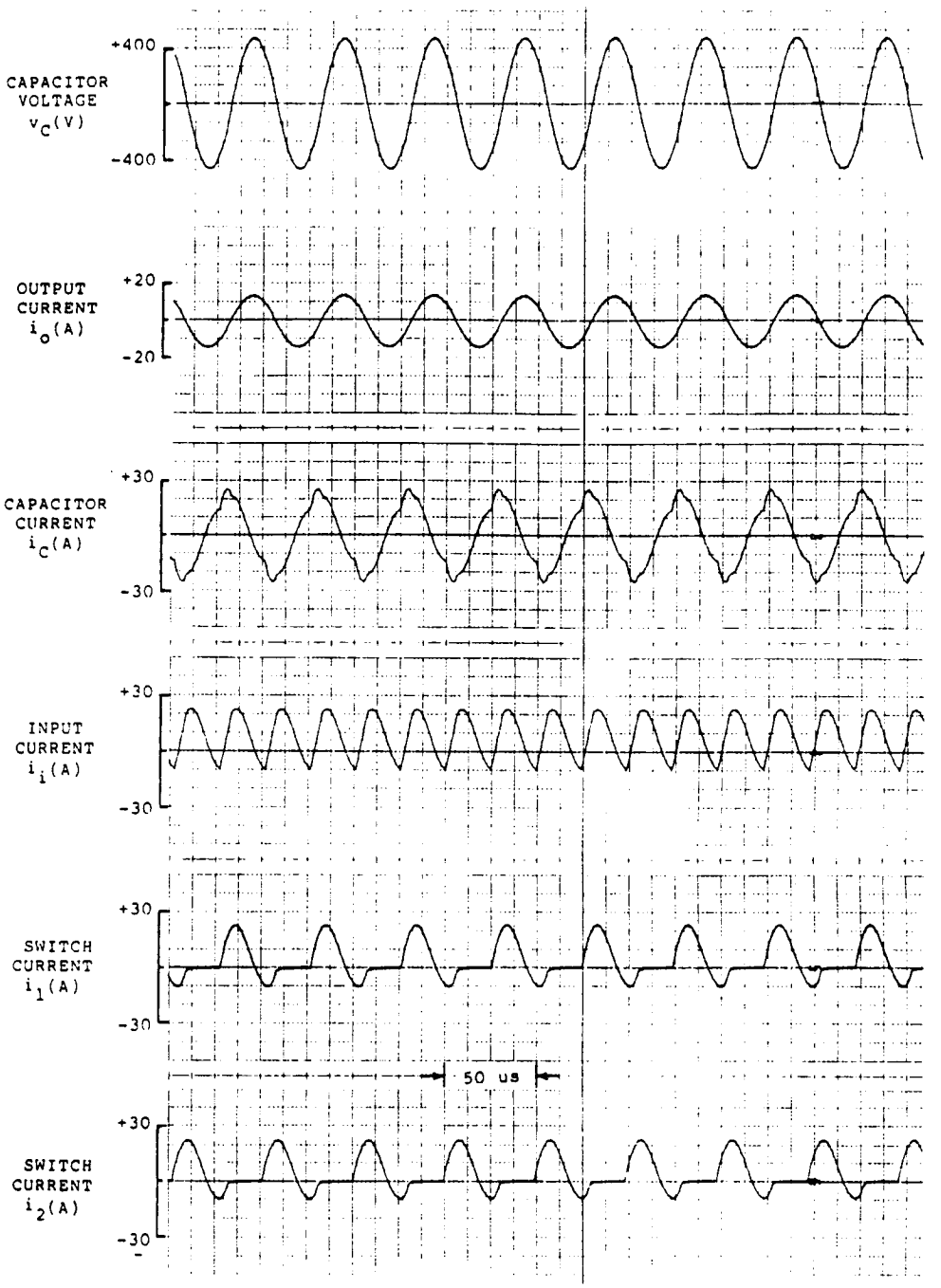

Figure B.8: Corresponding waveforms predicted by the POSR model for a 1.6 kW Load.

Appendix C

Modelling of Pulse Density Modulated (PDM) Converters

This appendix describes the development and verification of a hybrid computer model of the three-phase bridge PDM converter discussed in Sec. 4.4. Modeling of single-phase PDM converters for synthesizing ac and dc voltages or currents is also discussed.

C.1 Development of the Three-Phase Bridge Model

Development of a hybrid computer model for a power converter requires writing down the circuit equations for the converter and then transforming them into an integral form so that they can be solved using the analog integrators. Logic for switch selection and the timing waveforms required for the implementation of this logic are developed on the digital portion (PDP 11/23) of the hybrid computer.

C.1.1 Power Circuit.

Figure C.1 shows the detailed power circuit of the 3-phase bridge PDM converter prepared for simulation. Although a resonant LC tank filter has been assumed at the link side of the converter, other filter topologies can be considered by modifying this portion of the model. On the low-frequency side, a passive R-L load and a three-phase induction machine have been considered but clearly other loads are possible and can be modeled using the suggested procedure. Ideal switches S_1 to S_6 have been used to model the actual bi-

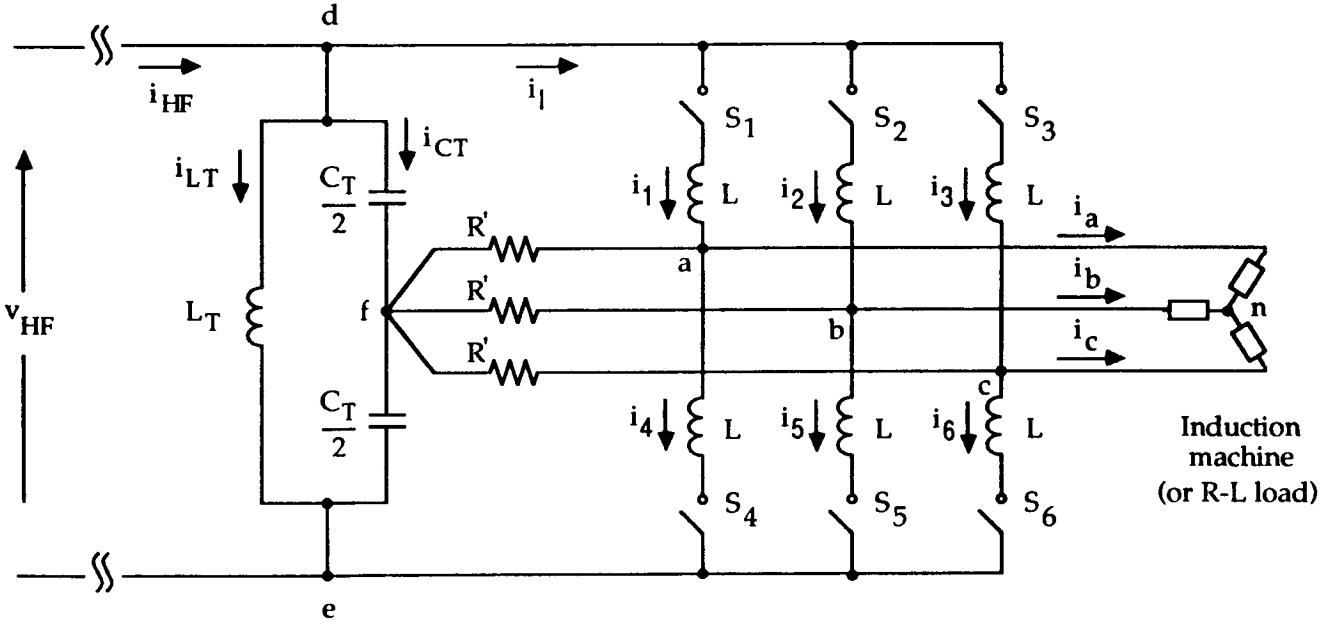

Figure C.1: Power circuit of three-phase PDM bridge converter prepared for simulation.

directional switches required in PDM converters. Inductance, l in series with each switch allows modeling the switch-inductor combination by a single integrator (Fig. C.2). Clearly, the circuit behavior related to nonideal characteristics of the devices (e.g finite switching times and losses, nonzero voltage drops, effects of snubbers when present, etc.) cannot be predicted from a such a simplified model and for these one must use breadboard systems. However, very useful information is obtained even from the simplified model. When the physical inductance in series with the devices is small in the actual circuit, (as it should be in a PDM power circuit so that current transfers among the switches can be completed with a minimum of voltage overshoots). it is then important to use the smallest possible value for l in the model. For the model described a value of 0.625 μH was used for the series inductor, l. Note that this value is not far from the stray inductance that can be present in an actual converter circuit of this type.

When ever switch of Fig. C.2 is ON, the integrator modeling the switch-inductor combination is enabled (i.e. $OP/\overline{IC} = 1$) and the voltage across the combination is integrated. The integrator is disabled when the switch turns OFF (i.e. $OP/\overline{IC} = 0$) either as a result of a gating signal (forced commutated devices) or due to the natural extinction of the current in the switch (natural commutated devices). Clearly, the commutation charateristics of the devices used in realization of the bi-directional switch have to be taken in account when generating the enable/disable signal for the integrator. Figure C.3 illustrates the generation of this integrator control signal for switch S_1 when forced commutated devices are used. Logic signal G1 is produced by the PDM based switch selection logic and indicates that switch S_1 has been selected for conduction. Switch S_1 is therefore closed by setting the integrator control signal, OPS1 (operate S_1) to high. OPS1 is forced low as soon as G1 goes low in order to simulate the gate controlled turn-off of the devices. OPS4, being the control signal for the complementary switch in the same pole of the converter, is logical complement of OPS1 When naturally commutated devices such as inverter grade SCRs are used in the realization of the bi-directional switch, the integrator control signal cannot be forced zero merely when the gating signal has gone low but must await the circuit forced extinction of the current through the switch.

In the model described here, only forced commutated devices have been assumed since they are the most likely choice in the physical circuit realization as discussed in Sec. 4.4. Modeling of a naturally commutated PDM circuit would differ in switch selection logic to ensure that circuit commutation currents are set up under all conditions of operation, and in the generation of the integrator control signal as discussed above. Resistors shown in dotted lines Fig. C.1 and labelled R' are present for assisting in the solution of circuit equations. They are of such high value as not to influence with the operation of the circuit directly.

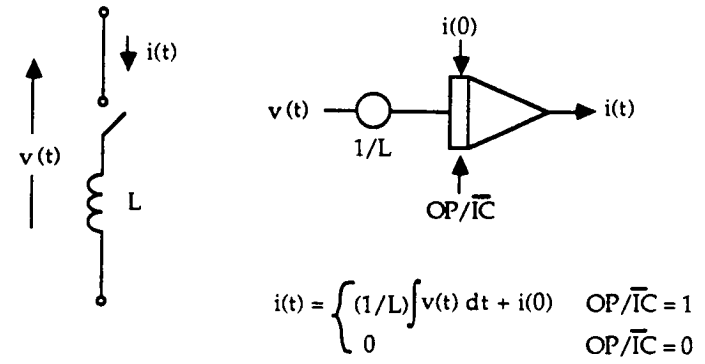

(a)

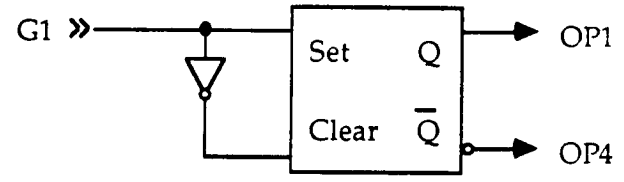

(b)

Figure C.2: Modelling of a PDM converter switch. (a) Single-integrator representation. (b) Generation of control signal (shown for switch S_1).

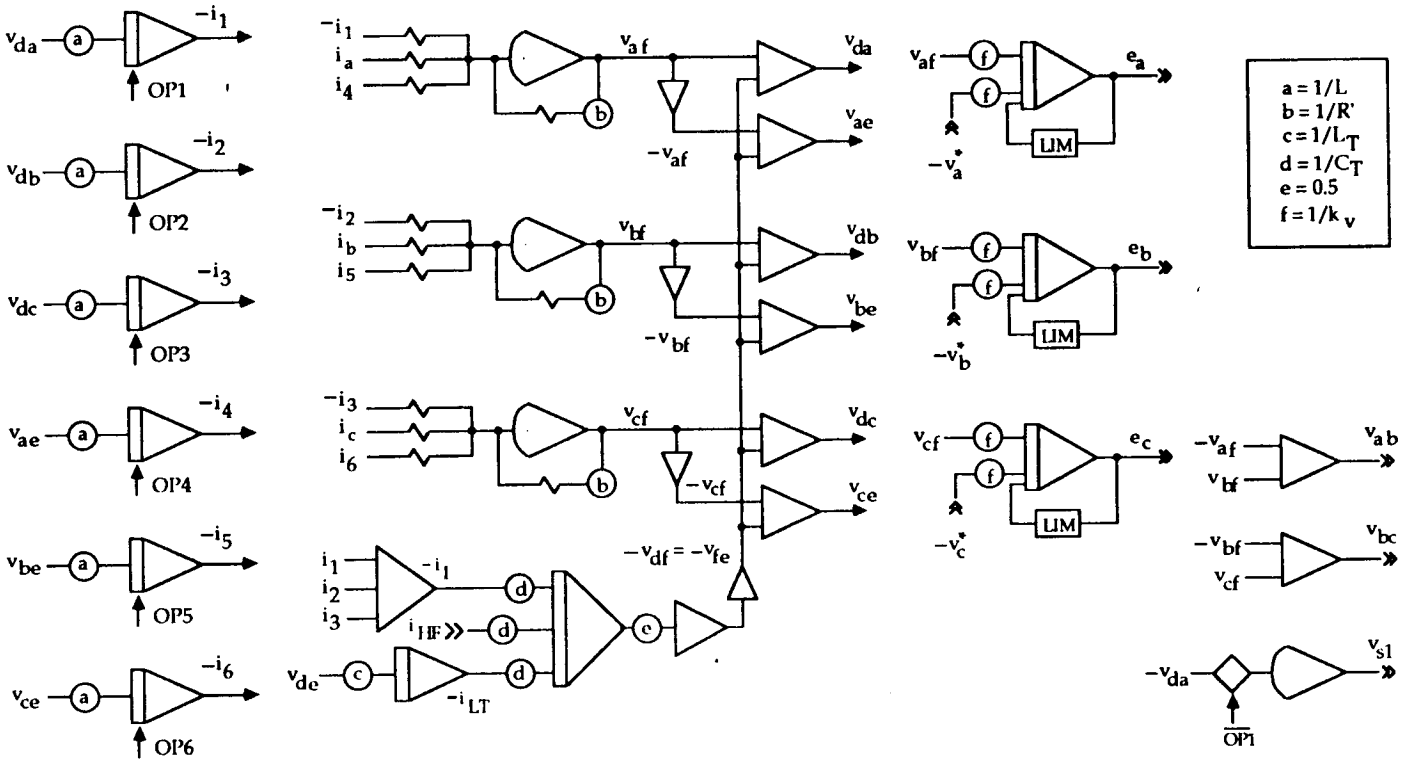

Figure C.3: Hybrid computer model of a three-phase PDM bridge converter.

C.1.2 Circuit Equations

. The circuit equations to be solved are *Switch Currents.*

$$i_1 = \begin{cases} \frac{1}{\ell} \int v_{da}\, dt & S_1 ON \\ 0 & S_1\ OFF \end{cases} \tag{C.1}$$

$$i_2 = \begin{cases} \frac{1}{\ell} \int v_{db}\, dt & S_2 ON \\ 0 & S_2\ OFF \end{cases} \tag{C.2}$$

$$i_3 = \begin{cases} \frac{1}{\ell} \int v_{dc}\, dt & S_3 ON \\ 0 & S_3\ OFF \end{cases} \tag{C.3}$$

$$i_4 = \begin{cases} \frac{1}{\ell} \int v_{ae}\, dt & S_4 ON \\ 0 & S_4\ OFF \end{cases} \tag{C.4}$$

$$i_5 = \begin{cases} \frac{1}{\ell} \int v_{be}\, dt & S_5 ON \\ 0 & S_5\ OFF \end{cases} \tag{C.5}$$

$$i_6 = \begin{cases} \frac{1}{\ell} \int v_{ce}\, dt & S_6 ON \\ 0 & S_6\ OFF \end{cases} \tag{C.6}$$

High-Frequency Port

$$i_I = i_1 + i_2 + i_3 \tag{C.7}$$

$$i_{CT} = i_{HF} - i_{LT} - i_I \tag{C.8}$$

Tank Filter

$$i_{LT} = \frac{1}{L_T} \int v_{de}\, dt \tag{C.9}$$

$$v_{de} = \frac{1}{C_T} \int i_{CT}\, dt \tag{C.10}$$

Voltage Relations Pole voltages:

$$v_{af} = R' (i_1 - i_a - i_4) \tag{C.11}$$

$$v_{bf} = R' (i_2 - i_b - i_5) \tag{C.12}$$

$$v_{cf} = R' (i_3 - i_c - i_6) \tag{C.13}$$

Switch-inductor voltages:

$$v_{da} = v_{df} - v_{af};\quad v_{db} = v_{df} - v_{bf};\quad v_{dc} = v_{df} - v_{cf} \tag{C.14}$$

$$v_{ae} = v_{fe} + v_{af};\quad v_{be} = v_{fe} + v_{bf};\quad v_{ce} = v_{fe} + v_{cf} \tag{C.15}$$

Line voltages:

$$v_{ab} = v_{af} - v_{bf};\quad v_{bc} = v_{bf} - v_{cf};\quad v_{ca} = v_{cf} - v_{af} \tag{C.16}$$

If the R''s are sufficiently large, then

$$v_{df} = v_{fe} = \frac{v_{de}}{2} \tag{C.17}$$

Voltage across a switch can be derived from the corresponding voltage across the switch-inductance combination. For example, the voltage across switch S_1 is given by

$$v_{S_1} = \begin{cases} v_{da} & S_1\ ON \\ 0 & S_1\ OFF \end{cases} \tag{C.18}$$

Low-Frequency Port with a balanced wye connected passive (R_{LF}, L_{LF}) load:

$$v_{an} = \frac{2}{3} v_{af} - \frac{1}{3} v_{bf} - \frac{1}{3} v_{cf} = \frac{2}{3} v_{ab} + \frac{1}{3} v_{bc} \tag{C.19}$$

$$v_{bn} = -\frac{1}{3} v_{af} + \frac{2}{3} v_{bf} - \frac{1}{3} v_{cf} = \left(-\frac{1}{3} v_{ab} + \frac{1}{3} v_{bc} \right) \tag{C.20}$$

$$i_a = \frac{1}{L_{LF}} \int \left(v_{an} - i_{LF} R_{LF} \right) dt \tag{C.21}$$

$$i_b = \frac{1}{L_{LF}} \int \left(v_{bn} - i_{LF} R_{LF} \right) dt \tag{C.22}$$

$$i_c = -\left(i_a + i_b \right) \tag{C.23}$$

Three-phase three-wire induction machine load:

$$v_{qs} = v_{an} = \left(\frac{2}{3} v_{ab} + \frac{1}{3} v_{bc} \right) \tag{C.24}$$

$$v_{ds} = -\frac{1}{\sqrt{3}} v_{bc} \tag{C.25}$$

$$v_{ns} = 0 \tag{C.26}$$

Corresponding machine currents i_{qs} and i_{ds} are obtained from the induction machine model described in Appendix A. These $d-q$ current components can then be transformed to yield line currents i_a, i_b and i_c .

The converter model that results from these equations is shown in Fig. C.4. .

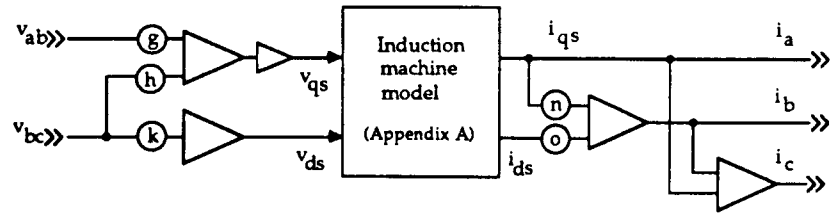

(a)

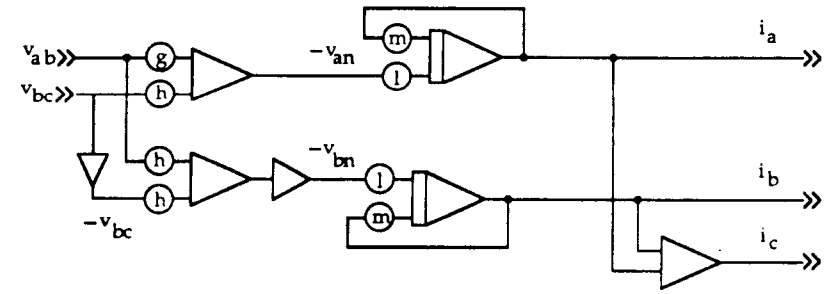

(b)

$g = 2/3$; $h = 1/3$; $k = 1/\sqrt{3}$; $l = 1/L_{LF}$
$m = R_{LF} / L_{LF}$; $n = 1/2$; $o = \sqrt{3/2}$

Figure C.4: Modelling of the low frequency end circuit. (a) Induction machine (See Appendix A). (b) Passive R-L load.

C.1.3 PDM Logic.

Implementation of PDM scheme requires integration of the difference between the reference and the synthesized signal. For the case when pole voltages of the three-phase PDM bridge are synthesized individually the equations that apply are

$$e_a(t) = K_v \int (v_a^* - v_{af})\, dt \tag{C.27}$$

$$e_b(t) = K_v \int (v_b^* - v_{bf})\, dt \tag{C.28}$$

$$e_c(t) = K_v \int (v_c^* - v_{cf})\, dt \tag{C.29}$$

Where K_v is the gain of the PDM difference integrator. Error signals e_a, e_b and e_c with the polarities of the link and the reference signals determine the switch selection in the PDM converter. Zero voltage switching requires that the device selection for the next half-cycle of the link voltage be made somewhat in advance of the zero crossing so that the actual switching can take place at or near the zero crossings. This advance sensing is reflected in the switch selection logic in the form of the reversed polarity of the link voltage as seen below. To help write the logic expressions for switch selection, define the following logic variables

G1 = 1 if switch S_1 is to be selected for the *next* half-cycle of the link voltage.

VA = 1 if the reference signal $v_a^*(t)$ has positive polarity in the *present* half-cycle of the link voltage.

VHF = 1 if the link voltage, v_{HF} is positive during the *present* half cycle of the link voltage.

TGA = 1 if the pole "a" needs to be toggled.

A value of 1 (0) denotes a logic value of TRUE (FALSE) in the expressions above. With these definitions, the logic needed to operate pole "a" is given by

$$TGA = (e_a > \epsilon)\ .\text{AND.}\ (e_a < -\epsilon)\ .\text{AND}\ \overline{VA} \tag{C.30}$$

$$S_1 = \overline{S_4} = (\text{VA .XOR. VHF}) \text{ .XOR. TGA} \qquad \text{(C.31)}$$

Where .AND. and .XOR. indicate "and" and "exclusive or" logic operations. Similar equations apply for switch pairs S_2, S_5 and S_3, S_6 for poles "b" and "c" respectively.

Implementation of the PDM logic requires detection of the zero crossing of the link voltage and preselection of the switches as discussed above. Flow chart of Fig. C.5 shows how the logic of C.31 and C.32 was implemented on the PDP 11/23 portion of the hybrid computer using built in analog-to-digital and digital-to-analog conversion capability when needed.

C.2 Verification of the Model

A qualitative verification of the model was carried out by comparing the predicted and observed waveforms of a PDM bridge converter for the case of a passive R-L load. For example, Fig. C.6 shows key waveforms observed on the laboratory converter supplying a wye connected R-L load measured to have an inductance of 30 mH per phase. Effective resistance was determined using power and current measurement to have a value of 3.5 ohms per phase. Link voltage was 252 V rms at a frequency of 19.3 kHz. Reference signal corresponding to a low-frequency line voltage of 104 V rms at a frequency of 28 Hz. With these parameters as the input, the corresponding waveforms predicted by the PDM model are shown in Fig. C.7. The differences that are present can be attributed to one or more of the features (e.g. capacitive snubbers, device turn-on and turn-off times, recovery currents, losses associated with devices and passive L and C components etc.) of a real system that had to be neglected so that the model does not become so large as to be of no practical use. Note, however, that even a simple one-integrator model of the bi-directional switch provides a wealth of information on the fundamental behavior of the PDM converter.

C.3 Modeling Single-Phase PDM Converters

Full- or half-bridge power circuit configurations of the PDM converter can be modeled using exactly the same procedure discussed for the three-phase configuration. A single-phase power circuit can be used to synthesize ac or dc, voltage or current signals with only minor modification in the controller. No changes are needed in the modeling of the basic power circuit.

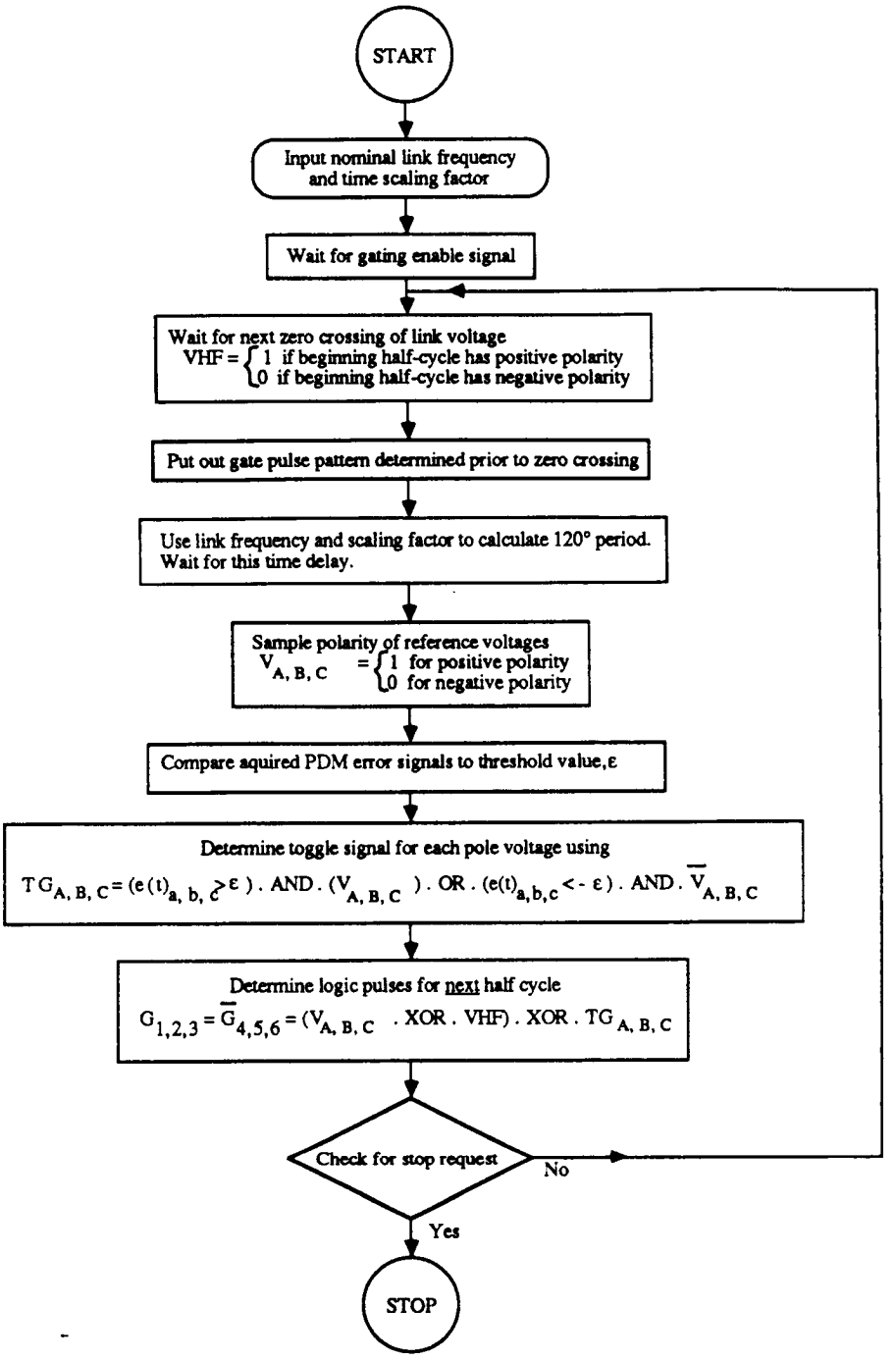

Figure C.5: Flow chart showing hybrid computer implementation of the PDM logic for a three-phase bridge converter.

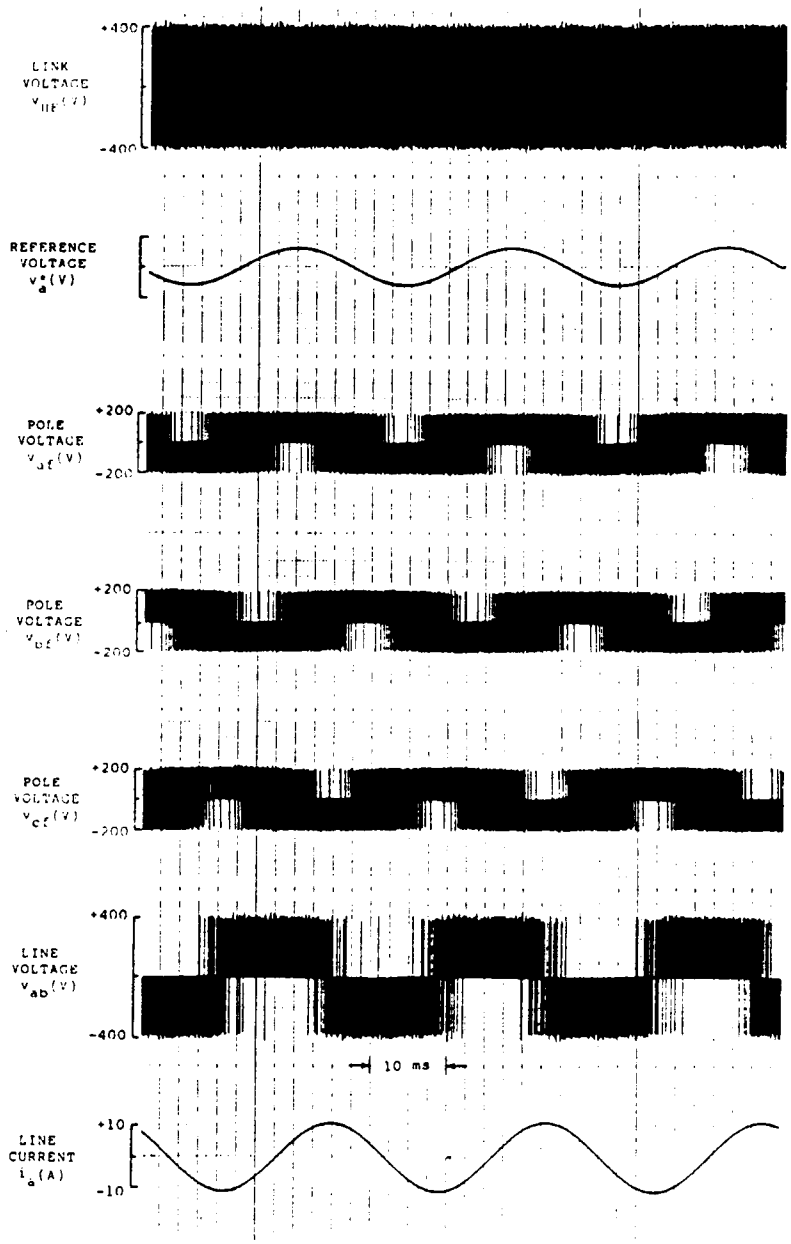

Figure C.6: Simulated waveforms for PDM converter supplying a wye connected R-L load. R = 6 ohms, L = 40 mH, f_{HF} = 36 Hz, v_{LF} = 145 V rms line-to-line, V_{HF} = 400 V peak, and f_{HF} = 19.3 Hz.

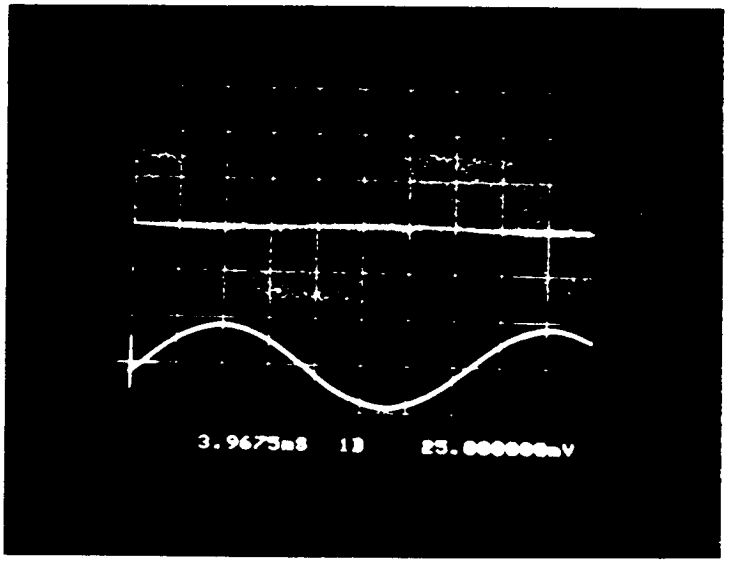

Figure C.7: Corresponding waveforms observed on the breadboard converter. Upper trace: Line voltage, v_{ab}; 250 V/div. Lower trace: Line current, i_a; 12.5 A/div.

C.4 Voltage Synthesis.

Using the single-phase power circuit model (for example, the full-bridge power circuit model), either an ac voltage or a dc voltage of positive or negative polarity may be synthesized by simply using the appropriate reference signal. If a half-bridge is used then the synthesis is exactly like the control of one pole of a three-phase bridge PDM converter discussed earlier. When full-bridge circuit is used, options discussed in Sec. 6.1 are available and can all be implemented with only minor changes in the basic PDM logic of Eqns. C.30 and C.31. For example, instead of synthesizing individual pole voltages using two phase displaced reference signals, the line voltage (difference of the two pole voltages) can be synthesized directly using a single reference signal with an added restriction of commutated waveform (not permitting pulses with polarity opposite to the instantaneous polarity of the reference signal). Synthesis of 120 V rms 60 Hz ac voltage of Fig. 6.4 was an example of this type of synthesis.

C.5 Current Synthesis.

The power circuit modification for basic current synthesis that may be needed is the addition of a current ripple limiting inductor in case such an inductor in not already a feature (as in machine, or R-L load) of the load/source present of the low-frequency side. The major change in the controller is that the feedback to the AC-PDM controller must now be from the resulting low-frequency current. It has been observed that that the gain of the difference integrator has to be increased roughly by the factor of $1/L_{LF}$ over the corresponding value used for voltage synthesis and appears to be a consequence of the indirect control of current through application of voltage pulses. Figs. 6.5 and 6.6 shown in Chapter 6 are examples of the current synthesis implemented in the described manner using the full bridge model.

1. Report No.	2. Government Accession No.	3. Recipient's Catalog No.
NASA CR-179600		

4. Title and Subtitle	5. Report Date
Study of the Generator/Motor Operation of Induction Machines in a High Frequency Link Space Power System	March 1987
	6. Performing Organization Code

7. Author(s)	8. Performing Organization Report No.
Thomas A. Lipo and Pradeep K. Sood	None
	10. Work Unit No. 481-54-02

9. Performing Organization Name and Address	11. Contract or Grant No.
University of Wisconsin Dept. of Electrical and Computer Engineering 1415 Johnson Drive Madison, Wisconson 53706	NAG3-631
	13. Type of Report and Period Covered Contractor Report Final
12. Sponsoring Agency Name and Address	14. Sponsoring Agency Code
National Aeronautics and Space Administration Lewis Research Center Cleveland, Ohio 44135	

15. Supplementary Notes

Project Manager, Irving G. Hansen, Electrical Systems Division, NASA Lewis Research Center.

16. Abstract

Static power conversion systems have traditionally utilized dc current or voltage source links for converting power from one ac or dc form to another since it readily achieves the temporary energy storage required to decouple the input from the output. Such links, however, result in bulky dc capacitors and/or inductors and lead to relatively high losses in the converters due to stresses on the semiconductor switches. This report examines the feasibility of utilizing a high frequency sinusoidal voltage link to accomplish the energy storage and decoupling function. In particular, a new type of resonant six pulse bridge interface converter is proposed which utilizes zero voltage switching principles to minimize switching losses and uses a novel, easy to implement technique for pulse density modulation to control the amplitude, frequency, and the waveshape of the synthesized low frequency voltage or current. Adaptation of the proposed topology for power conversion to single-phase ac and dc voltage or current outputs is shown to be straight forward. The feasibility of the proposed power circuit and control technique for both active and passive loads are verified by means of simulation and experiment.

17. Key Words (Suggested by Author(s))	18. Distribution Statement
Aerospace power Motor drive	Unclassified - unlimited STAR Category 20

19. Security Classif. (of this report)	20. Security Classif. (of this page)	21. No. of pages	22. Price*
Unclassified	Unclassified	184	A09

*For sale by the National Technical Information Service, Springfield, Virginia 22161